The effect of vagus nerve stimulation on the brain of epilepsy patients

Simon Wostyn

Supervisors: Prof. dr. Stefaan Vandenberghe, Prof. Kristl Vonck
Counsellors: Ir. Willeke Staljanssens, Dr. ir. Pieter van Mierlo

Master's dissertation submitted in order to obtain the academic degree of
Master of Science in Biomedical Engineering

Department of Electronics and Information Systems
Chairman: Prof. dr. ir. Rik Van de Walle

Vakgroep Inwendige ziekten
Chairman: Prof. dr. Guy Joos

Faculty of Engineering and Architecture
Academic year 2014-2015

UNIVERSITEIT GENT

Ghent, June 2015

Simon Wostyn

Preface

This master thesis is a final milestone in my five-year journey of engineering studies. Although the road was bumpy at times, it was a wonderful experience. Therefore, I'd like to thank some people who supported me over the last five years and during this master thesis.

First, I would like to thank ir. Willeke Staljanssens for her superb guidance. She provided motivation when needed and help when asked. I would also like to thank dr. ir. Pieter van Mierlo for helpful insights in technical issues and useful feedback.

Next, I would like to thank my promoters prof. dr. Stefaan Vandenberghe and prof. Kristl Vonck. They provided me the opportunity to do my research in the wondrous neuroscience field.

Writing this master thesis was intense and I therefore would like to express my sincerest gratitude to all of my close friends and in particular to Glenn and Tim for their mental support and relaxing table tennis matches.

A very special 'thank you' goes to Valérie for her everlasting support. She is the most amazing person I know. I hope that our time in Lausanne was only the beginning. You make me a better person.

Lastly, I would like to thank my family and especially my brother and parents. Their ever-present warmth, many encouragements and unconditional faith mean the world to me.

Simon Wostyn
Ghent, June 2015

"The core of mans' spirit comes from new experiences.
I don't want to know what time it is.
I don't want to know what day it is or where I am.
None of that matters.
I now walk into the wild."

Christopher McCandless (Alexander Supertramp), May 1992

The effect of vagus nerve stimulation on the brain of epilepsy patients

Simon Wostyn

Supervisors
prof. dr. Stefaan Vandenberghe
prof. Kristl Vonck

Counsellors
ir. Willeke Staljanssens
dr. ir. Pieter van Mierlo

Master's dissertation submitted in order to obtain the academic degree of
Master of Science in Biomedical Engineering
Faculty of Engineering and Architecture
Ghent University
Academic year 2014-2015

Department of Electronics and Information Systems
Chairman: prof. dr. ir. Rik Van de Walle

Vakgroep Inwendige ziekten
Chairman: prof. dr. Guy Joos

Abstract

The mechanism of action (MOA) of vagus nerve stimulation (VNS) is yet to be elucidated. To that end, the effect of VNS on the brain of epilepsy patients is studied and possible biomarkers for VNS efficacy are identified. Both when VNS is On and Off, the brain of responders (>50% seizure frequency reduction) is compared to the brain of non-responders (<50% seizure frequency reduction) at three levels: the sensor level, the source level and the brain connectivity level. At the sensor level, several differences are found in P300 amplitude between responders (R) and non-responders (NR). Increase in P300 amplitude for R only is present in literature and confirmed in this research with the extension of significant decrease in P300 amplitude for NR. Some of these results can be used as biomarkers for VNS efficacy with higher accuracy than features reported in literature to date, pointing to one of the following hypotheses: (1) P300 features recorded in non-midline electrodes are better P300 biomarkers for VNS efficacy, and (2) VNS-dependent brain signals other than P300 can be used as biomarkers for VNS efficacy with higher accuracy. At source level and brain connectivity level, the activity of the limbic system, insula, frontal orbital lobe and temporal structures is found to be highly dependent on VNS and patient group. The importance of the insular and limbic area in the brain network is found to be altered between R and NR due to VNS. Therefore, the results of this research point to a key role for the limbic and temporal area in the MOA of VNS.

Keywords

Epilepsy, VNS, P300, ESI, effective connectivity, graph theory

The effect of vagus nerve stimulation on the brain of epilepsy patients

Simon Wostyn

Supervisors: prof. dr. Stefaan Vandenberghe, prof. Kristl Vonck
Counsellors: dr. ir. Pieter van Mierlo, ir. Willeke Staljanssens

Abstract **The mechanism of action (MOA) of vagus nerve stimulation (VNS) is yet to be elucidated. To that end, the effects of VNS on the brain of epilepsy patients are studied and possible biomarkers for VNS efficacy are identified. Both when VNS is On and Off, the brain of responders (>50% seizure frequency reduction) is compared to the brain of non-responders (<50% seizure frequency reduction) at three levels: the sensor level, the source level and the brain connectivity level. In the sensor level, several differences are found in P300 amplitude between responders (R) and non-responders (NR). Increase in P300 amplitude for R only is present in literature and confirmed in this research with the extension of significant decrease in P300 amplitude for NR. Some of these results can be used as biomarker for VNS efficacy with higher accuracy than features reported in literature to date, pointing to one of the following hypotheses: (1) P300 features recorded in non-midline electrodes are better P300 biomarkers for VNS efficacy, and (2) VNS-dependent brain signals other than P300 can be used as biomarkers for VNS efficacy with higher accuracy. At source level and brain connectivity level, the activity of the limbic system, insula, frontal orbital lobe and temporal structures is found to be highly dependent on VNS and patient group. The importance of the insular and limbic area in the brain network is found to be altered between R and NR due to VNS. Therefore, the results of this research point to a key role for the limbic and temporal area in the MOA of VNS.**

Keywords **Epilepsy, VNS, P300, ESI, effective connectivity, graph theory**

I. Introduction

Epilepsy is a neurological disorder characterized by unprovoked, recurrent seizures and affects 50 million people worldwide [1]. Anti-epileptic drugs can adequately help about 70% of the patients. For the other 30%, the refractory epilepsy patients, resective surgery or neuromodulation are considered [2]. Here, focus is on VNS and its effects on the brain of epilepsy patients. Although several studies and clinical practice confirm the efficacy and safety of VNS as epilepsy treatment, little is known on the cause of the anti-epileptic effect; the MOA of VNS is yet to be elucidated. Currently, about 1/3 of the patients that undergo a VNS implantation are 'responders' (R), indicating seizure frequency reduction of over 50%. Thus, 2/3 of the patients, the 'non-responders' (NR), obtain a seizure frequency of less than 50% [2]. Biomarkers to assess the VNS efficacy pre-operatively would be highly valuable and could reduce the number of superfluous and risky VNS implantations. To that end, the MOA is studied by identifying differences between the brain of R and NR with respect to VNS. Possible biomarkers for the VNS efficacy are analyzed and discussed.

Over the last 20 years, research indicates an important role for the locus coeruleus – norepinephrine (LC-NE) system in the anti-epileptic effect of VNS [3], [4]. The activity of this system is assessed indirectly via the P300 amplitude of the auditory Event-Related Potential (ERP) [5]. Interesting features of the P300 wave are discussed regarding their potential to estimate VNS efficacy and thus to separate R from NR based on the value of a certain feature. These analyses are further referred to as the sensor level. Based on the recorded EEG, active regions in the brain can be estimated, which is further referred to as the source level. Effective brain connectivity deals with the interconnections between active brain regions. By representing the brain network as a graph, specific measures can identify key regions in the overall brain network. This last part is further referred to as the brain connectivity level.

II. Methods

ERP and auditory oddball task - In this research, the P300 component of the ERP is used, which is registered by recording an EEG during an auditory oddball experiment. During such an experiment, patients press a button upon hearing a target tone (low frequency) and should not press the button upon hearing a standard tone (high frequency).

Patients - Data of twenty epilepsy patients was recorded for both VNS On and Off by De Taeye et al. [6] by means of a scalp video-electroencephalogram in the Reference Center for Refractory Epilepsy, Ghent University, Ghent, Belgium. Patients were classified based on the reduction in mean monthly seizure frequency as being either R (>50% reduction) or NR (≤50% reduction). This resulted in 10 R and 10 NR. All of the included patients had been implanted chronically with a VNS device (Cyberonics, Houston, TX, USA). No significant differences in stimulation parameters were present between R and NR. More details on the patients and stimulation parameters can

S. Wostyn is a master student in the research group on Medical Imaging and Signal Processing (MEDISIP), Ghent University (UGent), Ghent, Belgium. E-mail: Simon.Wostyn@UGent.be

be found in the original research by De Taeye et al. [6].

Electrophysiological recordings - A Micromed System Plus (Micromed, Mogliano, Italy) in combination with Ag/AgCl electrodes was used to record the electroencephalogram (EEG) at 60 standard locations according to the extended International 10-20 System using an electrode cap (WaveGuard EEG cap system, Eemagine, Berlin, Germany). The online reference electrode and the ground electrode were placed at electrode locations CPz and AFz respectively. Ocular, cardiac and VNS artifacts were measured by respectively a vertical electrooculogram (EOG), an electrocardiogram (ECG) and two additional electrodes in the neck. The EEG, EOG, ECG and VNS signals were digitized online using a sampling frequency of 1024 Hz, antialiasing filter of 250 Hz, gain of 50 dB and a resolution of 16 bits.

Pre-processing – The data was filtered by a 50 Hz notch filter and a band-pass filter (0.1-30 Hz) with slope of 12 dB/Oct and then downsampled to 256 Hz. Artifacts were corrected by EOG, ECG and VNS signal measurements. The data was re-referenced to the average of the recorded EEG channels.

Epoching and averaging - The EEG was split into epochs from 200 ms pre-stimulus to 1000 ms post-stimulus, which were baseline corrected on the 200 ms pre-stimulus interval. To increase the signal-to-noise ratio, epochs were averaged, resulting in two average epochs for each patient and each condition: a non-task-related standard-stimulus epoch and a task-related target-stimulus epoch. To isolate the P300 component, a target-standard difference waveform is calculated. Sensor and source level analyses use this difference waveform.

P300 features - The peak latency in the P300 wave was determined in the 300-900 ms post-stimulus interval at the parietal midline electrode Pz. At this latency, the amplitude of the P300 wave in all EEG channels was extracted. These features are used to perform statistical analyses at the sensor level. Data in this research is analyzed by a mixed-model ANOVA with one between-subjects factor (group or R vs. NR) and one within-subjects factor (condition or VNS On vs. Off). Post-hoc two-tailed independent samples t-tests for the factor group and post-hoc two-tailed paired samples t-tests for the factor condition are used. Cross-validation allows estimating how accurate an unknown patient can be classified as being either R or NR based on a certain feature. Combining the results of 10-fold cross-validation in a binomial distribution allows calculating mean and standard deviation for the cross-validation accuracy. Both single-channel and two-channel features are used.

Electrical source imaging (ESI) – ESI was performed from the EEG channel amplitudes in the target-standard difference waveform in an 80 ms interval around the P300 peak using statistical parametric software (SPM, Wellcome Trust Centre for Neuroimaging, London, Great Britain). The head models, used for ESI, were patient-specific for 14 patients (5-layered segmentation based on individual MRI images: scalp, skull, CSF, gray matter, white matter). For 6 patients a template head model (SPM's 4-layered T1 template) was used because their MRI images were too poor. A multiple sparse volumetric priors algorithm based on region growing in gray matter was used, which was developed by Strobbe et al. in the Medical Imaging and Signal Processing (MEDISIP) research group, Ghent University, Ghent, Belgium [7]. Gridpoints in the distributed source model are 3 mm apart. Source priors were grown in the gray matter and are volumetric bell-shaped. FWHM depends on the maximum distance r to a seed point and smoothing σ. The maximum distance r was chosen to be 7 mm and the smoothing σ was 0.7. The number of patches used as prior was 512. To compare activity between R vs. NR and VNS On vs. Off, all activity was projected (warped) onto the template head model using SPM. A flexible factorial design for the brain activity was performed using a 2nd-level analysis in SPM.

Brain connectivity - The Automated Anatomical Labeling (AAL) template was used to define 27 regions of interest (ROI) in the brain. These were chosen as the second-to-last level of regional split in the AAL template [8]. ESI was performed at each sample of a 9 s interval in the pre-processed EEG channels. This interval was chosen to include both standard and trigger stimuli. All activity was warped to the template model. Dipole activity is linked to the appropriate brain region using the AAL toolbox for Matlab (Groupe d'Imagerie Neurofonctionnelle, Bordeaux, France). Performing a Single Value Decomposition (SVD) analysis for the dipole time series in each ROI with preservation of the first component extracted a single activity time series for each brain region or ROI. Effective connectivity measures iADTF, iAPDC, ffADTF and ffAPDC were used to calculate connection strengths between the ROIs. A model order of 10, a Kalman smoother with value 100 and an update coefficient of 0.001 were used. More information on these effective connectivity measures and their implementation is given in [9]. The effective connectivity analysis was performed in 5 frequency bands: δ, θ, α, β and γ or 0-4 Hz, 4-8 Hz, 8-16 Hz, 16-32 Hz and 32-64 Hz. Time-averages and standard deviations of the time-dependent connection strengths were calculated. Mixed model ANOVA and post-hoc t-tests were performed. Bonferroni (family wise error rate of 0.05) and Benjamini-Hochberg (false discovery rate of 0.1 and significance level of 0.05) multiple comparison corrections were applied to the post-hoc t-test results. The whole-brain network was analyzed by calculating the betweenness centrality of the 27 ROIs defined in the previous section, which are used as nodes in a graph. Betweenness centrality indicates

the importance of a node in the network. iADTF, iAPDC, ffADTF and ffAPDC mean connection strengths were used as edge weights. Betweenness centrality is calculated for each node, for each effective connectivity measure and in each frequency band. Mixed-model ANOVA and post-hoc t-tests identified differences between groups and conditions.

III. Results

Sensor level - No significant main effect of group, condition or interaction effect was found for the P300 latency. No significant main effect of condition was found for the P300 amplitude in any of the EEG channels, but 23 EEG channels show a significant main effect of group (left panel of Figure 1).

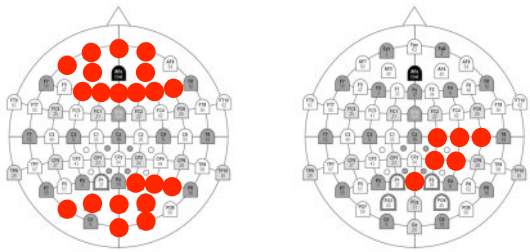

Figure 1: Red dots indicate the EEG channels that exhibit a significant main effect of group (left) and a significant interaction effect (right) for the P300 amplitude.

Six EEG channels (right panel of Figure 1) show a significant interaction effect, namely CP2 (p=0.004), C2 (p=0.017), C4 (p=0.006), Pz (p=0.034), C6 (p=0.016) and CP4 (p=0.012). For these channels the P300 amplitude is larger for NR than for R and when VNS is switched On, the P300 amplitude increases for R while it decreases for NR.

Post-hoc t-tests reveal that for VNS Off 15 EEG channels and for VNS On 20 EEG channels show a significant difference between R vs. NR. From the significant interactions, channels C4 (p=0.0079) and C6 (p=0.023) display a significant difference between VNS Off and On for NR. Channels CP2 (p=0.009) and Pz (p=0.014) display a significant difference between VNS Off and On for R. The relative change in P300 amplitude is (On-Off/On) exhibits a significant difference (p=0.014) between R and NR.

Cross-validation showed that for single-channel features when VNS is Off, CP4 and CP2 perform best in classifying an unknown subject as being either R or NR. The obtained accuracy is 72.22% or 13 out of 18 patients (two patients were not used due to errors in the data). For VNS On, channels Oz and F2 obtain an accuracy of 83.33%. The accuracy when using the relative P300 amplitude change in the Pz channel is 61.11%. Using two features simultaneously can result in accuracies up to 88.89%. The sum or product of the P300 amplitudes in two EEG channels, results in accuracies up to 94.44%, e.g. for the sum or product of the P300 amplitudes of channel CP2 (Off) and channel PO5 (On).

Source level - Using ESI, the brain activity of all patients was estimated. Several brain areas are significantly more active for R than for NR independent of VNS On or Off. These areas are the right hippocampus (p=0.059, 3.7 cm^3), the left hippocampus and amygdala (p=0.054, 1.1 cm^3) and the anterior cingulate cortex (p=0.094, 1.6 cm^3). The indicated volumes represent the size of the significant zones. For the left hippocampus and amygdala (p=0.007, 12.3 cm^3), the right and middle cingulate cortex (p=0.022, 8 cm^3) and the right hippocampus and amygdala (p=0.078, 1.6 cm^3) the activity is larger for NR than for R independent of VNS On or Off. Activity is larger when VNS is Off than when VNS is On in the right hippocampus and amygdala (p=0.076, 1.4 cm^3), the right precuneus (p=0.046, 5.2 cm^3) and the left hippocampus and amygdala (p=0.056, 1.1 cm^3) independent of R or NR. Activity is larger when VNS is On than when VNS is Off in the right superior frontal gyrus (p=0.053, 1.2 cm^3), the left hippocampus (p=0.058, 3.3 cm^3) and the right calcarine gyrus (p=0.041, 4.3 cm^3). The difference in activity between R and NR in the right insula (p=0.091, 0.2 cm^3), the left superior parietal lobe (p=0.067, 4.5 cm^3) and the left frontal orbital lobe (p=0.035, 18 cm^3) depends significantly on whether VNS was switched On or Off.

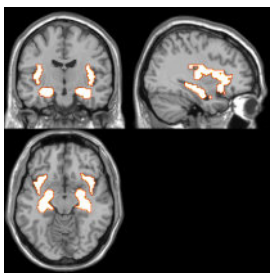

Figure 2: The activity of the indicated brain regions is significantly altered due to VNS between R and NR and between VNS Off and On. These regions include the hippocampus, amygdala and insula and are highlighted bilaterally.

From these results, it is clear that the activity in the hippocampus, amygdala and insula is highly dependent on whether the patient is R or NR and whether VNS was On or Off. These brain regions are shown in Figure 2.

Brain connectivity - No significant differences in connection strength between the 27 ROIs are found after Bonferroni correction (family wise error rate of 0.05). Benjamini-Hochberg multiple comparison correction (false discovery rate of 0.1 and significance level of 0.05) delivers significant results for both mean and standard deviation. For the mean connection strength, significant differences are found for R in the connection from the occipital lobe to the frontal lobe dependent on VNS. For VNS On, 312 significant features in 50 different connections are found between R and NR for several frequency bands and measures. These are situated over the entire brain

but mainly in the right temporal lobe, left occipital lobe and the right frontal lobe. For the standard deviation, the autospectra of the right limbic lobe and the right temporal lobe are significantly different in NR between VNS switched On and Off. For VNS On, 295 features show significant differences in 47 different connections for several frequency bands and measures between R and NR. These are mainly situated in the central gyri, the right temporal lobe and the left insula.

Using betweenness centrality, mixed-model ANOVAs and post-hoc t-tests, the right insula is found to increase in importance in the whole-brain network for R when VNS is switched On. This effect is observed in the τ–frequency band. In the γ–frequency band, the importance of the right limbic lobe is significantly larger for R than for NR when VNS is On. These regions are shown in Figure 3.

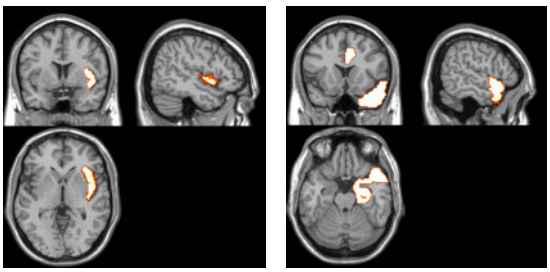

Figure 3: Significantly altered brain regions in the whole-brain network due to VNS. The right insula (left) increases in importance for R when VNS is switched On. The right limbic lobe (right) is more important in R than in NR for VNS On.

IV. Discussion

Sensor level - No differences in P300 latency were found between R vs. NR and VNS Off vs. On. This is in agreement with other research [6], [10]. In many EEG channels, the P300 amplitude was found to be larger for NR than for R, which is consistent with the reported values by De Taeye et al. [6] and Neuhaus et al. for VNS Off [11]. This result was significant in 23 EEG channels and these are situated both frontally (possibly linked to the P3a wave) and parietally (possible linked to P3b) as shown in the left panel of Figure 1. The non-significant result for the Pz channel is consistent with De Taeye et al. [6]. The Fz channel indicates a larger P300 amplitude for NR than for R in this research, which is inconsistent with Neuhaus et al.[11]. However, in that research, the P300 amplitude in the Fz channel was detected at the moment of peak in the Fz, while in this research it was detected at the moment of peak in the Pz channel, making the comparison difficult. To the knowledge of the author, no results are present in previous research in which the P300 amplitude was analyzed between R and NR in non-midline electrodes. The result that significant differences between R vs. NR are found in other EEG channels than Pz, Cz and Fz is therefore novel.

At the moment of P300 wave, many brain regions are thought to be processing information from the stimulus. Therefore, one should be watchful that significant results recorded in other than centroparietal regions could also be due to activity of other brain areas. Especially the six EEG channels showing significant interaction between group and condition are situated towards right parietal and temporal regions (right panel of Figure 1). A possible explanation could be the VNS-dependent limbic system activity [12], [13]. But, the origin of the P3b wave is thought to be situated more temporoparietally as well, meaning that the results could also be due to the P3b wave [14]. Further research should clarify these results. The P300 amplitude was found to increase significantly in channels Pz and CP2 for R only. This result is consistent with De Taeye et al.[6] and Neuhaus et al. [11]. Channels C4 and C6 show a significant decrease in P300 amplitude for NR only. The result that VNS induces not only P300 amplitude changes for R but also specific changes for NR is interesting and could lead to more effective separation of R from NR. The relative P300 amplitude increase was significant for channel Pz, a result consistent with De Taeye et al. [6]. The results of P300 increase for R and P300 decrease for NR support the hypothesis that VNS activates the LC-NE system and that this activation is critically linked to the anti-epileptic effect of VNS. This proposes the amount of NE release in the brain as biomarker for VNS efficacy, as supported in literature [3], [4], [15].

The larger P300 amplitude for NR than for R is specifically found in the P300 wave, showing a key role for the LC-NE system in the difference between these two groups. The inhibitory signaling as a result of the activation of the LC-NE system is suggested to be a key anti-epileptic actor since it is thought to arrest and cancel the spatial spread of seizures, which is nicely linked to the better VNS outcome for R, since an increase in P300 amplitude is observed upon VNS being switched On in R only [3].

The strength of this research is the use of cross-validation to indicate the potential of P300 features to classify unknown patients as R or NR. This is not the case for logistic regression analyses or ROC curves, which are used in other research [6]. For VNS Off, channels CP4 and CP2 perform best and obtain an estimated accuracy of 72%. For VNS On, channels Oz an F2 obtain accuracies of 83%, which is relatively high. De Taeye et al. used the relative P300 amplitude increase in the Pz channel as a biomarker for VNS efficacy [6]. However, using cross-validation in this research, it was found that this feature only obtains 61% classification accuracy. This is an important result and could lead to shifting the focus of future research in identifying clinically applicable predictive biomarkers for VNS efficacy. It is important to be cautious about these results, because it is not clear whether they originate from the P300 wave or from other VNS-dependent brain

signals. Future research should provide a clearer insight. Two-channel features are either two features used simultaneously or combined in a new single feature. Two features simultaneously results in accuracies of 89% for several features. Using the sum of the P300 amplitudes in two EEG channels obtains accuracies as high as for the simultaneous use of two features (89%) and summing the P300 amplitudes of channels CP2 for VNS Off and PO5 for VNS On even leads to an estimated accuracy of 94%. To the knowledge of the author, these results for cross-validation are not present in other research.

The novel results for cross-validation indicate intriguing possibilities to find biomarkers for clinical efficacy of VNS treatment. However, these results also point to the main drawback of this research. One of the main objectives of the research was to identify predictive biomarkers to be used before VNS surgery. Therefore, predictive biomarkers should be identified in pre-operative recordings. All data in this research was recorded in patients that underwent VNS surgery and received at least 18 months of VNS therapy. It is attempted to overcome this problem by recording ERPs of patients when VNS was switched Off. However, the anti-epileptic effects of VNS are present during Off-time as well [16]. Results shown in this research are thus poor indicators of differences between R and NR pre-operatively and thus have little predictive value in clinical practice. The results at sensor level remain valuable since they indicate that P300 features, previously thought to be good biomarkers for VNS efficacy, are out-performed by other features. These results can point to one or both of the following hypotheses: (1) P300 features recorded in non-midline electrodes are better P300 biomarkers for VNS efficacy, and (2) VNS-dependent brain signals other than P300 can be used as biomarkers for VNS efficacy with higher accuracy.

Source level - Several brain regions are found to be significantly influenced by VNS. The main result consistent with other research is the diminished activity of the limbic system (hippocampus and amygdala) [12], [13], [17]. Also the influence of VNS on the activity of the insular region and frontal orbital lobe is interesting and can be linked to the reported VNS-dependent changes in activity in other research [18], [19].

Brain connectivity - For R, differences are found in the mean connection strength from occipital to frontal lobe when VNS is On vs. Off. For VNS On, many mean connection strengths show a significant difference between R and NR. These connections mainly involve the right temporal lobe, the left occipital lobe and the right frontal lobe. They indicate that VNS could have an effect on the whole brain.

Analyzing the standard deviation of the time-dependent connection strengths, for NR, the autospectra for the right limbic lobe and right temporal lobe are significantly different for VNS On vs. Off. This again indicates an effect of VNS on the activity and connectivity with and within the right temporal lobe and limbic lobe, as was also discussed for source and sensor level. For VNS On, the standard deviation is significantly different between R and NR in connections situated in the central gyri, the right temporal lobe and the left insula. The strength of this research is to analyze connectivity between activity time series of brain regions and not between EEG electrode potentials, as is often done in research [20]. This approach is interesting because it can provide insight in the involved brain areas and allows easier clinical and physiological interpretation. The presence of the temporal area with inclusion of the limbic system and insula is undeniable in this research and presented by others as well [21], [22].

Using betweenness centrality in the graph representation of the brain network, the right insula was found to be of higher importance in the brain network of R when VNS was switched On than when VNS was Off. This result was present only in the θ-band. The θ-band is found to be crucially involved in epileptic brain alterations [23]. When VNS is switched On, the right limbic lobe was found to be of higher importance in the γ-band in R than in NR. For both the right insula and limbic lobe, the relative importance increases when VNS is switched On for R while it decreases for NR.

In research on the brain network for epilepsy patients, many inconsistencies are present, but a main conclusion is that a shift towards a less efficient organization increases the epilepsy burden [24]. Fraschini et al. [20] found this result when comparing R and NR for VNS Off and On. They computed a minimum spanning tree to characterize VNS-induced alterations in the network topology. In the research presented here, the right insula and limbic lobe increase in importance in R when VNS is switched On while it decreases for NR. Also, these nodes are relatively more important in R than in NR. It is possible that these nodes perform a hub-like function and therefore can relay information more efficient to more nodes to create a more integrated network, consistent with Fraschini et al. [20]. They also showed an increased minimum spanning tree hierarchy in R only, which indicates a decreased overloading of central nodes, inconsistent with results in this research. Fraschini et al., however, used EEG electrodes as nodes whereas in this research brain areas were used. Thus, comparison between this research and Fraschini et al. is not trivial. Importantly, again the insular and limbic area in the brain seem to be critically involved in the differences between R vs. NR and VNS On vs. Off. This result is consistent with the conclusions in the source level analysis and the effective connectivity results.

Limitations - The limited amount of patients and the absence of pre-operative recordings reduce the clinical applicability of the results. P300 amplitudes were extracted in all EEG channels at the moment of peak in the Pz channel and not in each channel

separately. Differences between P3a and P3b should be incorporated. Warping the head models to the template head models was performed accurately, but the anatomically defined ROIs on the template head model do not perfectly delineate the same brain regions in the individual head models. Using 27 large ROIs limits the anatomical accuracy of the results. Due to computational issues in the ESI, EEG signals of 9s were used, which is short compared to the recordings of +10 min and could possibly generalize the results incorrectly. It is possible that differences in the anti-epileptic drugs regimes altered the brain functioning in patients.

V. Conclusion

The effects of VNS on the brain of epilepsy patients were explored at three levels: sensor level, source level and brain connectivity level. Possible biomarkers for pre-operative assessment of the VNS efficacy are analyzed and discussed.

The increase in P300 amplitude for R only is reported in literature and confirmed in this research with the extension of finding a significant decrease in P300 amplitude for NR as well. Results indicate that treating the P3a and P3b components of the P300 wave separately could be valuable. Cross-validation revealed that several features in the ERP have a large potential to estimate VNS efficacy of an unknown patient with higher accuracy than the P300 amplitude recorded from the midline electrodes, which is proposed in literature. Results point to one or both of the following hypotheses: (1) P300 features recorded in non-midline electrodes are better P300 biomarkers for VNS efficacy, and (2) VNS-dependent brain signals other than P300 can be used as biomarkers for VNS efficacy with higher accuracy. However interesting, the reported results have little predictive value due to the absence of pre-operative ERP recordings.

Several brain regions are significantly influenced by VNS treatment, including the limbic system, insula, frontal orbital lobe and several temporal structures. These results are consistent with the VNS mediated activity in limbic and temporal lobe structures presented in literature. Analyzing the brain connectivity and whole-brain network identified shifts in the brain functioning between R and NR due to VNS. The importance of the insular and limbic area in brain functioning seems to be altered between R and NR. Future research should elaborate on unraveling the role of these structures in the anti-epileptic effect of VNS. Consistent with literature, analyzing the epileptic brain by connectivity and graph theory measures proves to be useful to find insights in the mechanism of action of VNS.

References

[1]"WHO | Epilepsy," *WHO*. [Online]. Available: http://www.who.int/topics/epilepsy/en/. [Accessed: 15-Apr-2015].

[2]F. A. Al-Otaibi, C. Hamani, and A. M. Lozano, "Neuromodulation in epilepsy," *Neurosurgery*, vol. 69, no. 4, pp. 957–979; discussion 979, Oct. 2011.

[3]F. Fornai, R. Ruffoli, F. S. Giorgi, and A. Paparelli, "The role of locus coeruleus in the antiepileptic activity induced by vagus nerve stimulation.(Report)," *Eur. J. Neurosci.*, vol. 33, no. 12, 2011.

[4]R. Raedt, R. Clinckers, L. Mollet, K. Vonck, el Tahry, T. Wyckhuys, de Herdt, E. Carrette, W. J. Wadman, Y. Michotte, I. Smolders, P. Boon, and A. Meurs, "Increased hippocampal noradrenaline is a biomarker for efficacy of vagus nerve stimulation in a limbic seizure model.," *J. Neurochem.*, vol. 117, 2011.

[5]S. Nieuwenhuis, G. Aston - Jones, and J. D. Cohen, "Decision Making, the P3, and the Locus Coeruleus--Norepinephrine System," *Psychol. Bull.*, vol. 131, no. 4, 2006.

[6]L. De Taeye, K. Vonck, M. van Bochove, P. Boon, D. Van Roost, L. Mollet, A. Meurs, V. De Herdt, E. Carrette, I. Dauwe, S. Gadeyne, P. van Mierlo, T. Verguts, and R. Raedt, "The P3 event-related potential is a biomarker for the efficacy of vagus nerve stimulation in patients with epilepsy," *Neurother. J. Am. Soc. Exp. Neurother.*, vol. 11, no. 3, pp. 612–622, Jul. 2014.

[7]G. Strobbe, P. van Mierlo, M. De Vos, B. Mijović, H. Hallez, S. Van Huffel, J. D. López, and S. Vandenberghe, "Multiple sparse volumetric priors for distributed EEG source reconstruction," *NeuroImage*, vol. 100, pp. 715–724, Oct. 2014.

[8]N. Tzourio-Mazoyer, B. Landeau, D. Papathanassiou, F. Crivello, O. Etard, N. Delcroix, B. Mazoyer, and M. Joliot, "Automated anatomical labeling of activations in SPM using a macroscopic anatomical parcellation of the MNI MRI single-subject brain," *Neuroimage*, vol. 15, no. 1, pp. 273–289, 2002.

[9]Pieter van Mierlo, "Epileptic focus localization using functional brain connectivity," 2013.

[10]E. J. Hammond, B. M. Uthman, S. A. Reid, and B. J. Wilder, "Electrophysiologic Studies of Cervical Vagus Nerve Stimulation in Humans: II. Evoked Potentials," *Epilepsia*, vol. 33, no. 6, 1992.

[11]A. H. Neuhaus, A. Luborzewski, J. Rentzsch, E. L. Brakemeier, C. Opgen-Rhein, J. Gallinat, and M. Bajbouj, "P300 is enhanced in responders to vagus nerve stimulation for treatment of major depressive disorder," *J. Affect. Disord.*, vol. 100, no. 1, pp. 123–128, 2007.

[12]K. Vonck, V. De Herdt, T. Bosman, S. Dedeurwaerdere, K. Van Laere, and P. Boon, "Thalamic and limbic involvement in the mechanism of action of vagus nerve stimulation, a SPECT study," *Seizure*, vol. 17, no. 8, pp. 699–706, Dec. 2008.

[13]T. R. Henry, "Therapeutic mechanisms of vagus nerve stimulation," *Neurology*, vol. 59, no. 6 Suppl 4, pp. 3–14, 2002.

[14]T. W. Picton, "The P300 wave of the human event-related potential.," *J. Clin. Neurophysiol.*, vol. 9, no. 4, pp. 456–479, 1992.

[15]S. E. Krahl, K. B. Clark, D. C. Smith, and R. A. Browning, "Locus Coeruleus Lesions Suppress the Seizure-Attenuating Effects of Vagus Nerve Stimulation," *Epilepsia*, vol. 39, no. 7, 1998.

[16]E. Ben-Menachem, A. Hamberger, T. Hedner, E. J. Hammond, B. M. Uthman, J. Slater, T. Treig, H. Stefan, R. E. Ramsay, and J. F. Wernicke, "Effects of vagus nerve stimulation on amino acids and other metabolites in the CSF of patients with partial seizures," *Epilepsy Res.*, vol. 20, no. 3, pp. 221–227, Mar. 1995.

[17]K. Van Laere, K. Vonck, P. Boon, J. Versijpt, and R. Dierckx, "Perfusion SPECT changes after acute and chronic vagus nerve stimulation in relation to prestimulus condition and long-term clinical efficacy," *J. Nucl. Med. Off. Publ. Soc. Nucl. Med.*, vol. 43, no. 6, pp. 733–744, Jun. 2002.

[18]T. Kraus, K. Hösl, O. Kiess, A. Schanze, J. Kornhuber, and C. Forster, "BOLD fMRI deactivation of limbic and temporal brain structures and mood enhancing effect by transcutaneous vagus nerve stimulation," *J. Neural Transm.*, vol. 114, no. 11, pp. 1485–1493, Jun. 2007.

[19]C. R. Conway, Y. I. Sheline, J. T. Chibnall, M. S. George, J. W. Fletcher, and M. A. Mintun, "Cerebral blood flow changes during vagus nerve stimulation for depression," *Psychiatry Res. Neuroimaging*, vol. 146, no. 2, pp. 179–184, Mar. 2006.

[20]M. Fraschini, M. Demuru, M. Puligheddu, S. Floridia, L. Polizzi, A. Maleci, M. Bortolato, A. Hillebrand, and F. Marrosu, "The re-organization of functional brain networks in pharmaco-resistant epileptic patients who respond to VNS," *Neurosci. Lett.*, vol. 580, pp. 153–157, 19.

[21]J. Fang, P. Rong, Y. Hong, Y. Fan, J. Liu, H. Wang, G. Zhang, X. Chen, S. Shi, L. Wang, R. Liu, J. Hwang, Z. Li, J. Tao, Y. Wang, B. Zhu, and J. Kong, "Transcutaneous Vagus Nerve Stimulation Modulates Default Mode Network in Major Depressive Disorder," *Biol. Psychiatry*.

[22]F. Pittau, C. Grova, F. Moeller, F. Dubeau, and J. Gotman, "Patterns of altered functional connectivity in mesial temporal lobe epilepsy," *Epilepsia*, vol. 53, no. 6, pp. 1013–1023, Jun. 2012.

[23]L. Douw, E. van Dellen, M. de Groot, J. J. Heimans, M. Klein, C. J. Stam, and J. C. Reijneveld, "Epilepsy is related to theta band brain connectivity and network topology in brain tumor patients," *BMC Neurosci.*, vol. 11, p. 103, 2010.

[24]W. M. Otte, R. M. Dijkhuizen, M. P. A. van Meer, W. S. van der Hel, S. A. M. W. Verlinde, O. van Nieuwenhuizen, M. A. Viergever, C. J. Stam, and K. P. J. Braun, "Characterization of functional and structural integrity in experimental focal epilepsy: reduced network efficiency coincides with white matter changes," *PloS One*, vol. 7, no. 7, p. e39078, 2012.

Table of contents

List of figures

List of tables

List of acronyms

ADTF	Adaptive Directed Transfer Function
AED	Anti-Epileptic Drug
AIS	Axon Initial Segment
AP	Action Potential
APDC	Adaptive Partial Directed Coherence
AR	Autoregressive
BEM	Boundary Element Method
CI	Confidence Interval
CNS	Central Nervous System
CSF	Cerebrospinal Fluid
CT	Computed Tomography
DBS	Deep Brain Stimulation
DC	Directed Coherence
DTF	Directed Transfer Function
DTI	Diffusion Tensor Imaging
DWI	Diffusion Weighted Imaging
ECD	Equivalent Current Dipole
ECG	Electrocardiogram
ECoG	Electrocorticogram
EEG	Electroencephalogram
EOBL	End Of Battery Life
EOES	End Of Effective Stimulation
EOG	Electrooculogram
EP	Evoked Potential
EPSP	Excitatory Post-Synaptic Potential
ERP	Event-Related Potential
ESI	Electrical Source Imaging
FDA	Food and Drug Administration

FDM	Finite Difference Method
FEM	Finite Element Method
ffADTF	Full-Frequency ADTF
ffAPDC	Full-Frequency APDC
fMRI	Functional MRI
FWHM	Full-width at half maximum
GABA	γ-aminobutyric acid
Glut	Glutamate
HD EEG	High-Density EEG
iADTF	Integrated APDC
iAPDC	Integrated ADTF
IBE	International Bureau for Epilepsy
ICA	Independent Component Analysis
IED	Interictal Epileptiform Discharges
IEEG	Intracranial EEG
ILAE	International League Against Epilepsy
IPI	Initial Precipitating Insult
IPSP	Inhibitory Post-Synaptic Potential
LC	Locus Coeruleus
MEG	Magnetoencephalogram
MI	Mutual Information
MOA	Mechanism Of Action
MRI	Magnetic Resonance Imaging
NE	Norepinephrine
NIRS	Near-Infrared Spectroscopy
OR	Odds Ratio
PC	Partial Coherence
PDC	Partial Directed Coherence
PET	Positron Emission Tomography
PNS	Peripheral Nervous System
RNS	Responsive Neurostimulator
ROC	Receiving Operator Characteristic
RRE	Relative Residual Energy
SPECT	Single Photon Emission Computed Tomography
SVD	Single Value Decomposition
SVEM	Scalp-Video EEG Monitoring
tDCS	Transcranial Direct Current Stimulation

TMS	Transcranial Magnetic Stimulation
TNS	Trigeminal Nerve Stimulation
TRD	Treatment Resistant Depression
TVAR	Time-Varying AR
VNS	Vagus Nerve Stimulation
WMN	Weighted Minimum Norm

Chapter 1

Introduction

Epilepsy is a neurological disorder characterized by unprovoked, recurrent seizures. Worldwide, fifty million people are diagnosed with epilepsy making it the second most common neurological problem following cerebrovascular disorders [1]. The estimated number of new cases per year in Europe is around 300,000 [2]. In current clinical practice, around 70% of the patients can be adequately helped by anti-epileptic drugs. For the other 30%, the so-called refractory epilepsy patients, resective surgery and neuromodulation are considered [3]. Resective surgery aims to surgically remove the epileptogenic focus in the brains. However, the eligibility of a patient for surgery depends on many factors and it is a drastic decision that poses several risks. Neuromodulation can provide a solution for ineligible patients. It encompasses technology that alternates or modulates nerve activity by delivering electrical stimulation, which is typically done by using (micro)electrodes as interface with the excitable tissues. Deep Brain Stimulation (DBS) and Vagus Nerve Stimulation (VNS) are the two main neuromodulatory techniques for epilepsy. In this research, focus will be on VNS and its effects on the brain of epilepsy patients. These effects are assessed at three levels: sensor level, source level and brain connectivity level.

Although several studies and clinical practice confirm the efficacy and safety of VNS as epilepsy treatment, little is known on the cause of the anti-epileptic effect; the Mechanism of Action (MOA) of VNS is yet to be elucidated [4], [5]. Currently, about a third of the patients that undergo a VNS implantation are termed 'responders', indicating seizure frequency reduction of over 50%. Therefore, 2/3 of the patients, the non-responders, obtain a seizure frequency reduction of less than 50% [6]. It is clear that biomarkers to assess the VNS efficacy pre-operatively would be valuable and could reduce the number of superfluous and risky VNS implantations. To that end, the MOA of VNS is studied by identifying differences between the brain of responders and non-responders with respect to the electrical stimulation. Possible biomarkers for the VNS efficacy are analyzed and discussed.

Over the last 20 years, experiments indicate an important role for the locus coeruleus – norepinephrine (LC-NE) system in the anti-epileptic effect of VNS [7]. Direct assessment of the

LC-NE activity is non-trivial. Therefore, the activity is assessed indirectly via a parameter that can be measured easily and is modulated by this LC-NE activity [8]. The parameter used in this research is the P300 amplitude of the Event-Related Potential (ERP). An ERP is a voltage deflection in an electroencephalogram (EEG) after a certain sensory (e.g. visual or auditory) stimulus is given to a patient. The P300 wave is a well-known component of the ERP and the amplitude of this wave is modulated by the LC-NE activity [9]. The P300 wave can be registered by recording an EEG during an auditory oddball experiment. During such an experiment, patients press a button upon hearing a target tone (low frequency) and should not press the button upon hearing a standard tone (high frequency). This experiment was performed for 10 responders and 10 non-responders for both VNS switched Off and VNS switched On in the Reference Center for Refractory Epilepsy, Ghent University, Ghent, Belgium [8]. By doing so, the P300 amplitude can indicate differences between responders and non-responders due to the VNS stimulation in terms of LC-NE activity, which is termed the sensor level analysis. The sensor level is discussed in Chapter 4.

Based on the recorded EEG, active regions in the brain can be estimated. To do so, Electrical Source Imaging (ESI) is performed, which results in the estimation of the brain activity. Differences in the brain activity are investigated between responders vs. non-responders and VNS On vs. Off. This is the source level analysis and is discussed in Chapter 5.

Brain connectivity deals with the functional interconnections between brain regions. This connectivity can be focused on anatomical links (structural connectivity), statistical dependencies of activity (functional connectivity) or causal interactions (effective connectivity). In this research, functional and effective connectivity are investigated in terms of responders, non-responders, VNS Off and VNS On. This is done by defining Regions of Interest (ROI) in the brain and by using ESI to extract the activity time series of each ROI. These time series are analyzed using several connectivity measures. Graph theory measures can identify key regions in the overall brain network. Therefore, the brain network is represented as a graph. By using betweenness centrality as measure, the importance of several brain regions in the overall brain network is calculated [10]. Shifts in this brain network and changes in the functional and effective connections are analyzed in the brain connectivity analysis between responders and non-responders with respect to VNS stimulation. This brain connectivity level is shown in Chapter 6.

The results at the sensor level, source level and brain connectivity level are discussed in Chapter 7, where similarities and discrepancies with previous research are explored. Lastly, in Chapter 8 a final conclusion of this master thesis is given.

Chapter 2

Literature review

2.1 Introduction

This literature review recapitulates and summarizes the required biological, pathological, methodological and mathematical concepts to be able to fully comprehend the framework of the performed research. First, the anatomy, physiology, electrophysiological properties and functioning of the brain are explained. Next, the possible neuroimaging techniques are defined with emphasis on electroencephalography (EEG) and electrical source imaging (ESI). Then, epilepsy is described in different aspects and current treatment possibilities are highlighted. Subsequently, vagus nerve stimulation is explored in greater detail, followed by a description of brain connectivity as well as different mathematical considerations for connectivity calculations. Lastly, graph theory is introduced and network measures are given.

2.2 The brain

2.2.1 Brain anatomy and functioning

The brain is a vital organ in the body. It is considered the most complex of all human organs and in combination with the spinal chord it makes up the central nervous system (CNS). The brain (and in part the spinal chord) analyses and integrates sensory and motor information in order to supervise, control and coordinate human activity. The CNS is one of the main components of the nervous system, next to the peripheral nervous system (PNS) (Figure 2.1)

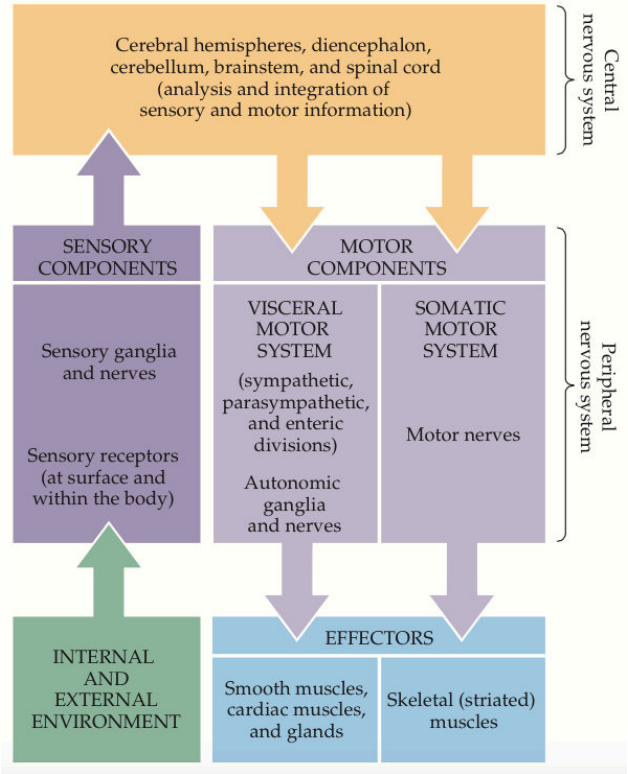

Figure 2.1: The main components of the nervous system and their functional relationships [11].

2.2.1.1 The neuron as fundamental building block

Neurons or neuronal cells are the basic functional units of any nervous system. The brain contains approximately 86 billion neurons and around the same amount non-neuronal cells (glial or supporting cells) [12]. Several varieties of neurons come and work together in so-called neural circuits, which are the primary components for integration and analysis of information. Neural systems are defined to comprise neurons and circuits in a number of discrete anatomical locations in the brain. These systems (but also neural circuits and neurons) can be classified into three categories based on their function. On the one hand there are sensory systems that acquire information about the organism and its environment. Motor systems on the other hand control and coordinate several kinds of action. Thirdly, associational systems link the sensory components to the motor components and bridge the information flow between information input and behavioral output. These associational systems also provide the framework for higher-order capabilities of the brain such as emotions, logical reasoning, attention, etc.

Although the basic cellular organization of neurons resembles that of other cells, their morphology is highly specialized for intercellular communication. Characteristic for neurons is their extensive branching (Figure 2.2). Dendrites arise from the neuronal cell body (or soma) and are the primary target to receive communication from other neurons. The dendrites themselves have many branches, which are called the dendritic processes. A second typical

branching of the neuronal cell is the axon, which is a unique extension from the neuronal cell body. The axons transfer the information integrated in the cell body towards other cells. They can vary immensely in length from up to a few mm to over 1 m. The connection between the axon and the soma is called the axon initial segment (AIS) or axon hillock. To increase information transfer, axons are electrically insulated by a myelin sheath, which is a phospholipid layer wrapped around the axon. At distinct locations along the axons, the myelination is interrupted at the so-called nodes of Ranvier.

Another characteristic aspect of the neuronal cells is the morphology of their connections with other neuronal cells. The connection between neuronal cells is called a synapse. Typically, an axon carrying information has a presynaptic terminal. The other end of the communication line is the dendrite of the neuronal cell to receive the information. Dendrites possess postsynaptic specializations to acquire information coming from the axon of the previous cell. Between the presynaptic terminal and the postsynaptic specialization there is a small zone of extracellular space (typically 50 nm wide), which is called the synaptic cleft (Figure 2.2) [11].

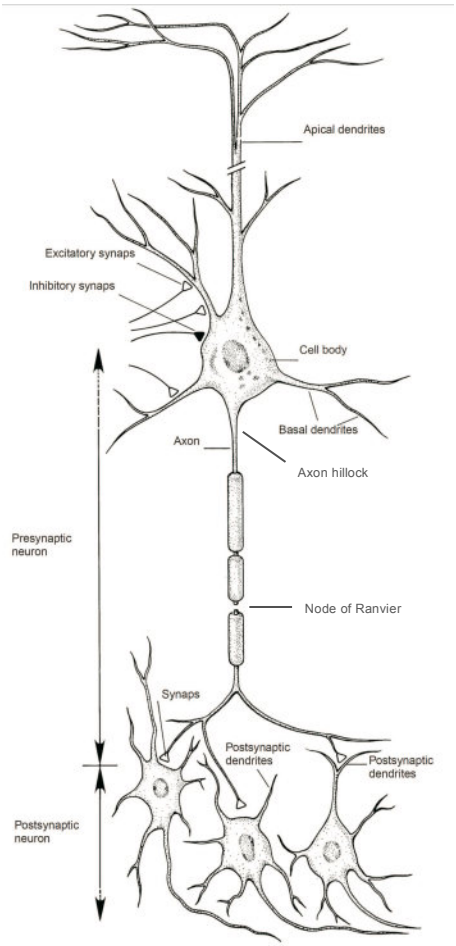

Figure 2.2: Anatomy of a neuron and the synapse as an interneuron connection. Adapted from [13].

2.2.1.2 Neuronal signaling

Internally, neurons transmit information through electrical signals. Specific ionic concentration differences between the inside and the outside of the cell govern the resting electrical properties and the so-called resting membrane potential of a neuron. The neuronal cell membrane possesses channels for sodium (Na^+) and potassium (K^+) ions. Due to the specific voltage dependent permeability of these ion channels and ion pumps, there exists a concentration difference between the inside and the outside of the nerve cell ($[Na^+]_{in}$ = 12 mM, $[Na^+]_{out}$ = 145 mM, $[K^+]_{in}$ = 150 mM, $[K^+]_{out}$ = 4 mM). The Goldman-Hodgkin-Katz equation provides the resulting resting membrane potential of the neuron of around -70 mV, meaning the inside is less positive [14], [15].

In the transmission from dendrite to soma, the conduction occurs passively. In axons, the distance that the signal needs to travel is much longer. Due to the poor electrical conductance in axons, the signal would fade away relatively fast compared to the length of the axon. Therefore, a specialized mechanism ensures the propagation of the signal along the length of the axon. This mechanism is called the action potential (AP), which is the fundamental building block for axonal signal conduction. Upon depolarization of the membrane, the membrane potential can reach a certain threshold. When this threshold is reached, the cell 'fires'. The Na^+-channels open very quickly upon depolarization allowing a massive influx of Na^+-ions into the cell, generating a fast upward burst of the membrane potential (up to approximately +60 mV, depending on the type of nerve cell). After some time (a few ms), the slower K^+-channels open, allowing outward flow of K^+-ions and at the same time the Na^+-channels close again. These changes allow the repolarization of the membrane potential to a level around the original resting membrane potential. The actual conduction of the signal occurs due to the propagation of the AP. The Na^+-ions that entered the cell spread in the axon and are able to depolarize the next part of the axon. Due to the depolarization of the next axonal part above threshold level, this part fires an AP as well. The AP generated here can then again depolarize the next part and so on. Due to this consecutive AP firing, the signal can be conducted through the entire neuronal cell without loss of signal, which would be the case for passive conduction. Myelin sheaths insulate the neuron electrically to improve the AP propagation. The mechanisms of AP generation (top) and propagation (bottom) can be seen in Figure 2.3 [11], [15].

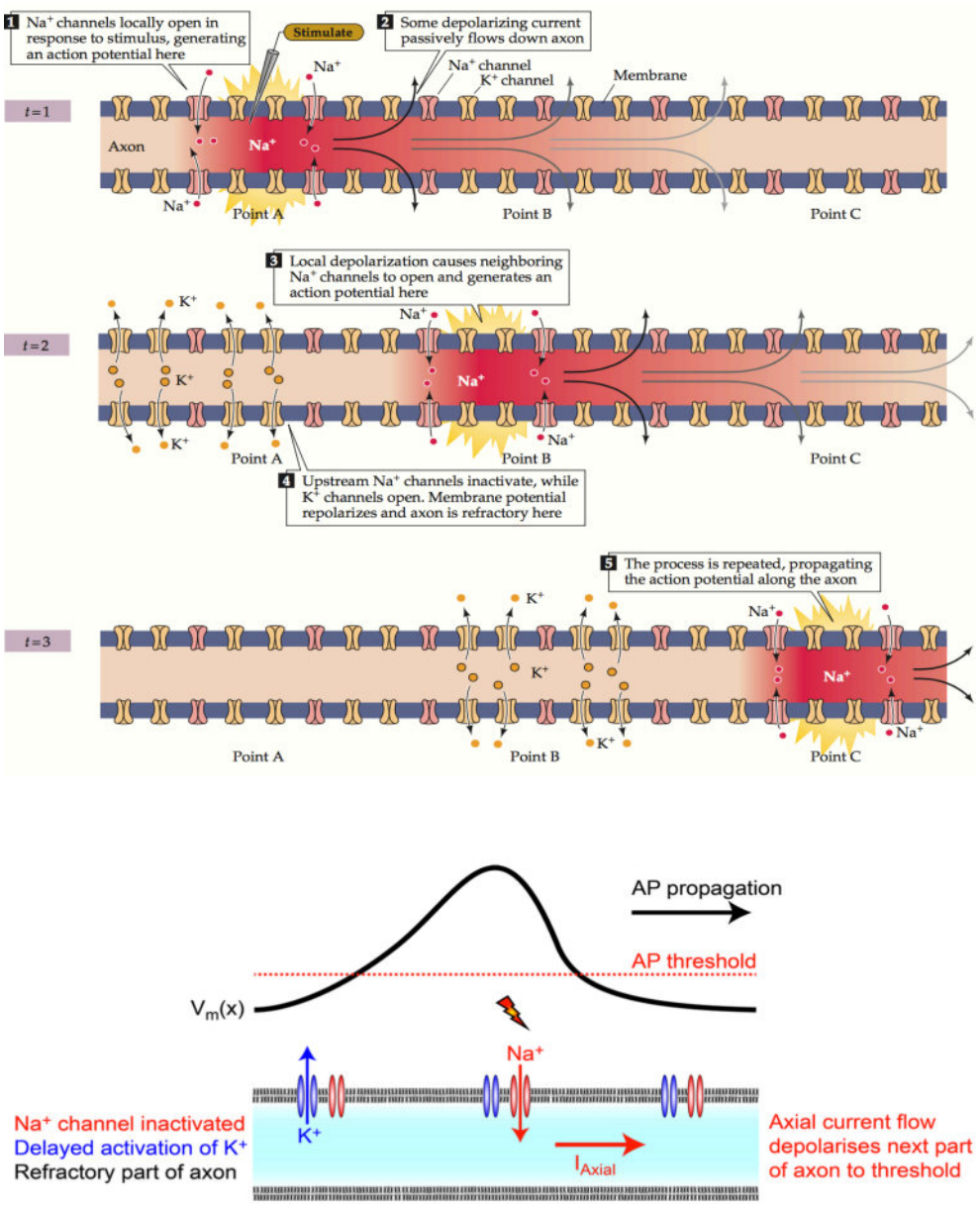

Figure 2.3: Generation (top) and propagation (bottom) of the action potential [11], [15].

In the synapse, the connection between neurons, the information transfer occurs chemically. The conversion between intraneuronal electrical signals and extraneuronal chemical signals is performed in the presynaptic terminal of the axon and the postsynaptic specialization of the dendrite. Once the AP reaches the end of the axon, it enters the presynaptic terminal and causes the opening of calcium (Ca^{2+}) channels. These channels allow the influx of Ca^{2+}-ions into the presynaptic terminal. There, these ions allow small spherical reservoirs (vesicles) to release their content, namely the chemical signaling molecules or neurotransmitters. The vesicles are refilled and replaced continuously in the presynaptic terminal. The Ca^{2+}-ions allow the vesicles to fuse with the cell membrane thereby releasing their content, the neurotransmitter molecules. A large variety of neurotransmitters has been discovered of which the most well known are glutamate (Glut), γ-aminobutyric acid (GABA), dopamine and acetylcholine. At the

postsynaptic specialization specific ligand-gated ion channels are present. These ion channels possess receptors that are highly specific for certain neurotransmitters. The most common receptors are the glutamatergic and GABAergic receptors. Upon binding of the correct ligand on these receptors, the ion channel opens and ions can flow in. Similarly as during AP generation, these ion fluxes result in membrane potential changes. In case of glutamatergic receptors and synapses, Na^+ rushes inwards causing depolarization of the cell membrane. Thus, glutamatergic synapses are excitatory since they depolarize the postsynaptic membrane potential in the direction of the AP threshold. The potential that is generated in the postsynaptic specialization is called the excitatory postsynaptic potential (EPSP). In case of opening of GABAergic channels, Cl^--ions flow into the postsynaptic specialization. Since these ions are negatively charged they cause a hyperpolarization of the cell membrane leading the membrane potential away from AP threshold. Therefore, these GABAergic synapses are inhibitory and cause inhibitory postsynaptic potentials (IPSP).

Inhibitory and excitatory synapses are the two main types of synapses present in the human brain. The dendrites of each cell receive input from many other cells, which creates multiple EPSPs and/or IPSPs in a single neuron. All these PSPs enter the soma where they are integrated. If the depolarization is large enough to reach the AP threshold, an AP will be fired at the axon hillock where the AP threshold is lowest. Upon firing of an AP, the neuronal signal is conducted through the axon. This completes the sequence in which neuronal signals are transmitted in the nervous system [16]–[19].

2.2.1.3 Brain anatomy

Macroscopically, the brain can be divided into gray and white matter. The neuronal cell bodies are situated in the gray matter while the axons make up the white matter. The lighter appearance of white matter results from the presence of the lipid content of myelin sheaths. Surrounding the brain are the scalp, skull and three meninges. The scalp is the skin on top of the skull. The meninges are membranes covering the brain. The skull is a bony structure creating a cavity for the brain and protecting it from trauma. The dura mater is the outermost membrane just below the skull; the arachnoid and the pia mater are closer to the brain with the pia mater attached to the brain surface. Furthermore, the cerebrospinal fluid (CSF) is very important for proper and long-lasting functioning of the brain. On top of that it serves as buffer to protect the brain from trauma. It flows between the pia mater and arachnoid matter and inside the ventricles. These ventricles are cavities inside the brain and they contribute to the circulation of the CSF, which delivers nutrients to and removes waste from the brain. This global organization can be seen in Figure 2.4 [13].

The brain is usually considered to have six basic parts with distinct functions: the medulla, the pons, the cerebellum, the midbrain, the diencephalon and the cerebral hemispheres. The cerebral hemispheres are connected by the corpus callosum and together they are called the

cerebrum. The medulla, pons and midbrain are referred to as the brainstem. The diencephalon together with the cerebral hemispheres is defined as the forebrain. The brainstem serves as a gateway between the forebrain and spinal chord: it relays sensory information from the spinal chord to the forebrain and sends motor commands from the forebrain to the spinal chord. It is also a key structure in the regulation of primary vital functions. The cerebellum is situated at the dorsal side of the brain and is essential in coordination and planning of movements (Figure 2.5) [11].

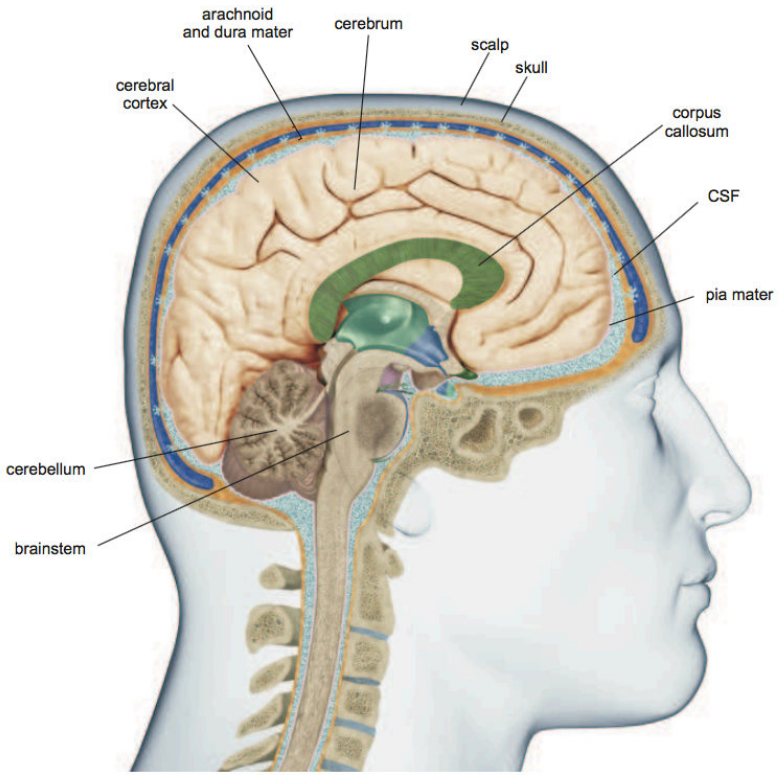

Figure 2.4: Global organization and surroundings of the brain. Adapted from [20].

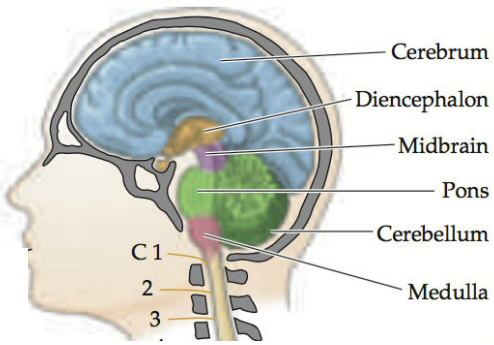

Figure 2.5: The six basic parts of the brain [11].

The brain tissue is folded to maximize its surface area. Due to these folds, characteristical crests are present, which are called gyri. Grooves that divide gyri from one another are called sulci. These gyri and sulci vary slightly from individual to individual but provide an overall division of the brain into four lobes: occipital, temporal, parietal and frontal lobe (Figure 2.6). The outer layer of the cerebrum is often called the cerebral cortex [11].

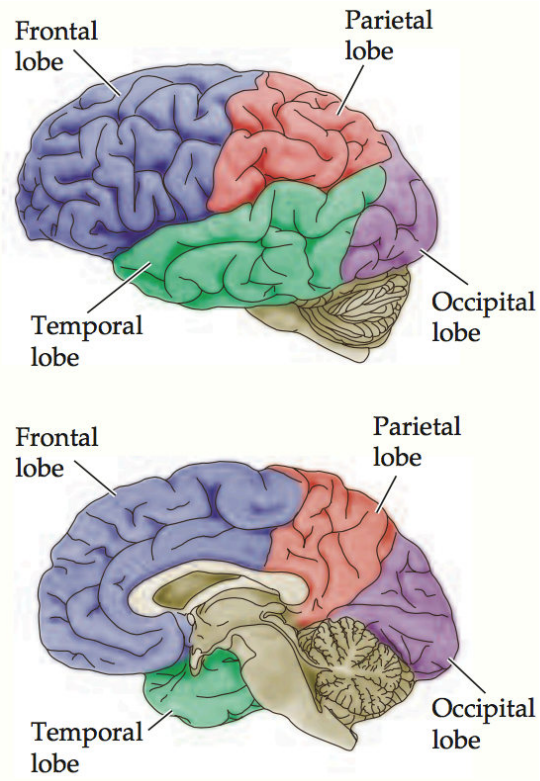

Figure 2.6: Structural anatomy of the brain with frontal, parietal, occipital and temporal lobe [11].

2.2.1.4 Brain functions

The brain cannot only be divided anatomically; also functionally the brain consists of distinct regions. The frontal lobe is important for thinking, organizing, speech production and executive function as well as performing movements via the primary motor cortex. The parietal lobe is involved in perception and spelling while the main function of the occipital lobe is vision. The temporal lobe is used for memory and listening.

Another very interesting division in terms of brain function is by means of the Brodmann areas. These areas have been identified on the cerebral cortex and perform specific functions. Different regions are distinguished by their specific cytoarchitecture and organization of cells [13].

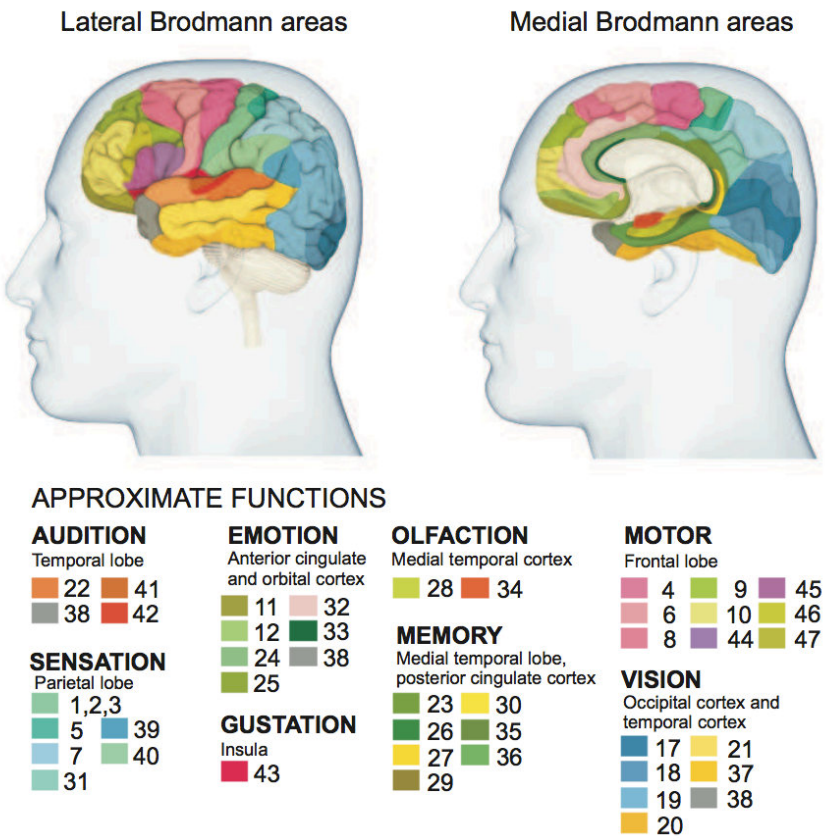

Figure 2.7: The Brodmann areas in the brain. Adapted from [20].

2.2.2 Neuroimaging and electroencephalography

2.2.2.1 Overview

In order to study the brain, one needs to be able to look (in)to the brain and the nervous system. Different modalities have been developed and they are termed 'neuroimaging' techniques (Figure 2.8). A brief overview is given of the most important modalities before electroencephalography will be explained in greater detail.

Neuroimaging techniques are often classified as being either structural or functional. Structural modalities target to visualize the anatomical structure of the brain while functional techniques are used to investigate function and activity. Examples of structural techniques are Computed Tomography (CT) and Magnetic Resonance Imaging (MRI) and important functional modalities are functional MRI (fMRI), Positron Emission Tomography (PET), Single Photon Emission Computed Tomography (SPECT), Near-Infrared Spectroscopy (NIRS), Magnetoencephalography (MEG), and Electroencephalography (EEG). Within these functional techniques, EEG and MEG measure the electrical activity of the neurons directly while other techniques such as PET and fMRI perform indirect measurements based on the increased blood

flow or metabolic activity in active neurons. Functional techniques can be used to diagnose metabolic or cognitive disorders [13], [21], [22].

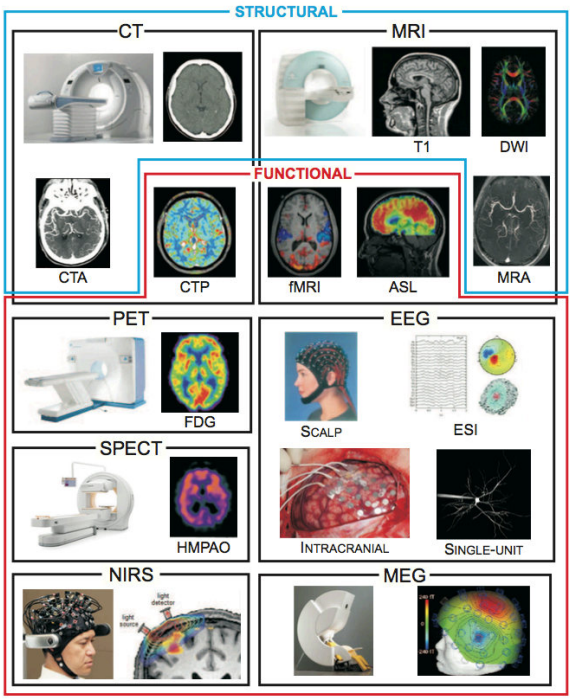

Figure 2.8: Overview of different structural and functional neuroimaging techniques [13].

Each of the techniques mentioned above has specific advantages and drawbacks. Next to general aspects such as size, cost, availability, complexity, etc., neuroimaging techniques are often discussed in terms of spatial and temporal resolution (Figure 2.9). Spatial resolution expresses the smallest spatial difference between two points that can still be resolved while time resolution indicates the necessary time interval between instances to be detected individually. In order to overcome the specific drawbacks of each technique, different methods are often combined in so-called multimodal neuroimaging [23].

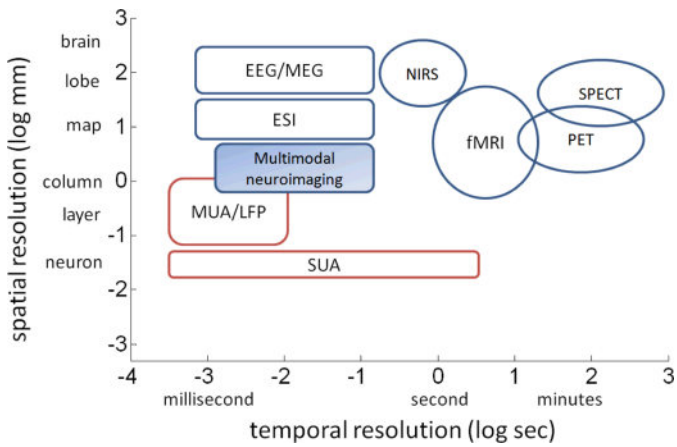

Figure 2.9: Spatial and temporal resolution of different neuroimaging techniques [23].

2.2.2.2 Electroencephalography

Electroencephalography or EEG is the oldest functional brain imaging technique. It dates back to Berger's discovery in 1929 that brain electrical activity could be recorded from electrodes placed on the scalp. It is still widely used due to very good temporal resolution (below 100 ms), which even allows acquiring real-time measurements [24].

Generators of the EEG

Currents generated by a single neuron are very small. In order to be able to pick up the electrical fields generated by the currents on the scalp, superposition of many neural currents is needed. APs are larger in amplitude then EPSPs (100 mV vs. 1 mV) but EPSPs last longer (10 ms vs. 0.1 ms). Thus, APs are much less likely to sum up. Therefore, EPSPs are thought to give rise to the underlying currents that generate the measured electrical fields on the scalp. Currents generated by single neurons are in the order of 10 fA while sources of around 10 nA are needed to be detected, meanings millions of neural currents need to fire simultaneously. On top of that, the dendrites need to be spatially aligned in order to contribute to a large overall current. In terms of brain volume, a volume of 5 mm x 5 mm x 5 mm is assumed to be able to generate a sufficiently large amount of current to be detected [25], [26].

To generate an EPSP, neurotransmitters at the apical (furthest away from the soma) dendritic postsynaptic specialization cause a large amount of positive ions to enter the nerve cell. This results in a lack of extracellular positive ions at the apical dendrites. Intracellularly, the ions flow towards the basal (close to the soma) dendrites and cell body, which is called the primary current. By depolarizing the cell body, positive ions become available extracellularly. These ions can fill the lack of positive ions apically and thereby generate an extracellular current, the secondary current. A simplified electrical model of an active neuron consists of two current monopoles: a current sink at the apical dendrites removing positive ions from the extracellular space and a current source at the cell body injecting positive ions in the extracellular space. Therefore, the electrical activity of a neuron is often represented as a current dipole (see 2.2.3.1) [26], [27].

Pyramidal neurons, which are characterized by a typical pyramidal-shaped soma, fulfill the requirements to be the generators of the EEG signals. These pyramidal cells lie perpendicular to the cortical surface and are thought to be the main generators of the EEG signal (Figure 2.10) [28], [29]. In order to reach the scalp electrodes, the pyramidal currents need to pass the 3 meninges, the CSF, the skull and the scalp. The signal is thereby attenuated and distorted resulting in EEG recordings in the order of 100 μV [13].

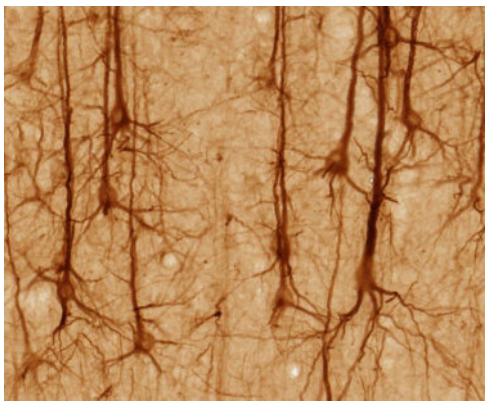

Figure 2.10: Pyramidal neurons in the cerebral cortex [30].

Recording EEG

Recording an EEG comprises measuring potential differences with scalp electrodes and plotting them in function of time. A typical measurement setup consists of electrodes with conductive media to reduce the scalp-electrode impedance, amplifiers with filters, A/D conversion and a recording device. Since the EEG is measured as potential differences between electrodes, the minimal configuration (for a so-called mono-channel EEG) consists of three electrodes: a measuring electrode, a reference electrode and a ground electrode to provide a ground for the measurement and to reduce interference. Different amounts of electrodes can be used. Internationally, the 10-20-electrode system is often used. However, to improve the spatial sampling, high-density arrays (HD EEG) are used that can consist of up to 256 measuring electrodes. The electrodes can be glued directly to the skin or incorporated in an elastic cap to ensure fast attachment and fixed configuration. Depending on the amount of electrodes, a standardized electrode placement is used, which can vary for different applications. In Figure 2.11 the 10-20-electrode configuration is shown.

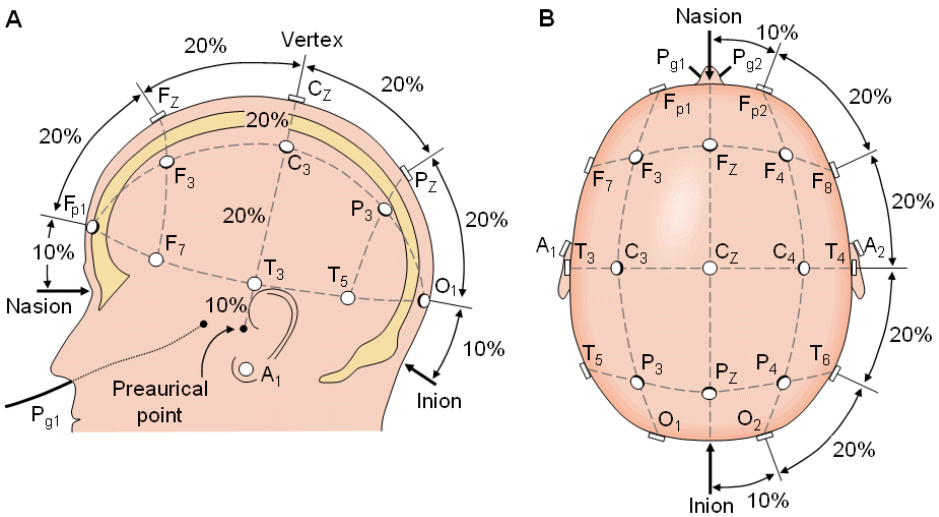

Figure 2.11: The 10-20 electrode configuration [31].

Anatomical landmarks on the human head are used to position the electrodes correctly. Depending on the number of electrodes, the spatial sampling is different, although there is a

trend to use a higher number of electrodes for better sampling. In order to identify the electrodes easily, the electrodes have specific labels consisting of a character (one or two) and a number. Frontal, temporal, parietal, occipital, and central electrodes are indicated with the labels 'F', 'T', 'P', 'O' and 'C' respectively while electrodes on the forehead and at the earlobe are labeled 'Fp' (frontal polar) and 'A' (auricular). Electrodes over the midline have a 'z' as second character. Odd numbered electrodes are situated on the left hemisphere; even numbers are used on the right hemisphere.

The amplifiers used for EEG measurements have to satisfy very specific requirements. They should provide specific amplification of the physiological signal, reduce noise and interference from the electrical grid and guarantee protection to patient and equipment through voltage and current surges. The A/D converter transforms the signals from analog to digital to be stored easily [24], [32].

2.2.3 Electrical source imaging

Computing power has allowed researchers to use EEG to find active regions inside the brain by locating the underlying sources that generate the measured EEG. This method is referred to as electrical source imaging (ESI). Using this technique requires solving the so-called forward model and inverse problem. The forward model models the propagation of the sources to the electrodes. The inverse problem starts from the measured electrode potentials and estimates the underlying generating sources. The discussion of ESI, the forward model and the inverse problem is based on [13], [24], [26], [33]–[35].

2.2.3.1 Current dipole

As stated above, the neuronal pyramidal cell can be represented by a current dipole [36]. Characterizing a given dipole is done by defining its location $\mathbf{r}_{dip}$ and dipole moment $\mathbf{d}$. The dipole moment $\mathbf{d}$ is characterized by a unit vector $\mathbf{e}_d$ directed from sink to source and a magnitude $d = ||\mathbf{d}||$. Often, the dipole is decomposed into three orthogonal dipoles oriented along the three Cartesian axes. Each dipole is then defined by the orthogonal projections of the original dipole onto one of the axes. Therefore, the dipole moment is indicated as follows:

$$\boldsymbol{d} = d_x\boldsymbol{e}_x + d_y\boldsymbol{e}_y + d_z\boldsymbol{e}_z \quad (1)$$

Conversion to spherical coordinates allows full characterization of a current dipole by 6 parameters: 3 parameters for the location (r_x, r_y, r_z), 2 orientation parameters (Φ, ϕ) and intensity d (Figure 2.12).

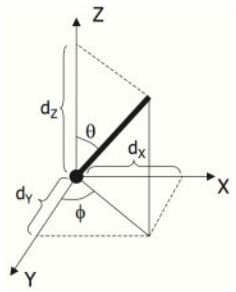

Figure 2.12: Representation of a current dipole as EEG generator [33].

2.2.3.2 Forward model

The forward model consists of calculating the scalp potentials given the activity of all dipoles in a certain electrical source distribution (the source model). To project the sources to the scalp electrodes, the source model and a model of the head are needed. The head model includes the volume conduction and the electrode positions. The forward model is illustrated in Figure 2.13.

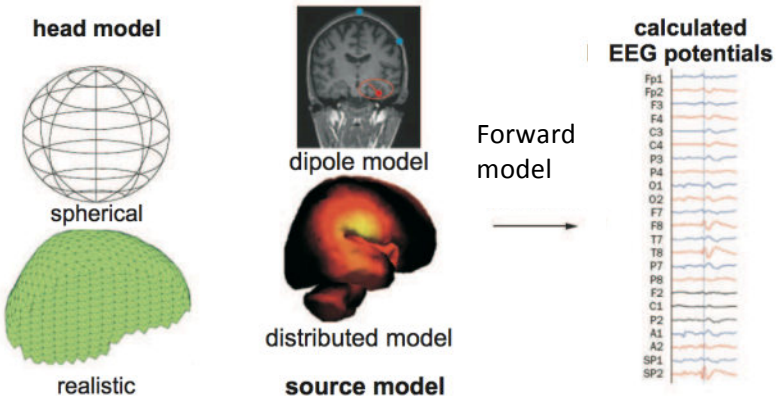

Figure 2.13: The forward problem in electrical source imaging (ESI). The EEG scalp potentials are calculated from a source distribution with respective dipole activity and a head model. Adapted from [37].

Head model

The head model contains the geometrical and electromagnetical properties of the head as well as the location of the electrodes. More specifically, the model incorporates the electrical conductivities (isotropic or anisotropic) of the brain and its different tissues. Different types of head models are available with increasing complexity and accuracy. Simple head models or spherical head models consist of one or more concentric shells depending on the amount of different types of brain tissues included in the model. Conductivities are homogeneous and isotropic in each compartment. These head models are easy to use and the scalp potentials can be calculated analytically, but they are a severe simplification of the real human head. In order to approximate reality better, realistic head models are built based on anatomical data from MRI or CT images, which allows to use patient-specific head models. The images are segmented, meaning that the boundaries for the different tissues are defined. Usually 3 or 4 compartments are identified: the brain, skull and scalp with the addition of CSF in 4-layered

head models. Each compartment is given a specific conductivity. By using other modalities such as Diffusion Weighted MRI it is possible to incorporate anisotropic conductivities in the head model.

Source model

The source model contains the properties of the sources thought to underlie the EEG. As indicated above, the pyramidal neurons can be modeled as current dipoles defined by six parameters. Different source models can be used with varying complexity. The dipole is used as the basic building block for different source models. In case of a single dipole model, the brain activity is represented by a single dipole. If different areas of the brain are active, a multiple dipole model can be used. The number of variables to be determined depends on the number of dipoles chosen and is equal to six times the number of dipoles since for each dipole six parameters need to be estimated. These single or multiple dipole models are often termed Equivalent Current Dipole (ECD) approaches. A relatively small number (<10) of focal sources are usually assumed.

In distributed source models the brain is segmented into volume or surface elements. In case the full brain is used, the brain volume is divided into small (often cubic) volume elements, which are called voxels. In other applications, only the brain surface or cortex is investigated and a mesh with specific faces and vertices divides it into elementary zones. To each of the elementary voxels or surfaces a single dipole with fixed location is assigned. Therefore, all possible source locations (usually around 10,000) are considered at the same time. In this distributed source model the only unknown per dipole is the intensity. However, due to the large number of voxels, distributed source models have a large amount of unknowns. ECD models tend to have less variables than measured data points making the forward problem easy to solve but it is important to properly choose the amount of dipoles. In distributed source models, the amount of dipoles is fixed but the amount of unknowns is much higher than the measured data points, making the problem ill-posed (highly underdetermined), so it needs regularization. A large drawback of multiple dipole models compared to distributed source models is that it is required to know the amount of active brain regions in advance since for the multiple dipole models one dipole is assigned to each investigated region while for distributed source models this is no issue.

Solving the forward problem

The measured potential at a given electrode with position $\mathbf{r}$ due to a dipole with location $\mathbf{r}_{dip}$ and intensities d_x, d_y and d_z can be expressed as follows:

$$V(\boldsymbol{r}, \boldsymbol{r}_{dip}, \boldsymbol{d}) = d_x V(\boldsymbol{r}, \boldsymbol{r}_{dip}, \boldsymbol{e}_x) + d_y V(\boldsymbol{r}, \boldsymbol{r}_{dip}, \boldsymbol{e}_y) + d_z V(\boldsymbol{r}, \boldsymbol{r}_{dip}, \boldsymbol{e}_z) \quad (2)$$

This equation can be elaborated and rewritten to include all electrode potentials:

$$\boldsymbol{V} = \begin{bmatrix} V(\boldsymbol{r}_1, \boldsymbol{r}_{dip}, \boldsymbol{e}_x) & V(\boldsymbol{r}_1, \boldsymbol{r}_{dip}, \boldsymbol{e}_y) & V(\boldsymbol{r}_1, \boldsymbol{r}_{dip}, \boldsymbol{e}_z) \\ \vdots & \vdots & \vdots \\ V(\boldsymbol{r}_M, \boldsymbol{r}_{dip}, \boldsymbol{e}_x) & V(\boldsymbol{r}_M, \boldsymbol{r}_{dip}, \boldsymbol{e}_y) & V(\boldsymbol{r}_M, \boldsymbol{r}_{dip}, \boldsymbol{e}_z) \end{bmatrix} \begin{bmatrix} d_x \\ d_y \\ d_z \end{bmatrix} \quad (3)$$

$$\boldsymbol{V} = \boldsymbol{L}(\boldsymbol{r}_{dip}).\boldsymbol{d} \quad (4)$$

Where **V** is a M x 1 matrix consisting of the electrode potentials (EEG measurements) with M the number of electrodes and $\mathbf{L}(\mathbf{r}_d)$ is a M x 3 matrix, the so-called lead field matrix, which depends on the dipole position, electrode positions and the properties of the head model.

As stated before, when using a spherical head model, the forward problem can be solved analytically. For realistic head models numerical methods are required. Three main methods are used to solve the forward problem with realistic head models: the boundary element method (BEM) [38], the finite element method (FEM) [39] and the finite difference method (FDM) [40].

2.2.3.3 Inverse problem

The inverse problem in ESI is the estimation of the neural current sources from the measured scalp potentials. It is an ill-posed problem when using distributed source models, meaning that an infinite number of source configurations can be found to explain the measured EEG. The inverse problem is represented in Figure 2.14.

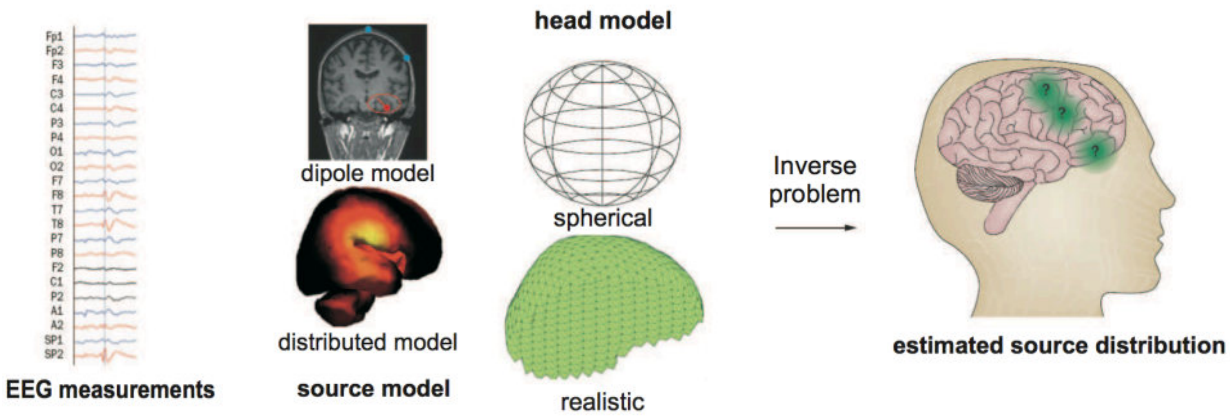

Figure 2.14: The inverse problem in electrical source imaging (ESI). The neural current sources are estimated given the measured EEG potentials. Adapted from [37].

To overcome the issue of the ill-posedness and to impose a unique solution to the inverse problem, a source model is chosen and regularization is performed. This regularization consists of adding requirements such as a cost function or restrictions on certain characteristics to impose a single solution. In solving the inverse problem, two general approaches exist: a parametric approach and an imaging approach. The parametric approach uses the dipole source models whereas the imaging approach utilizes the distributed source model. Solving the inverse problem means that the parameters of the chosen source model are estimated. In the parametric approach the number of unknown parameters is much smaller than the measured data points, while in the imaging approach the number of unknowns is much larger.

Solving the inverse problem

Instantaneous single dipole

Solving the inverse problem by using the parametric approach consists of an iterative approach. Initial distributions, orientations and intensities of the dipoles are chosen and by using the forward model the electrode potentials are calculated. The difference between the actual measured EEG potentials and the calculated electrode potentials is then incorporated in a cost function. Depending on the outcome of the cost function, dipole parameters are re-estimated to calculate new electrode potentials. This iterative loop is repeated until the cost function is below a certain threshold. The cost function that is often used is the relative residual energy (RRE, equation 5) with ||.|| the L_2-norm, $\mathbf{V}_{measured}$ the recorded EEG data, $\mathbf{V}_{calculated}$ the electrode potentials calculated using the forward model and **d** and **r** the dipole parameters.

$$RRE = \frac{|| \boldsymbol{V}_{measured} - \boldsymbol{V}_{calculated} ||}{|| \boldsymbol{V}_{measured} ||} = \frac{|| \boldsymbol{V}_{measured} - \boldsymbol{L}(\boldsymbol{r})\boldsymbol{d} ||}{|| \boldsymbol{V}_{measured} ||} \quad (5)$$

Six dipole parameters need to be estimated by minimizing the RRE. However, this can be reduced by deriving the optimal dipole moment at position **r** with $\mathbf{L}(\mathbf{r})^{\dagger}$ the Moore-Penrose pseudo-inverse of matrix L. This optimal dipole moment is obtained as the solution of the over-determined system of linear equations $\mathbf{x} = \mathbf{L}.\mathbf{d}$ [41].

$$\boldsymbol{d}_{opt}(\boldsymbol{r}) = \boldsymbol{L}(\boldsymbol{r})^{\dagger} \ .\boldsymbol{V} \quad (6)$$

The parameters in this overdetermined problem can be estimated in least-squares sense or by a non-linear algorithm such as MUSIC or the Nelder-Maede simplex method [42].

Time-varying single dipole

To estimate the parameters of a time-varying single dipole, Singular Value Decomposition (SVD) of the electrode potentials **V** can be used:

$$\boldsymbol{V} = \boldsymbol{USD}^T \tag{7}$$

where **U** defines the topographies, **S** contains the singular values and **D** represents the time series corresponding to the topographies. We can simplify the problem by only retaining the topography corresponding to the highest singular value. Thereby, the RRE can be written as

$$RRE = \frac{|| \boldsymbol{U}(:,1) - \boldsymbol{L}(\boldsymbol{r})\boldsymbol{L}(\boldsymbol{r})^{\dagger} \ \boldsymbol{U}(:,1)||}{|| \boldsymbol{U}(:,1) ||} \tag{8}$$

Multiple dipole model

The measured EEG signals can be rewritten as:

$$\boldsymbol{V} = \boldsymbol{AS}^T \tag{9}$$

With **A** an M x p matrix and **S** a p x N matrix with p a number of sources. Each column of **A** represents the fixed topography of source p and each row of **S** represents the time varying amplitude of source p. Optimal time series are given by $\mathbf{S}_{\text{opt}} = \mathbf{A}^{\dagger}\mathbf{V}$ which leads to a minimization problem with respect to **A**:

$$RRE = \frac{|| \boldsymbol{V} - \boldsymbol{AS}^T||_F}{|| \boldsymbol{V} ||_F} = \frac{|| \boldsymbol{V} - AA^{\dagger}\boldsymbol{V} ||_F}{|| \boldsymbol{V} ||_F} \tag{10}$$

With $||.||_F$ the Frobenius-norm. Direct optimization methods suffer from some drawbacks. Optimization techniques such as MUSIC or RAP-MUSIC deliver good results.

Imaging methods

In the imaging approach, a distributed source model is used. This results in a highly underdetermined system since the number of assumed dipoles is much higher than the number of EEG channels. Unique solutions are achieved by optimizing a goodness-of-fit term together with a regularization term. The classical and most popular distributed approach is the Weighted Minimum Norm (WMN) solution or Tikhonov regularization method [43]. In this approach the reconstructed source distribution is constrained by minimization of a linear mixture of some weighted norm ||**HJ**|| of the source amplitudes **J** and the residuals of the fit. The regularized problem can be expressed as:

$$\boldsymbol{J'} = argmin_{\boldsymbol{j}}(\| \boldsymbol{LJ} - \boldsymbol{V_m} \| + \boldsymbol{\mu} \| \boldsymbol{HJ} \|) \tag{11}$$

With **J'** the estimated activity and parameter μ expressing the balance between fitting the model by the term ||**LJ-V**$_m$|| and minimizing the a priori constraint ||**HJ**||. The solution is given by:

$$\boldsymbol{J'} = (\boldsymbol{H}^T\boldsymbol{H})^{-1}\boldsymbol{L}^T[\boldsymbol{L}(\boldsymbol{H}^T\boldsymbol{H})^{-1}\boldsymbol{L}^T + \mu\boldsymbol{C}_\varepsilon]^{-1}\boldsymbol{V}_m \tag{12}$$

With C_ε the covariance matrix of the noise which is assumed to be Gaussian. It is clear that μ is the crucial parameter in this solution since it defines the balance between fitting of the model and the constraint on the solution. Typically, μ is estimated by an L-curve approach [44].

2.2.4 Applications

EEG is widely spread in clinics and research since it is a cheap, safe and easy technique. In current clinical practice several diseases can be diagnosed using EEG such as epilepsy, sleep disorders, coma and brain death. Often, it is used as a first step towards the final diagnose. Due to its superb temporal resolution, it is unlikely that EEG will lose its place in everyday clinical practice.

In research, the EEG signal is often recorded to include evoked potentials (EP) or event-related potentials (ERP). EPs are potentials recorded as a result of a certain stimulus presented to the subject. Usually, the amplitude of EPs is lower than the normal EEG signal. ERPs are potentials measured after specific sensory, cognitive or motor events. As is the case with EPs, the amplitude of ERPs is smaller than the normal EEG. Therefore, the ERP is often averaged across several trials in order to reduce noise. Typical characteristics of EPs and ERPs are

latency and amplitude, which are often used as measures to compare outcomes. ERPs will be used in the research in this master thesis and are explained further in Chapter 3.

2.3 Epilepsy

2.3.1 Definition

Epilepsy is the second most common neurological problem in the world following cerebrovascular disorders. Worldwide, there are approximately 50 million epilepsy patients [1]. Traditionally, it has been referred to as a disorder or a family of disorders, rather than a disease, to emphasize that it is comprised of many different diseases and conditions. In most of the definitions, epilepsy is described as a brain disorder characterized by an abnormally increased predisposition to seizures, which are recurrent and unpredictable interruptions of normal brain function. In order to ensure clear communication on the subject of epilepsy, the International League Against Epilepsy (ILAE) together with the International Bureau for Epilepsy (IBE) published definitions on epilepsy and epileptic seizures [45]–[51]:

"An epileptic seizure is a transient occurrence of signs and/or symptoms due to abnormal excessive or synchronous neuronal activity in the brain."

"Epilepsy is a disorder of the brain characterized by an enduring predisposition to generate epileptic seizures, and by the neurobiological, cognitive, psychological, and social consequences of this condition. The definition of epilepsy requires the occurrence of at least one epileptic seizure."

From the previous definitions it is clear that epileptic seizures are the main determinants of epilepsy. Operationally, the signs or symptoms mentioned include sudden and transitory abnormal phenomena such as alterations of consciousness, or involuntary motor, sensory, autonomic, or psychic events perceived by the patient or an observer.

The ILAE-definitions are commonly used as the standard definitions of epilepsy and epileptic seizures. However, in medical practice these definitions are rather vague and require elaboration in terms of diagnostic application. The ILAE proposed that epilepsy should be considered to be a disease of the brain in the following cases: (1) at least two unprovoked seizures occurring >24h apart, or (2) one unprovoked seizure and a probability of further seizures similar to the

general recurrence risk (at least 60%) after two unprovoked seizures, occurring over the next 10 years, or (3) diagnosis of an epilepsy syndrome [47].

2.3.2 Classification, epidemiology and pathophysiology

The ILAE proposes three main categories of seizures: (1) generalized seizures, (2) focal seizures, and (3) unknown seizures. Generalized seizures are occurring in and rapidly engaging bilaterally distributed networks. Focal epileptic seizures can be seen as originating within networks limited to one hemisphere. The site of the focus and the speed and extent of spread determine the clinical manifestation of the seizure [45], [46], [51]. Classification can also be made based on etiologic considerations. The ILAE suggests separation into the categories genetic, structural/metabolic and unknown cause [45], [52].

According to the World Health Organization (WHO) around 0.5-1% of the population or 50 million people suffer from epilepsy worldwide. In Europe the amount of people suffering from epilepsy was estimated to be 4.4 million in 2004. The estimated number of new cases per year in Europe is around 300,000 with the highest incidence rate for elderly people. In Figure 2.15, one can see the average rate per 100,000 of epilepsy cases at different ages [2], [53].

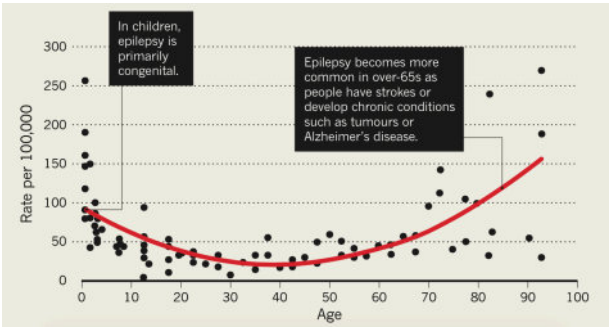

Figure 2.15: Number of epilepsy patients in terms of age on a global scale [54].

Epileptic seizures are defined as excessive or abnormal nervous activity. During these seizures, sudden bursts of uncontrolled electrical activity occur in a group or multiple groups of neurons. The etiology of epilepsy in a specific patient is often difficult to determine in part due to the fact that many factors can cause epilepsy: genetic predisposition, head trauma, tumors, dementia, oxygen deprivation, infectious diseases, developmental disorders, etc. These causes are termed the initial precipitating insult (IPI). Epileptogenesis is the process in which epilepsy evolves into the occurrence of spontaneous seizures [13], [55]. Depending on the type of epilepsy and the patient, the symptoms during an epileptic seizure can vary immensely. Symptoms are often classified as ictal (during seizure) or interictal (between seizures). Extensive lists of symptoms for different types of epilepsy can be found in several reference books, such as [56].

2.3.3 Epilepsy and EEG

EEG is often used to detect and classify epileptiform activity since it helps to answer three important questions concerning epilepsy: (1) does the patient have epilepsy, (2) where is the epileptogenic zone and (3) is the provided therapy effective. The International Federation of Clinical Neurophysiology defines EEG seizure patterns as repetitive discharges with relatively abrupt onset and termination and characteristic patterns of evolution lasting at least several seconds. Usually, this is observed as rhythmic displays of increasing amplitude and decreasing frequency. Also interictal epileptiform discharges (IED) can be detected. These IEDs are classified by their shape as sharp waves, spikes, spike-wave complexes, etc. Based on the type of epileptiform activity in the EEG and in combination with abnormalities seen on MRI, the source of neural activity can sometimes be identified but ESI can provide better results. EEG can also detect side effects of several anti-epileptic drugs such as dizziness, sedation, irritability, nausea or cognitive slowing [57]–[59].

Figure 2.16: Example of ictal and interictal epileptiform activity. Ictal rhythmic activity (left) and an interictal spike-wave complex (right) are shown. Adapted from [58].

2.3.4 Treatment

Treating epilepsy is focused on reducing the seizure frequency. Anti-epileptic drugs (AEDs) are usually the first option to help the patient. If the AED is not effective, a second or even third drug can be prescribed. However, chances of finding an effective AED after three attempts decrease dramatically [60]. Around 70% of the patients can be helped by AEDs. The other patients are diagnosed with 'refractory epilepsy'. For these patients, other options such as resective surgery or neuromodulation can be helpful. Resective surgery consists of the surgical removal of the ictal onset zone in the brain. Neuromodulation or neurostimulation therapy is the technology that alternates or modulates nerve activity by delivering electrical stimulation. A typical treatment algorithm is presented in Figure 2.17.

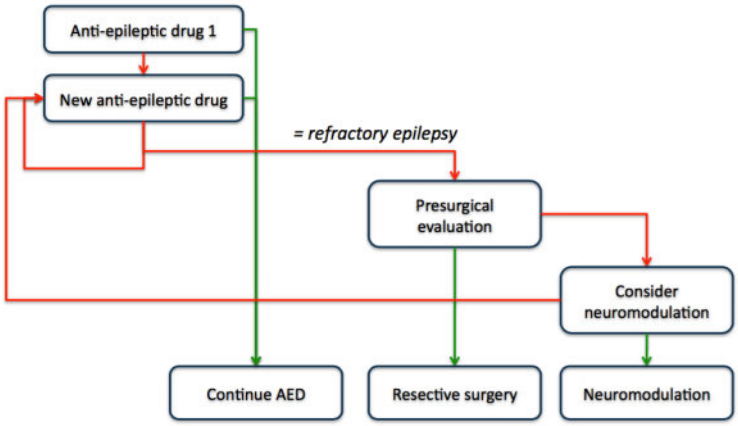

Figure 2.17: Treatment plan for newly diagnosed epilepsy patients. Green lines indicate possible positive outcomes, red lines indicate other options that can be considered [59].

2.3.5 Refractory epilepsy

The ILAE defines refractory epilepsy or drug resistant epilepsy as follows [61]:

"Drug resistant epilepsy may be defined as failure of adequate trials of two tolerated and appropriately chosen and used AE schedules (whether as monotherapies or in combination) to achieve sustained seizure freedom."

Treatment of refractory epilepsy can be resective surgery, neuromodulation or a ketogenic diet. Resective surgery consists of the surgical removal of the ictal onset zone in the brain. Neuromodulation techniques include deep brain stimulation (DBS) or vagus nerve stimulation (VNS) and will explained further.

2.3.5.1 Presurgical evaluation and resective surgery

Resective surgery requires careful preparation and evaluation. Several tests and evaluations need to be completed in order to continue with surgery. Three main questions need to be answered: (1) is the patient willing and motivated to undergo resective surgery, (2) is there a single epileptogenic focus and where is it situated and (3) is the focus resectable without serious functional deficit. A multidisciplinary team of neurologists, psychologists, neurosurgeons and engineers determines whether surgery is appropriate for the given patient. Seizure freedom is obtained in up to 60-90% of the patients depending on the localization of the focus [1], [6].

Determining if there is a single epileptogenic focus and where it is situated can be achieved in several ways. Clinical, paraclinical and imaging methods exist and are used. Depending on the level of consensus of several investigations, resective surgery can be advised. Structural

Magnetic Resonance Imaging is preferred as imaging method. This modality is used to identify anomalies in the brain such as atrophy or lesions. Identification of such anomalies is insufficient to determine (single focus) epilepsy so that other modalities need to accompany structural MRI. Clinically, scalp video-EEG-monitoring (SVEM) is used. Hereby, the patient is present in the hospital for several days during which scalp EEG is recorded continuously together with video monitoring. Interictal spikes and seizure semiology are used to determine the epileptogenic focus. In 15 to 25% of the refractory epilepsy patients, SVEM is not conclusive enough. For these patients an intracranial electroencephalogram (IEEG) or electrocorticogram (ECoG) is recorded. In these methods, electrodes placed on the cortex (ECoG) and depth electrodes in the brain's parenchyma (IEEG) measure the electrical activity. Some issues accompany ECoG: the skull needs to be opened, patients are scared, and infections are a real danger. On top of that ECoG is more labor intensive and that's why EEG is preferred. Although SVEM and structural MRI are commonly used in the presurgical evaluation, other techniques are used to come to a final conclusion, such as ESI, EEG/fMRI, MEG, PET and SPECT [59], [62], [63].

2.3.5.2 Neuromodulation

Neuromodulation or neurostimulation therapy is the technology that alternates or modulates nerve activity by delivering electrical stimulation or pharmaceutical agents. The electrical stimulation is delivered by using (micro)electrodes as interface with the excitable tissue. It is evaluated as an option if resective surgery is not advisable. Neuromodulation has some advantages over surgery: (1) it is usually reversible, (2) it is adjustable in a wide range of parameters, (3) multiple foci can be reached by a single target and (4) foci that cannot be removed safely can still be stimulated. However, the outcome of neurostimulation is highly variable depending on the patient's specific case. Better understanding of the mechanisms of action (MOA) of both epilepsy and neurostimulation could improve the outcome prediction. Future challenges will lie in sorting out the appropriate candidates for each procedure, in finding the optimal anatomic targets for each epileptic syndrome and in assessing long-term effects [3].

The first indication of neurostimulation dates back to the first century AD when epilepsy was treated by electricity from the torpedo fish. A century later, stimulation of limbs was used. Already in 1803, the first device was used to electrically stimulate the body. Jean Aldini operated a device that was designed by Alessandro Volta to electrically stimulate the body of a hanged criminal. In the 1950s, researchers Penfield and Jasper specifically found that cortical stimulation could interrupt seizure activity. Simultaneously, Robert Heath used electrodes deep in the brain to induce seizures. In 1954, the first use of chronic therapeutic brain stimulation was observed when Pool implanted an electrode in the caudate nucleus of a woman to treat depression and Parkinson's disease. Starting from 1973, several trials were conducted to treat epilepsy patients with chronic neurostimulation to reduce seizure frequency. To date, many (double-blind crossover) studies are conducted to find interesting targets for electrical

stimulation. Targets that are tested include the cerebellum, thalamic nucleus and hippocampus each with its own specific reasons why it could reduce seizure frequency. Results of these studies are rather inconclusive and often depend highly on stimulation parameters [1].

Next to these cerebral structures, also peripheral nerves and in particular the vagus nerve, became widely used to treat epilepsy. In 1938, Baily provided the first evidence that the inhibition of the nucleus of the tractus solitaries reduced susceptibility to limbic motor seizures in animals. Zabara reported the first use of vagus nerve stimulation (VNS), which consists of electrically stimulating the vagus nerve using a kind of brain pacemaker. In 1989, the first VNS system was implanted. VNS was the first electrical stimulation treatment method for epilepsy approved by the US Food and Drug Administration in 1997. To date, VNS proved to be effective, but the MOA remains to be elucidated. VNS will be discussed in more detail in part 2.4 of this literature review.

Deep Brain Stimulation (DBS) involves the electrical stimulation of specific parts of the brain by the implantation of electrodes (deep) in the brain. DBS is more invasive than VNS since the surgeon needs to drill in the skull to open it, and the MOA still needs to be determined as well. Characterization of the full MOA and long-term side effects can lead to optimal targets and stimulation parameters. In 2010, European regulatory bodies approved DBS of the anterior thalamic nucleus, but the FDA refused to do so to date [64].

Currently, many other modalities are under investigation as well. Stimulation of the trigeminal nerve (TNS) proves to be an important alternative for VNS and DBS [65]. Repetitive Transcranial Magnetic Stimulation (TMS) is a noninvasive stimulation method whereby a magnetic field generator or coil is placed near the head of the patient and is also considered for its anti-epileptic effects. By electromagnetic induction, the magnetic field produces small electrical currents in the brain regions lying just below the coil [66]. Transcranial Direct Current Stimulation (tDCS) delivers currents to the brain via electrodes on the scalp and is considered as well for neurostimulation therapy. In 2013, the responsive neurostimulator (RNS) was approved by the FDA. In RNS seizure detection and stimuli delivery occurs in real-time (Figure 2.18). In the future, new techniques will be investigated such as focal delivery of AEDs, neuronal grafting and tissue transplant, gene therapy and focal cortical cooling [67].

VNS, TNS, TMS, tDCS, and DBS are at different levels of availability and clinical applicability. VNS is an availably therapy for refractory epilepsy with proven efficacy and safety. For therapeutic TNS, only proof of concept has been shown to date. TMS protocols for epilepsy have been developed in centers with a large experience in diagnostics but at this time it is not a routinely available treatment, nor is tDCS. Importantly, some neuromodulation techniques such as VNS and DBS can be used to treat other patients as well. VNS can be used to treat depression and DBS is used clinically to treat Parkinson's disease [3].

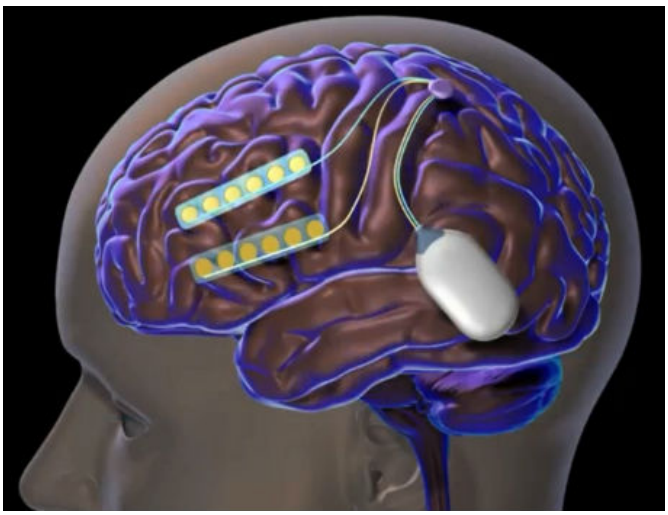

Figure 2.18: Responsive neurostimulation device implanted beneath the skull [68].

2.4 Vagus Nerve Stimulation

2.4.1 Introduction

As discussed above, Vagus Nerve Stimulation or VNS is the stimulation of the vagus nerve with electrical pulses. The pulses are delivered to the electrodes by a pulse generator implanted near the chest. Vagus nerve stimulation can be used to treat epilepsy and depression and is being studied for other conditions as well, such as multiple sclerosis or Alzheimer's disease. Due to the vast and widespread connections of the vagus nerve, stimulating it is thought to influence a large part of the brain including some key regulatory systems such as the locus coeruleus-norepinephrine system. However, research is still inconclusive and the MOA is yet to be elucidated.

2.4.2 History

Peripheral stimulation for seizure treatment dates back to several hundreds of years ago. Physicians in the 16^{th} and 17^{th} century described the use of ligatures around limbs in which a seizure commenced to arrest its progress. This hypothesis was described by the Greek author Pelops but was reviewed by Odier and Brown-Séquard in the 19^{th} century. They showed that ligatures could also arrest seizures caused by organic brain diseases [69]. At the end of the 19^{th} century, Glowers explained the spread of the discharge during epileptic seizures by increase in resistance of the nerves [70]. In 1989, Rajna and Lona demonstrated the concept of nerve

stimulation for epilepsy and in the same year the first vagus nerve stimulator was implanted in humans [5], [71], [72].

2.4.3 Anatomy of the vagus nerve

The vagus nerve (VN) is the 10th cranial nerve and is attached to the brainstem in the neck, which is shown in Figure 2.19. It is a mixed nerve, meaning it consists both of afferent and efferent fibers. Afferent fibers bring information to the brain and form about 80% of the fiber content of the VN [5]. Efferent fibers target several parts of the body. In case of the VN, the efferents innervate the heart, aorta, lungs and the gastrointestinal tract. These body parts are also the origins of the afferent fibers in the VN [1].

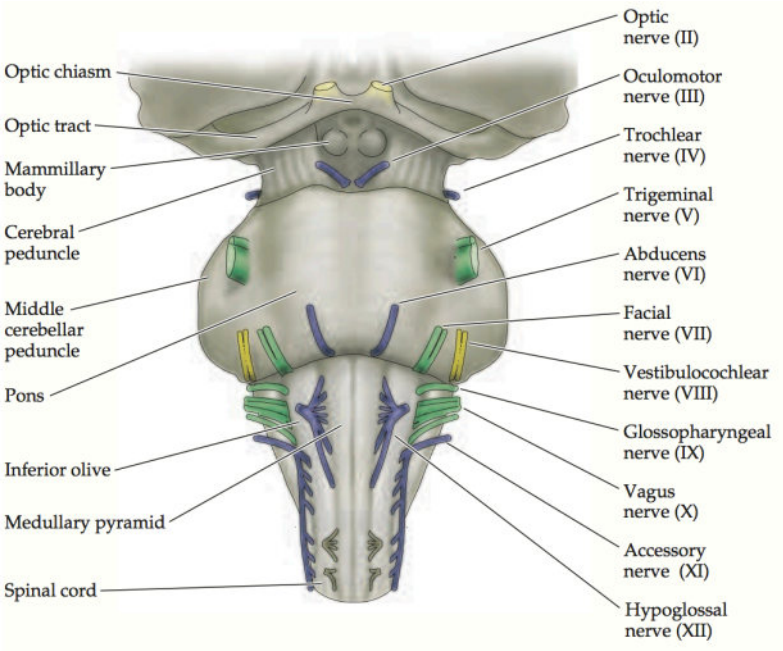

Figure 2.19: Ventral view of the brainstem and the cranial nerves. Nerves that are exclusively sensory are indicated in yellow, whereas motor nerves are blue. The vagus nerve or 10th cranial nerve (X) is green indicating it is a mixed nerve [11].

The vagus nerve is a mixed nerve projecting to various brain structures via the nucleus of the tractus solitaries (NTS). Of all the widespread connections, an important connection exists to the locus coeruleus (LC), which contains many noradrenergic neurons. The complex anatomical distribution resulted in the name of the vagus nerve since vagus is the Latin word for 'wanderer' [1], [3], [4], [71].

2.4.4 Device and surgery

Currently, VNS devices are produced by Cyberonics, Inc. (Houston, TX, USA) and are implanted as chronic, intermittent stimulators. The pulse generator is similar to a cardiac pacemaker. Two helical bipolar electrodes are wound around the left VN. The left vagus nerve is used to limit the risk of bradycardia or arrhytmias given the connections to the heart of the right vagus nerve. Patients are admitted to the neurosurgical department 1 or 2 days before surgery. Implantation procedures last around 1 hour and are usually performed under general anesthesia. The pulse generator is implanted below the left clavicle.

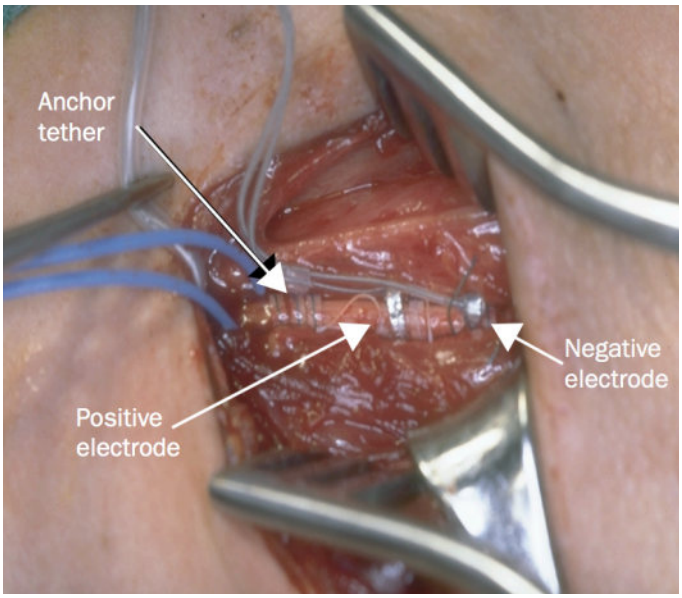

Figure 2.20: Implantation of the VNS electrodes. Adapted from [4].

Stimulation is initiated 2 to 4 weeks after surgery. A portable computer with specialized software initializes the stimulation parameters. This programming device is held directly against the patient's chest to set the parameters such as output current, frequency, pulse-with, and on/off periods. The output current is gradually ramped during 6-12 clinical visits over several weeks to reach individual patient threshold or a maximum of 3 mA. Maximal efficiency is usually obtained after 18 months. Other parameters are standard: frequency of 30 Hz, pulse width of 250-500 microseconds, and on/off periods of 30/300 to 600 seconds. Some other epilepsy centers prefer 7s on and 0-2s off [67], [68].

End of battery life (EOBL) and end of effective stimulation (EOES) are important points in time for VNS patients. EOES and EOBL are usually characterized by loss of seizure control (gradually or acutely), decreased or irregular perception of stimulation by the patient and loss of other VNS-induced effects. Postponing generator or battery replacement may result into permanent loss of seizure control. Battery life of the generator depends on the generator model, the programmed stimulation parameters and the lead impedance values of the stimulation

electrodes (<1-8kilo ohm). The newest models (Model 105, available since 2011) have life-expectancies of over 10 years [74].

Figure 2.21: Recent pulse generators of Cyberonics, Inc. for vagus nerve stimulation [75].

2.4.5 Efficacy and side effects

VNS was approved by the FDA for use in epilepsy in 1997 [76]. In general, about 1/3 of the patients has a seizure reduction of >50%. These patients are indicated as responders. Another third of the patients has a seizure reduction between 30-50% and the remaining third of the patients experiences little or no effect [3]. The latter groups are termed non-responders. To date, more than 100,000 people have received a VNS implantation [8], [77]. VNS is widely adopted and is now estimated to account for 50% of surgical procedures for epilepsy in the US and UK [78]. Efficacy seems to increase over time up to 18 months after implantation after which a plateau is reached [79].

Some side effects have been reported upon VNS implantation. Postoperative infections occur in 3-6% of the patients and are treated with oral antibiotics. Usually, side effects occur during the 'on' phase of the stimulation. Cough, hoarseness, voice alteration, lower facial weakness and paresthesias are observed but these effects diminish over time and can be accounted for by the electrical stimulation. No clear cognitive effects, as is the case with AEDs, are reported. There are no central nervous system side effects such as tiredness, psychomotor slowing, irritation, and nervousness. All this makes the side effect profile of VNS positive and the treatment option offers patients with refractory epilepsy prospects of good efficacy with only minor and often resolvable side effects. It is clear that VNS is considered a safe and relatively effective treatment with only mild side effects [4], [6], [80]. However, some recent studies also question the VNS efficacy [81]–[83].

2.4.6 Mechanism of action

Although vagus nerve stimulation proved to be effective, the mechanism of action (MOA) is not yet fully unraveled [84], [85]. A first part of the MOA that was uncovered was the influence of the afferent and efferent fibers. It is generally accepted that the afferent fibers are crucial for

the epilepsy suppressing effect whereas efferent fibers are thought to generate side effects and are not included in the positive effects.

Another part of the MOA of VNS that is assessed is whether VNS is anti-seizure (abort seizures), anti-epileptic (suppressing seizures, preventative effect) and/or anti-epileptogenic (reverse the development of the process, protective effect). Electrophysiological, functional and anatomical brain imaging and neuropsychological and behavioral studies have been conducted to investigate these properties. Due to its effective use in clinics, VNS clearly has an anti-seizure effect. Interestingly, it was found that VNS also influences seizures in off-time [86], suggesting an anti-epileptic effect. Pulsed stimulation also reduced seizure frequency in the off-periods and stimulation effects outlasted the stimulation period. The fact that seizures reoccur after battery life ended indicate VNS is not anti-epileptogenic.

Assessing the key brain structures involved is much more difficult. Unilateral stimulation influences both hemispheres and crucial brainstem and intracranial structures have been identified such as the locus coeruleus (LC), the nucleus of the solitary tract, the thalamus and the limbic structures. Neurotransmitters involved are GABA, serotonin and adrenaline. GABA receptor cell death was shown to be reduced due to VNS as well as conservation of the GABA receptor neuron density [87]. The thalamus is also involved as shown by increased blood flow in PET. Other researchers found that the areas of significant activation in response to VNS were the bilateral orbitofrontal and parieto-occipital cortex, the left temporal cortex, and the left amygdala. CSF studies showed an increase in several amino acids and neurotransmitters such as ethanolamine. This could be an indication of increased turnover of membrane components [88].

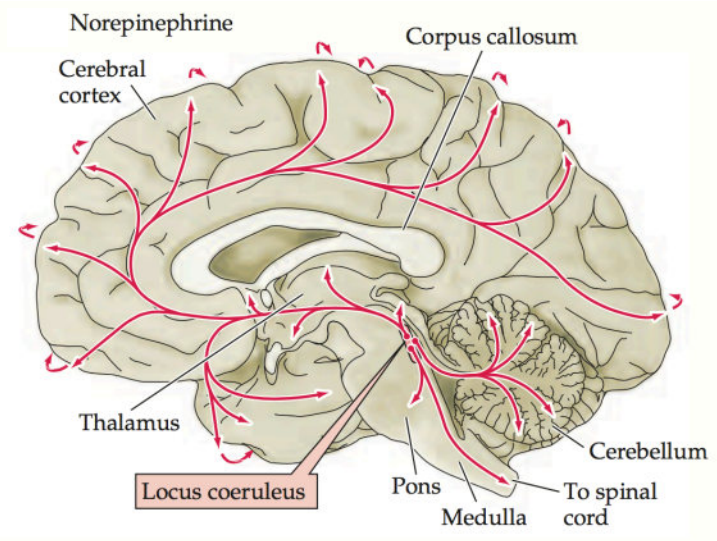

Figure 2.22: The locus coeruleus and norepinephrine system in the human brain. Adapted from [11].

Over the last 20 years, experiments indicate a crucial function for the LC and the norepinephrine system in the seizure suppressing characteristics of VNS (Figure 2.22) [7], [8]. VNS has been shown to result in a long-lasting increase in release of noradrenaline (NE) in the basolateral amygdala, the origin of which could be the locus coeruleus [89]. Researchers

inhibited the development of kindling of the amygdala by direct electrical stimulation [90], [91]. When NE was depleted by a 6-hydroxydopamine infusion into the LC of rats, the seizure-suppressive effect of VNS was abolished [89]. Some studies also found increased norepinephrine in the prefrontal cortex, the hippocampus and the amygdala [92]–[96]. A recent study found increased levels of NE, but not of serotonin, dopamine or GABA receptors [96]. Loss of LC activity reduces the efficacy of VNS while LC activation produces anti-epileptic effects. Due to the NE, LC-NE activity is crucial in limiting both spatial spreading and duration of different epileptic syndromes [7]. Therefore, there is growing consensus that the LC-NE activity is at least one of the key structures in the seizure suppressing effect of VNS [91].

2.4.7 Current research

VNS is still researched today. On the one hand, efforts focus on revealing the MOA of VNS, whereas other research focuses on the application of VNS in other (neurological) domains. VNS has been tested with regard to treatment-resistant depression (TRD) and pain, as well as memory and cognitive impairment [73]. In 2013, VNS was approved as an depression treatment by the FDA [76]. Recently, the crosstalk between the vagus nerve and the immune system has been described [5].

Research on elucidating the MOA of VNS is currently focusing on assessing the activity of the LC-NE system, which cannot be done through direct measurements at present. Indirectly, the activity levels are inferred from parameters modulated by the amount of noradrenergic signaling. In previous research this proved to be successful [8]. In this work, the P300 component of an event-related potential (ERP) is investigated during an auditory oddball experiment which is a parameter modulated by the activity levels of the LC-NE system [8]. More details will be provided in Chapter 3.

2.5 Brain connectivity

2.5.1 Introduction

Neuroscience research has been focusing on identifying key structures in the brain and which functions they exert. Current and future directions emphasize more on the integration of different brain structures and how they act and interact to perform the main functions of the human brain. Billions of neurons form patterns that flexibly integrate and are not limited to direct structural connections [97]. To understand the mechanisms that control complex brain

functioning such as emotions, perception, memory or decision-making, analysis of the brain and its structures needs to focus on integrating previous research and elucidating the overall circuitry in the brain. Connectomics, connectivity, causal modeling and analyses of distributed patterns of brain responses can indicate large distance co-activation and projections in order to make the next step in understanding how the brain is able to control and manage its highly complex functionality. These mathematical considerations and concepts are thought to be the main tools for future neuroscience research and will decipher the large-scale interregional symbioses and local intraregional circuitry in the human brain both functionally and structurally.

Defining and studying connections in the brain requires delineation of terminology and nomenclature. Ever since the formulation of phrenology by Gall in the 19th century, efforts have been made to link certain brain functions to anatomical delineated brain areas, referred to as functional segregation. Discoveries of brain areas with specific functions are usually made by finding activation of the area during a specific task or the inability of performing this task upon trauma in the specific area by using (functional) imaging modalities. On the other hand, research can be focused on functional integration or connectionism, which is explored by connectivity measures and tackles the issue of how different brain regions are connected and communicate with each other.

Brain connectivity is often divided into three types: structural, functional and effective connectivity. Structural or anatomical connectivity deals with the physical neural connections, often investigated using Diffusion Tensor Imaging (DTI). Assessing non-structural connectivity seems to be more daunting. One approach is to use functional connectivity, which is defined as the temporal correlations between spatially remote neurophysiological events [98]. It can be a theoretic information measure, which is essentially descriptive in nature. Often, this reduces to testing the null hypothesis that activities in two regions share no mutual information. Functional connectivity is therefore model-free. Integration is often better represented by effective connectivity, defined as the influence one neural system exerts over another, either synaptically or at population level [99]. This consists of the intuitive notion of coupling or directed causal influence. Therefore, effective connectivity is sometimes termed 'directed functional connectivity'. Effective connectivity depends explicitly on a model of the influence that one neural system exerts over another. Effective connectivity analysis can be interpreted as the comparison between models with and without certain connections to explain the cause of the observed data. To summarize the difference between functional and effective connectivity, the need for a model is a crucial point because it emphasizes the shift from a description of what the brain does (functional) to a theory of how it does it (effective) [100]–[102].

Brain signals used in connectivity measures can be recorded by EEG or fMRI time series. As discussed in section 2.2.2, these modalities have their own advantages and drawbacks. EEG is commonly used for its superior temporal resolution (a few ms) whereas fMRI excels in spatial resolution performance (a few mm).

2.5.2 Structural connectivity

Physical connections between brain regions can be studied using structural or anatomical connectivity. Diffusion Weighted Imaging (DWI) can be used to identify and visualize these fiber pathways [103]. This modality uses the diffusion of water molecules in vivo to image these tracts. As opposed to the free diffusion of water in a container, diffusion of water is easier in the direction of a tract than in the orthogonal direction. Using this technique in different directions results in Diffusion Tensor Imaging (DTI). Finally, by using tractography, the gathered directional information can be converted into white matter fiber pathways [104]. Structural connectivity can be used to detect altered fiber tracts related to disease. It can also help to identify key tracts to avoid during resective surgery [13].

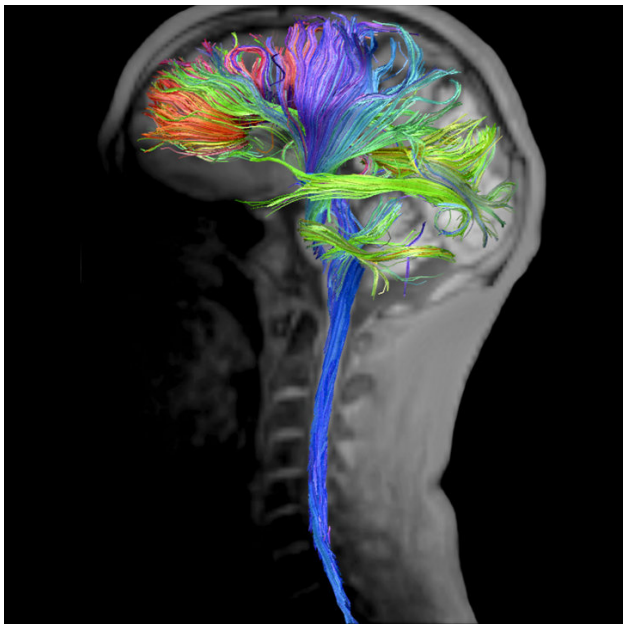

Figure 2.23: Example of the visualization of fiber pathways in the brain using tractography [105].

2.5.3 Functional connectivity

Functional connectivity deals with the temporal correlations between spatially remote events. Typically, two brain signals x(n) and y(n) are considered. Most functional connectivity measures are undirected, meaning the measures are symmetric: the connection from signal x to y is the same as from y to x. Essentially, there are three types of functional connectivity measures: linear, nonlinear and information-based. The following description is mainly based on [13], [106], [107].

2.5.3.1 Linear measures

Three linear measures are described here: correlation coefficient, coherence and partial coherence. Respectively, they incorporate two signals in the time domain, two signals in the frequency domain and multiple signals in the frequency domain.

Correlation

The correlation coefficient (ρ_{xy}) is a simple and easy to use measure. It is calculated by the following equation:

$$\rho_{xy} = \frac{E\left[(x - \mu_x)(y - \mu_y)\right]}{\sigma_x \sigma_y} = \frac{1}{N}\sum_{n=1}^{N}\frac{(x(n) - \mu_x)(y(n) - \mu_y)}{\sigma_x \sigma_y} \tag{13}$$

With N the number of samples, E[x] the expected value of x, σ_x and σ_y the standard deviations and μ_x and μ_y the mean values of the respective signals. Resulting values of the correlation coefficient lie between -1 and +1 meaning respectively full negative correlation and full positive correlation. A result equal to 0 indicates no correlation.

Cross-correlation and Coherence

The cross-correlation coefficient indicates the correlation between two signals with regard to a certain time lag τ:

$$\rho_{xy}(\tau) = \frac{1}{N - \tau}\sum_{n=1}^{N-\tau}\frac{(x(n) - \mu_x)(y(n + \tau) - \mu_y)}{\sigma_x \sigma_y} \tag{14}$$

In order to express the coherence, the cross-spectral density function is calculated by taking the Fourier transform of equation 5.2. Therefore, the coherence expresses the interdependency of two signals in the frequency domain:

$$C_{xy}(f) = \frac{|S_{xy}(f)|^2}{|S_{xx}(f)||S_{xy}(f)|} \tag{15}$$

Due to the normalization by the individual autospectral density functions, the resulting coherence values lie between 0 and 1. At each frequency, a value close to 1 indicates high dependence between the signals whereas a value of 0 indicates complete independence.

Spectral density function and Partial Coherence

Comparison between K signals $x_i(n)$ is possible by using partial coherence. In order to calculate this measure, the spectral density function is derived by the cross-spectral density functions of all pairwise combinations:

$$\boldsymbol{S}(f) = \begin{bmatrix} S_{11}(f) & \cdots & S_{1K}(f) \\ \vdots & \ddots & \vdots \\ S_{K1}(f) & \cdots & S_{KK}(f) \end{bmatrix} \tag{16}$$

The partial coherence indicates the coherence remaining between two time series after the influence of all the other time series is removed from each of the first two [108]:

$$PC_{ij}(f) = \frac{|M_{ij}(f)|^2}{|M_{ii}(f)|\,|M_{jj}(f)|} \tag{17}$$

Where $M_{ij}(f)$ is the minor of the spectral density function $\mathbf{S}(f)$, which is the determinant of $\mathbf{S}(f)$ without the i^{th} row and j^{th} column.

2.5.3.2 Nonlinear measures

Due to several nonlinear neural processes, nonlinear functional connectivity measures were introduced. They provide complementary information under strict assumptions [106]. Usually, nonlinear measures investigate phase synchronization between signals, e.g. in the Phase Locking Value [109].

2.5.3.3 Information-based measures

Information theory resulted in some information-based measures that can include both linear and nonlinear statistical dependencies. An important concept is the entropy which measures the uncertainty or impurity of a certain variable [110]–[112], e.g. the Shannon entropy of a set of probabilities of signal x:

$$I_{\boldsymbol{x}} = -\sum_{i=1}^{M} p_i \log(p_i) \tag{18}$$

With p_i indicating the probability that signal x has value x_i, calculated from an M-bin histogram. The entropy can be used to define information-based measures such as the information gain or mutual information (MI) [111], [112]:

$$MI_{xy} = \sum_{i,j} p_{ij} \log \frac{p_{ij}}{p_i p_j} \tag{19}$$

With p_{ij} the joint probability of x and y, derived from the joint histogram. Correct estimation depends highly on the amount of samples and the size of the histogram bins [113]. MI is zero for complete independent processes and equal to the entropy for identical signals. MI is often used in brain machine interfaces to perform feature selection or to prune in decision trees [111], [112].

2.5.4 Effective connectivity

An important drawback of functional connectivity is the lack of causation. Effective connectivity, often termed directed functional connectivity, can overcome this drawback and can describe the direction of the information flow in various ways: model based techniques such as structural equation modeling [114] and dynamic causal modeling [115] or derived from the data as with Granger causality measures [116]–[118].

Granger causality was derived by Clive Granger and was originally used in econometrics. A time series is said to Granger cause a second one if inclusion of the past values of the first into the modeling of the second significantly reduces the variance of the modeling error. This means that the past values of a signal x_1 should contain information that help to predict x_2 better than by past values of x_2 alone. This dependence can be investigated separately for both directions, making it a directed functional or effective connectivity measure [119].

The focus in this work will be data-driven effective connectivity techniques. Autoregressive modeling will be introduced. Similarly as was the case for functional connectivity, three categories exist: linear, nonlinear and information-based measures. Only linear measures, as they are used in this work, are considered here with their respective extension to include time-variances. For the others, the reader is referenced to [13]. This section is based on [13], [107], [120]–[123].

2.5.4.1 Autoregressive modeling

In order to assess the Granger causality, autoregressive (AR) models are often used. In these models, the signals are represented as a linear combination of their own past plus noise. Granger causality then reduces to comparing the univariate AR model fit to the bivariate model fit. A univariate AR model can be described by the following equation with p the model order, a(m) the model coefficients and e(n) the error. The model order defines the number of past time points that are included to estimate the current sample.

$$x(n) = \sum_{m=1}^{p} a(m)x(n-m) + e(n) \tag{20}$$

For two signals, an analogous but bivariate AR model can be constructed:

$$x_1(n) = \sum_{m=1}^{p} a_{11}(m)x_1(n-m) + \sum_{m=1}^{p} a_{12}(m)x_2(n-m) + e_1(n) \tag{21}$$

$$x_2(n) = \sum_{m=1}^{p} a_{21}(m)x_1(n-m) + \sum_{m=1}^{p} a_{22}(m)x_2(n-m) + e_2(n) \tag{22}$$

Or in matrix formulation:

$$\begin{bmatrix} x_1(n) \\ x_2(n) \end{bmatrix} = \sum_{m=1}^{p} \begin{bmatrix} a_{11}(m) & a_{12}(m) \\ a_{21\,(m)} & a_{22}(m) \end{bmatrix} \begin{bmatrix} x_1(n-m) \\ x_2(n-m) \end{bmatrix} + \begin{bmatrix} e_1(n) \\ e_2(n) \end{bmatrix} \tag{23}$$

Although, equation 23 is represented for two signals, it can be extended to K signals, in which case a multivariate autoregressive (MVAR) model is obtained:

$$\boldsymbol{X}(n) = \sum_{m=1}^{p} \boldsymbol{A}(m)\boldsymbol{X}(n-m) + \boldsymbol{E}(n) \tag{24}$$

A critical parameter is the model order p. It can be estimated using a criterion like the Akaike Information Criterion [124] or Schwarz's Bayesian criterion [125]. Coefficients are then estimated by the least squares method or method of moments [126]. Relations between the signals in the frequency domain are obtained by the Fourier transformation of equation 24:

$$\boldsymbol{E}(f) = \boldsymbol{A}(f)\boldsymbol{X}(f) \tag{25}$$

where

$$\boldsymbol{A}(f) = -\sum_{m=0}^{p} \boldsymbol{A}(m)\, e^{-i\,2\,\pi\,\frac{f}{f_s}m} \tag{26}$$

With f_s the sampling frequency and $\mathbf{A}(0)$ the negative of the K x K identity matrix. The equation can be rewritten as:

$$\boldsymbol{X}(f) = \boldsymbol{A}^{-1}(f)\,\boldsymbol{E}(f) = \boldsymbol{H}(f)\,\boldsymbol{E}(f) \tag{27}$$

$\mathbf{H}(f)$ is defined as the transfer matrix of the MVAR model. It is a K x K matrix in which $\mathbf{H}_{ij}(f)$ estimates the information flow from signal $\mathbf{x}_j$ to $\mathbf{x}_i$ at frequency f.

The different parameters in the above representation of the AR models can be used to describe several effective connectivity measures: G-causality, Directed Coherence (DC), Directed Transfer Function (DTF) and Partial Directed Coherence (PDC). These measures include respectively two signals in the time domain, two signals or multiple signals in the frequency domain, and DTF and PDC both include multiple signals in the frequency domain.

2.5.4.2 G-causality index

As stated before, the bivariate Granger causality compares the univariate AR models ($V_{x|x}$) with the bivariate model ($V_{x|xy}$):

$$G_{xy} = \ln\left(\frac{V_{x|x}}{V_{x|xy}}\right) \tag{28}$$

If past values of y do not improve the prediction of x, then G approaches 0 since $V_{x|xy}$ approaches $V_{x|x}$. The better the prediction by including past values of y, the larger G will be. As indicated before, G_{xy} can be calculated similarly, indicating that the G-causality index is a direct functional or effective connectivity measure.

2.5.4.3 Directed Coherence

Analogous to Coherence and Partial Coherence, the Directed Coherence can be calculated, but with the inclusion of directionality [127], [128].

$$\boldsymbol{DC}_{xy}(f) = \frac{\sigma_{xy}\boldsymbol{H}_{xy}(f)}{\sqrt{\sigma_{xx}^2\,|\boldsymbol{H}_{xx}|^2 + \sigma_{yy}^2\,|\boldsymbol{H}_{yy}|^2}} \tag{29}$$

Since this measure is bivariate, each pair of signals has to be considered separately [129].

2.5.4.4 Directed Transfer Function

The DTF was defined in 1991 and is calculated as follows:

$$\boldsymbol{DTF}_{ij}(f) = \frac{|\boldsymbol{H}_{ij}(f)|^2}{\sum_{k=1}^{K} |\boldsymbol{H}_{ik}(f)|^2} \tag{30}$$

With normalization condition:

$$\sum_{k=1}^{K} \boldsymbol{DTF}_{ik}(f) = 1 \tag{31}$$

Which signifies that the total incoming information flow into each channel is equal to 1 at each frequency. DTF consists of information with respect to the cascade of information flow.

2.5.4.5 Partial Directed Coherence

In 2001 Partial Directed Coherence was introduced as multivariate directional connectivity measure only showing direct relations between the signals [122]:

$$\boldsymbol{PDC}_{ij}(f) = \frac{|\boldsymbol{A}_{ij}(f)|^2}{\sum_{k=1}^{K} |\boldsymbol{A}_{kj}(f)|^2} \tag{32}$$

With normalization condition:

$$\sum_{k=1}^{K} \boldsymbol{PDC}_{kj}(f) = 1 \tag{33}$$

Which indicates the total outgoing flow from each channel is equal to 1 at each frequency. PDC can identify the direct flows of information much better than DTF.

2.5.4.6 Integrated and Full-Frequency Adaptive DTF and PDC

In current research, new concepts are developed to be able to apply connectivity measures to brain signals. Therefore, time-dependent versions of DTF and PDC were introduced: the Adaptive Directed Transfer Function (ADTF) and the Adaptive Partial Directed Coherence (APDC) [123], [130].

Time-variant autoregressive modeling

Instead of MVAR models, time-variant autoregressive (TVAR) models are introduced:

$$\boldsymbol{x}(t) = \sum_{m=1}^{p} \boldsymbol{A}_m(t)\, \boldsymbol{x}(t-m) + \boldsymbol{e}(t) \tag{32}$$

With K the number of signals, p the model order, $\mathbf{x}(t) = [x_1(t) \ldots x_K(t)]^T$ the K x 1 signal matrix, $\mathbf{e}(t)$ the K x 1 matrix containing the uncorrelated noise and $\mathbf{A}_m(t)$ the K x K coefficient matrix for delay m at time point t. Estimation of the TVAR coefficients is an ill-posed problem and can be done by Kalman filtering [13], [131], [132].

Similarly as done for the non-time-dependent MVAR models, equation 32 can be Fourier transformed:

$$\boldsymbol{A}(f,t) = -\sum_{m=0}^{p} \boldsymbol{A}_m(t)\, e^{-i\,2\,\pi \frac{f}{f_s} m} \tag{33}$$

Eventually, one can note the following system equation:

$$\boldsymbol{X}(f,t) = \boldsymbol{A}^{-1}(f,t)\, \boldsymbol{E}(f,t) = \boldsymbol{H}(f,t)\, \boldsymbol{E}(f,t) \tag{34}$$

Matrix $\mathbf{H}(f,t)$ is called the time-variant transfer matrix of the system. Each element $\mathbf{H}_{ij}(f,t)$ expresses the amount of information flow from signal $\mathbf{x}_j$ to $\mathbf{x}_i$ at frequency f at time point t.

Adaptive DTF and PDC

Several measures can be defined based on the variables from the TVAR model. The Adaptive Directed Transfer Function (ADTF) is defined as follows [131], [132]:

$$\boldsymbol{ADTF}_{ij}(f,t) = \frac{|\boldsymbol{H}_{ij}(f,t)|^2}{\sum_{k=1}^{K} |\boldsymbol{H}_{ik}(f,t)|^2} \tag{35}$$

Similarly, the APDC can be defined [123]:

$$\boldsymbol{APDC}_{ij}(f,t) = \frac{|\boldsymbol{A}_{ij}(f,t)|^2}{\sum_{k=1}^{K} |\boldsymbol{A}_{kj}(f,t)|^2} \tag{36}$$

Both APDC and ADTF are normalized similar to PDC and DTF meaning that for ADTF incoming information flow into each channel is equal to 1 at each frequency at each time point and analogously for the outgoing flow in APDC.

The integrated ADTF and APDC

The integrated ADTF or iADTF is the integration over a specific frequency band of the ADTF. It has been used to localize the epileptic focus in patients [123], [130], [133]–[135]:

$$\boldsymbol{iADTF}_{ij}(t) = \frac{1}{f_2 - f_1} \int_{f=f_1}^{f_2} \frac{|\boldsymbol{H}_{ij}(f,t)|^2}{\sum_{k=1}^{K} |\boldsymbol{H}_{ik}(f,t)|^2} \tag{37}$$

Normalization assures that the sum of incoming information flow into a channel at each time point is equal to 1. The values of iADTF lie within [0,1]. Analogously, iAPDC can be defined as well:

$$\boldsymbol{iAPDC}_{ij}(t) = \frac{1}{f_2 - f_1} \int_{f=f_1}^{f_2} \frac{|\boldsymbol{A}_{ij}(f,t)|^2}{\sum_{k=1}^{K} |\boldsymbol{A}_{kj}(f,t)|^2} \tag{38}$$

Normalization here assures that the sum of outgoing information flow into a channel at each time point is equal to 1.

The full-frequency ADTF and APDC

In the previous section on iADTF, the normalization at each frequency disregarded the frequency content at other frequencies of the interval. A new measure is introduced where normalization incorporates the frequency information of all frequencies in the defined frequency interval [136]:

$$\boldsymbol{ffADTF}_{ij}(t) = \int_{f=f_1}^{f_2} \frac{|\boldsymbol{H}_{ij}(f,t)|^2}{\sum_{k=1}^{K} \int_{f'=f_1}^{f_2} |\boldsymbol{H}_{ik}(f',t)|^2} \tag{39}$$

Normalization is done in such a way that the sum of incoming information flow into a channel at each time point is equal to 1. Similarly, ffAPDC can also be defined:

$$\boldsymbol{ffAPDC}_{ij}(t) = \int_{f=f_1}^{f_2} \frac{|\boldsymbol{A}_{ij}(f,t)|^2}{\sum_{k=1}^{K} \int_{f'=f_1}^{f_2} |\boldsymbol{A}_{kj}(f',t)|^2} \tag{40}$$

With normalization assuring the sum of outgoing information flow into a channel at each time point equals 1.

2.6 Graph theory

Graph theory is the study of graphs, which are mathematical structures formed by vertices (or nodes) and edges connecting the vertices. Simple graphs are therefore defined by a set of vertices and a set of connections between these vertices [137]. An example is given Figure 2.24.

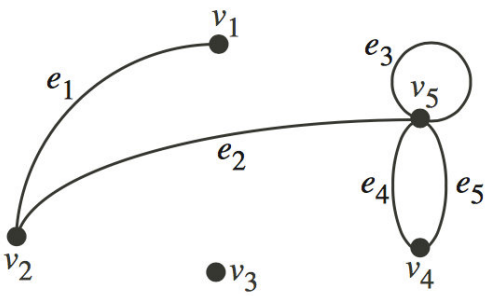

Figure 2.24: Example of a simple graph defined by vertices v and edges e [138].

Some extensions of the simple graph exist. Here, directed and weighted graphs are defined since these are useful in the performed research. A directed graph is a simple graph where the edges have a direction associated with them. An example is shown in Figure 2.25.

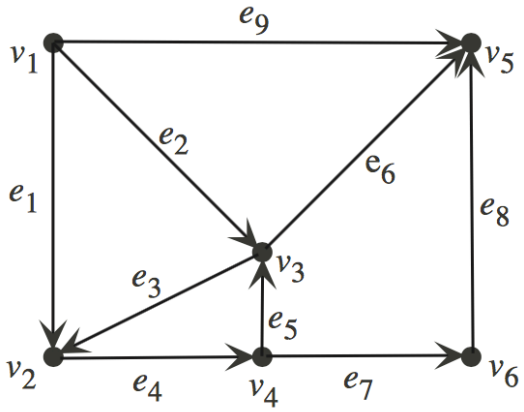

Figure 2.25: Example of a directed graph [138].

A weighted graph is a graph where edges are labeled with a certain weight (Figure 2.26). Typically, these weights are real numbers. Depending on the application, the significance of the labels is defined. For example, the shortest path between two vertices defines the path between two vertices such that the sum of the weights of the edges used is minimized. Weighted graphs can be directed or undirected.

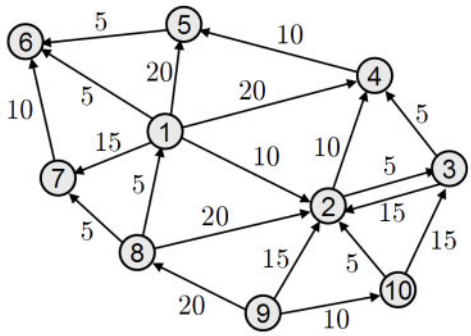

Figure 2.26: Example of a weighted directed graph [138].

Several measures, parameters and characteristics can be used to describe and analyze graphs. In this research, betweenness centrality is used as measure. Centrality measures indicate the importance of components within a graph. Betweenness centrality is a type of centrality measure that calculates the number of times a certain node is passed in the shortest paths from all nodes to all other nodes. Vertices that have a high probability to occur on a randomly chosen shortest path have a high betweenness value; the higher the betweenness value, the larger the importance of a node in a graph. Betweenness centrality can be defined for both undirected and directed graphs, but since directed graphs are used in this research, only the definition for the latter is defined here:

$$C_b(v_j) = \sum_{i=1}^{n} \sum_{k=1}^{n} \frac{g_{ik}(v_j)}{g_{ik}}, \forall\, i \neq j \neq k \tag{41}$$

In this equation $C_b(v_j)$ is the betweenness centrality value of node j, n is the amount of nodes in the graph, g_{ik} is the amount of shortest paths connecting node i to k and $g_{ik}(v_j)$ the amount of shortest paths from i to k that contain the node j [10].

Chapter 3

Methods

3.1 Introduction

In this master thesis, the effect of VNS on the brain of epilepsy patients is researched. The main focus is on identifying differences in brain activity and functioning between epilepsy patients in whom reduced seizure frequency due to VNS is observed (responders) and patients that experience little or no benefit (non-responders). Brain activity is measured with EEG and is investigated at three levels: sensor level, source level and brain connectivity level. For each of these levels, specific data is generated or calculated for two different conditions: VNS switched Off and VNS switched on. This allows elucidation of differences in brain activity and functioning between responders and non-responders due to the VNS treatment. Ultimately, significant differences could be helpful to unravel the mechanism of action (MOA) of VNS or to assess the efficacy of VNS treatment pre-operatively to avoid superfluous and risky implantation surgeries.

As discussed in section 2.4.6 of the literature review, current research indicates an important role for the locus coeruleus-norepinephrine (LC-NE) system in the therapeutic effect of VNS. Assessing the activity of the LC-NE system can be done indirectly by parameters modulated by the amount of noradrenergic signaling present in the brain. One of these parameters is the P3 or P300 component of the event-related potential (ERP) and it can be extracted from an EEG recorded during an auditory oddball experiment [9], [139]–[146].

Measuring and analyzing the P300 component of the ERP for both groups (responders and non-responders) and conditions (VNS Off and On) allows identifying differences in the influence of VNS on the LC-NE activity between responders and non-responders. This level of analysis is limited to the data directly recorded from the EEG and is further referred to as the sensor level analysis.

Estimating active brain regions during the auditory oddball experiment can be achieved by electrical source imaging (ESI). The obtained activity patterns are analyzed to identify differences with respect to group and condition, which is further referred to as the source level analysis.

The brain activity that is assessed in the source level analysis can also be used to go one step further in a brain connectivity analysis. Here, the interplay and functional connections between the active brain regions is investigated. Functional and effective connectivity measures indicate respectively the strength of functional interconnections between specific brain regions and the influence one neural system exerts over another. On top of that, the overall brain network can be analyzed using graph theory measures. In this research, betweenness centrality is used to identify important brain areas within the overall brain network. Differences in brain connectivity and network are studied to identify differences between responders vs. non-responders and VNS On vs. Off and this is further referred to as the brain connectivity analysis.

3.2 ERP and auditory oddball task

Event-related potentials or ERPs are defined as the potentials measured due to a brain response after a reference event. Typically, ERPs are extracted from an electroencephalogram (EEG). In practice this means that certain voltage deflections can be observed in the EEG after a given sensory stimulus is presented to the subject. ERPs consist of several components (Figure 3.2). Each component of the ERP has its specific characteristics and can be divided in smaller subcomponents. The P300 or P3 component is often used in research. P300 signifies that this wave is positive (P) and occurs around 300 ms after stimulus in young adults. P3 is often used as an alternative name and indicates that it is the third major positive peak in the ERP. The P300 or P3 wave contains a frontal P3a component and a parietal P3b component. The P300 wave can be evoked by a so-called oddball task where patients perform a task upon sensing a target stimulus but not when a standard stimulus is presented [147]. The meaning of the P300 wave is still under investigation, but much research has been done on factors influencing the amplitude and latency of this component. For example, the amplitude of the P300 wave is known to depend on the probability of the task-related target stimulus relative to the non-target-related standard stimulus. The amount of norepinephrine signaling in the brain also modulates the amplitude of the P300 wave and will be the underlying rationale for the data in this research [9], [148].

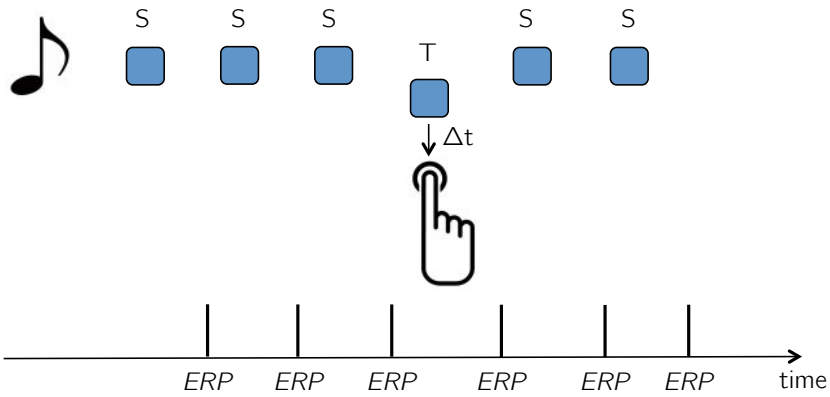

Figure 3.1: The auditory oddball paradigm. Patients press a predefined button only upon hearing a target tone (T) but not upon a standard tone (S). An ERP is generated after each stimulus.

The auditory oddball paradigm is a typical experimental paradigm to evoke a P300 wave in the recorded EEG. It consists of patients pressing a button in response to target tones (low frequency) and not to non-target or standard tones (high frequency) as presented in Figure 3.1 [147]. The P300 wave is larger after a task-related target stimulus (Figure 3.3). Due to the small single-trial response, the trials are often averaged (Figure 3.2).

Data used in this research was recorded by means of EEG during an auditory oddball experiment containing a series of 504 standard (or non-target) and 56 target tones presented randomly to the subject with 1s interstimulus intervals. This was done twice for all patients: once when VNS was switched On and once when VNS was switched Off, which allows to interpret the changes in P300 amplitude (and thus LC-NE activity) due to VNS [8]. To avoid learning/training as a cofounding factor, some patients started with VNS On trials, while others began with VNS Off trials.

3.3 Patients

Data of twenty epilepsy patients was recorded by De Taeye et al. by means of a scalp video-electroencephalogram in the Reference Center for Refractory Epilepsy, Ghent University, Ghent, Belgium [8]. Patients fulfilled three requirements: (1) at least 18 months of VNS treatment for refractory epilepsy, (2) older than 18 years, and (3) full-scale IQ score $\geq$ 70 on the Wechsler Adult Intelligence Scale, Third Edition. The first requirement stems from the fact that VNS efficacy tends to increase up to 18 months after implantation, as discussed in section 2.4.4 of the literature review. Patients were classified based on the reduction in mean monthly seizure frequency as being either a responder (>50% reduction) or a non-responder (≤50% reduction). This resulted in 10 responders and 10 non-responders.

All of the included patients had been implanted chronically with a VNS device (Cyberonics, Houston, TX, USA) and time since start of the VNS treatment varied between 1.5 and 16.2 years. Stimulation parameters were individual and gradually adjusted according to a standard ramping-up scheme as discussed in section 2.4.4 of the literature review. No significant differences in stimulation parameters were present between the groups of responders vs. non-responders. More details on the patients and stimulation parameters can be found in the original research by De Taeye et al. [8].

3.4 Electrophysiological recordings

A Micromed System Plus (Micromed, Mogliano, Italy) in combination with Ag/AgCl electrodes was used to record the EEG. The electrodes were placed at 60 standard locations according to the extended International 10-20 System using an electrode cap (WaveGuard EEG cap system, Eemagine, Berlin, Germany). The online reference electrode and the ground electrode were placed at electrode locations CPz and AFz respectively. Two facial electrodes on inferior and superior areas of the left orbit recorded a vertical electrooculogram (EOG). An electrocardiogram (ECG) was recorded using 2 ECG electrodes above the heart. In order to monitor the VNS artifacts, two additional electrodes were placed in the neck cranial and caudal with respect to the vagus nerve electrode. The EEG, EOG, ECG and VNS signals were digitized online using a sampling frequency of 1024 Hz, antialiasing filter of 250 Hz, gain of 50 dB and a resolution of 16 bits.

3.5 Processing

3.5.1 Pre-processing

Extracting the ERP and P300 component from the measured EEG signals requires further processing of the data. This was done by a commonly used sequence of data transformations and was performed separately for each patient and condition [149]. First, the data was filtered by a 50 Hz notch filter to reduce interference from the electricity grid and by a band-pass filter between 0.1 and 30 Hz with slope of 12 dB/Oct to reduce other unwanted influences such as muscle artifacts. Next, the data was downsampled to 256 Hz. Artifacts coming from eye movements, eye blinks, heartbeat and VNS signals were removed using the EOG, ECG and VNS

signal measurements. Performing Independent Component Analysis (ICA) and subsequent removal of the components generating the artifacts of the eyes, heartbeat and VNS removed them from the EEG data. Then, the data was re-referenced to the average of the recorded EEG channels. All pre-processing was performed in BrainVision Analyzer 2.0 (Brain Products GmbH, Gilching, Germany).

3.5.2 Epoching

After the initial pre-processing steps were performed, the EEG was cut into small segments (epochs) with a single epoch starting 200 ms pre-stimulus and ending 1000 ms post-stimulus. An example of the principle of epoching can be seen in Figure 3.2. The data used in this research was recorded during a series of 504 standard (or non-target) and 56 target tones. This means that 560 epochs were created and labeled by the appropriate marker (target or standard). The epochs were baseline corrected on the 200 ms pre-stimulus interval. All epoching was performed in BrainVision Analyzer 2.0 (Brain Products GmbH, Gilching, Germany).

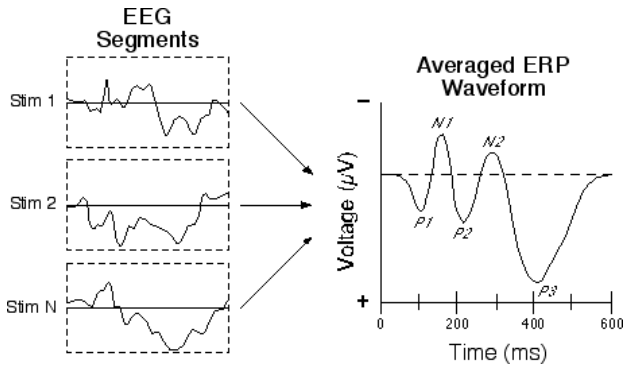

Figure 3.2: Event-related potentials (ERPs) are generated after a certain sensory stimulus. Recording is done by EEG. The EEG is split into segments or epochs with respect to the presented stimuli (left). Averaging all trials reveals different components in the ERP (right). Adapted from [148].

3.5.3 Averaging

Epochs after a single stimulus are often noisy and an ERP can be hard to detect (as in the example on the left in Figure 3.2). Therefore, epochs belonging to the same type of stimulus are averaged together. This results in two average epochs for each patient and each condition: one for the non-task-related standard stimulus and one for the task-related target stimulus. Due to averaging, the signal-to-noise ratio is increased and the P300 component of the ERP is visible. An example can be seen in Figure 3.3 for one patient and one condition in the Pz channel. It is clear that the P300 wave is mainly visible after task-related target stimuli and not after non-task-related standard stimuli.

To isolate the P300 component from other ERP waves, a target-standard difference waveform is calculated since other ERP components are thought to show no or much less differences between the standard and target epoch in auditory oddball experiments. The difference waveform is calculated by subtracting the average epoch for the standard stimulus from the average epoch for target stimulus for each patient, each condition and each EEG channel separately. The difference waveforms form the basis for subsequent sensor and source space analyses and represent the difference in P300 wave after target stimuli compared to standard stimuli. All averaging was performed in BrainVision Analyzer 2.0 (Brain Products GmbH, Gilching, Germany).

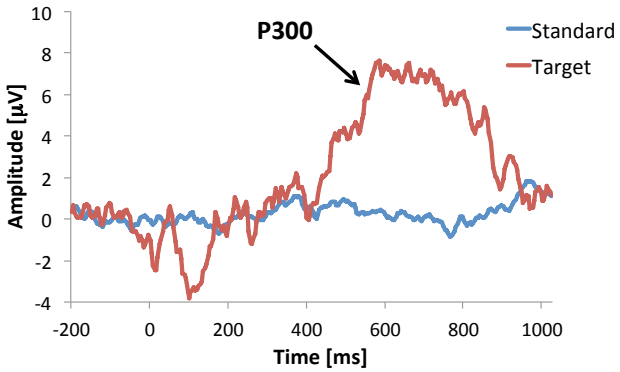

Figure 3.3: Average epoch after task-related target stimulus and non-task-related standard stimulus for the auditory oddball experiment. Time is given relative to the moment of stimulus. The P300 wave is larger after a task-related target stimulus.

3.5.4 P300 features

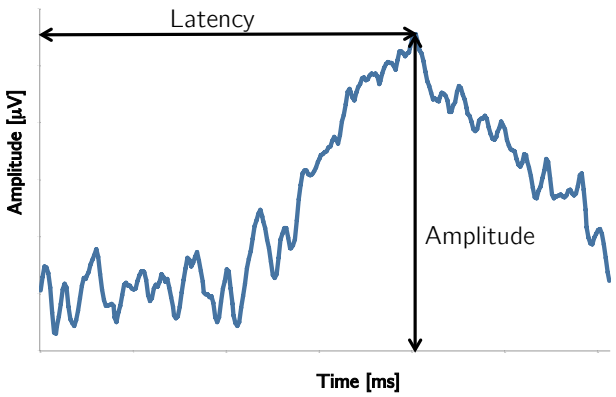

Figure 3.4: Schematic representation of the features extracted at the sensor level from the target-standard difference waveform. For each patient and each condition the P300 latency is determined in the Pz channel. The amplitude of the P300 wave in each channel at the peak moment in the Pz channel is extracted. The latency in the Pz channel and the P300 amplitude in all EEG channels are the features for the statistical analyses at sensor level.

Several characteristics or features of the P300 wave in the target-standard difference waveform can be identified and analyzed (Figure 3.4). The moment of the peak in the P300 wave or peak

latency was determined automatically using Analyzer in the 300-900 ms post-stimulus interval at the parietal midline electrode Pz since the P300 wave is known to be mainly present parietocentrally [8]. At this latency the amplitude of the P300 wave in all EEG channels was extracted. Extraction of the P300 amplitude in all EEG channels was performed for all patients and all conditions using Matlab R2012a (Mathworks, Natick, MA, USA). These features are used to perform statistical analyses at the sensor level.

3.5.5 Electrical source imaging

To analyze the data at source level, the activity in the brain is estimated for each patient and each condition. Therefore, electrical source imaging (ESI) was performed from the EEG channel amplitudes in the respective target-standard difference waveform in an 80 ms interval around the P300 peak using Matlab and statistical parametric software (SPM, Wellcome Trust Centre for Neuroimaging, London, Great Britain). A detailed description of the ESI principle is given in section 2.2.3 of the literature review. The used head models for ESI were patient-specific for 14 patients (5-layered segmentation based on individual MRI images: scalp, skull, CSF, gray matter, white matter). For 6 patients a template head model (SPM's 4-layered T1 template) was used since their MRI images were too poor. A multiple sparse volumetric priors algorithm based on region growing in gray matter was used, which was developed by Strobbe et al. in the Medical Imaging and Signal Processing (MEDISIP) research group, Ghent University, Ghent, Belgium [150]. The distributed source model in this approach consists of gridpoints in the gray matter (not in the cerebellum) with a spacing of 3 mm. Therefore, a cubic voxel containing one dipole has a volume of 27 mm^3. Source priors were grown in the gray matter and are volumetric bell-shaped. Full-width at half maximum (FWHM) depends on the maximum distance r to a seed point and smoothing σ. The maximum distance r was chosen to be 7 mm and the smoothing σ was 0.7. These values proved to be successful in previous research [151]. The number of patches used as prior was 512.

To compare the resulting dipole activity patterns or brain activity between patients and conditions, all activity was projected (warped) onto the template head model by aligning the individual head models with the template head model. Warping was achieved by using SPM. First, the individual head models were reoriented so that their origin was situated on the anterior commissura. Next, the individual head models were coregistered with the template head model as reference image. Normalized Mutual Information was used as objective function for the coregistration. Default SPM settings for separation, tolerance, histogram smoothing and interpolation parameters were used. After the coregistration, the images were normalized with default SPM settings and the template head model as template image. Lastly, the images were smoothed with FWHM of 8 in each coordinate.

3.5.6 Brain connectivity

The analysis of the brain activity can also be extended to investigate how the active brain regions interact with each other. In research, the importance of including connectivity and whole-brain network analyses in understanding epilepsy is prominently present [152]–[155]. This third level of analysis combines source imaging with connectivity measures. This consists of determining differences in the connectivity between different brain regions with respect to group and condition. To do so, first ESI was performed at each sample of a 9s interval of the original pre-processed EEG channels. This interval was chosen to include both standard and trigger stimuli. To calculate connectivity between brain regions, so-called Regions of Interest (ROI) are identified. The Automated Anatomical Labeling (AAL) template was used to define 116 standard regions of interest (ROI) in the brain volume (Appendix Table A) [156]. The images at each interval are warped to the template model as explained in the previous section. Each dipole from the source model is then linked to the appropriate brain region using the AAL toolbox for Matlab (Groupe d'Imagerie Neurofonctionnelle, Bordeaux, France). Performing a Single Value Decomposition (SVD) analysis for the dipole time series in each ROI with preservation of the first component, extracted a single activity time series for each brain region or ROI.

Correlation, a functional connectivity measure, is calculated between the two time series in all combinations between two different brain regions for all patients and all conditions. Statistical analysis was performed to identify differences in correlation between brain regions with respect to group and condition. More information on the correlation is given in section 2.5.3 of the literature review.

Next to correlation, also the effective connectivity measures iADTF, iAPDC, ffADTF and ffAPDC were used. These measures were applied similarly as in [13] and are discussed in section 2.5.4.6 of the literature review. To reduce the computation time, the 116 ROIs from the AAL template were reduced to 27 larger ROIs (Appendix Table A). These were chosen as the second-to-last level of regional split in the AAL template as presented in [156] and they were determined by combining the activity time series from the corresponding 116-regional ROIs by SVD. A model order of 10, a Kalman smoother with value 100 and an update coefficient of 0.001 were used.

A last analysis on the brain connectivity level was performed by analyzing the betweenness centrality of all brain regions. This measure requires representing the brain network as a graph. In this research, the 27 ROIs as used for the effective connectivity were used as nodes of the graph and the strengths of the connections as calculated by the effective connectivity measures were used as the edge labels or connection weights for the connections between the nodes. To reduce computation time, the warping was done inversely, meaning that the ROIs of the template head model were warped onto the individual head models. The betweenness centrality

value of each node indicates the importance of this region in the global brain network. More information on graph theory and betweenness centrality is given in section 2.6 of the literature review.

3.5.7 Statistical analysis

Mixed-model ANOVA, post-hoc t-tests and multiple comparison corrections

In the following analyses, several ways of analyzing data in a statistical manner are used. In this research, each data point belongs to one of the following 4 categories: responders with VNS On, responders with VNS Off, non-responders with VNS On and non-responders with VNS Off. Therefore, all data can be sorted based on two factors: the factor 'group' (responder or non-responder) and the factor 'condition' (VNS On or Off). The factor 'group' is a so-called between-subjects factor because the subjects (patients) present in the responder category are not the same patients as in the non-responder category. On the other hand, the factor 'condition' is a within-subjects factor because the patients present in the VNS On category are the same as the patients present in the VNS Off category because for all patients an EEG was recorded twice (once when VNS was switched On and once when VNS was switched Off).

Therefore, all data in this research can be analyzed in three ways, based on the factor of interest. This analysis is performed by using a so-called mixed-model analysis of variance (ANOVA), which allows identifying differences in terms of two or more different types of factors. A first comparison can be made between the two conditions independent of the group. This means that the data is analyzed to identify differences between the situation where VNS was switched On in comparison with VNS Off without taking into account if the patients where responders or non-responders. This comparison is termed 'main effect of condition'. Similarly, data can be analyzed to identify differences between responders and non-responders independent of VNS being switched On or Off, which is called the 'main effect of group'. Lastly, mixed-model ANOVA also analyzes the so-called interaction effect. This interaction effect indicates if the difference in one factor depends significantly on the level of the other factor and vice versa. This means that the interaction effect indicates whether the differences between responders and non-responders depend significantly on whether VNS was switched On or Off.

The main effect of group, the main effect of condition and the interaction effect are the three analyses that are incorporated in a mixed-model ANOVA. A significance level of 0.05 is used in all ANOVA analyses, meaning that a result is labeled as 'significant' if the probability that the data in both categories is actually sampled from the same population distribution is less than 5%.

After a mixed-model ANOVA is performed, the results can be analyzed in greater detail by so-called post-hoc t-tests. Of the four categories introduced in the previous paragraph, t-tests can

compare two with each other. This means that four t-tests are performed. A first t-test compares the categories VNS On and Off (condition) for responders, meaning that differences between the situation when VNS was switched On and when VNS was switched Off are compared for responders only. Similarly, a second t-test compares the VNS categories (condition) for non-responders. Thirdly, the data can be compared between responders and non-responders (group) for VNS On only and fourthly this comparison between groups can also be done for VNS Off. The t-tests where the effect of condition is investigated for one level of the group factor are performed by a paired samples t-test because the patients are the same in the two compared categories. On the other hand, investigating the effect of group for one level of condition is done by an independent samples t-test because the patients are not the same in both categories. All t-tests performed in this research are two-tailed meaning that the analyses investigate whether the data differs significantly between categories. One-tailed analyses can be used to detect significant increases and decreases, but it is required to know in advance which of the two groups will have higher values, which is not the case in this research. In this research, all t-tests are performed with a significance level of 5%.

Just by chance, due to the significance level of 5%, when many comparisons are made between the same patients, several comparisons (5% of all comparisons) will deliver significant results. These significant results by chance are termed Type I errors. Several techniques are developed to overcome this 'multiple comparison problem'. No golden standard exists for this problem. In this research, the Bonferroni and the Benjamini-Hochberg correction are applied. The Bonferroni correction reduces the significance level for a single comparison to make sure that the probability that one or more of all the comparisons made result in a Type I error, is limited to 5%. This is done by dividing the significance level of 5% by the amount of comparisons made and using this new value as significance level for each single comparison [157]. Therefore, the Bonferroni correction has very low power (probability of detecting the difference if there is a true difference) for a large amount of comparisons. Another option to limit the false discovery rate by chance is to use the Benjamini-Hochberg approach. By choosing a certain parameter (the false discovery rate) only a certain portion of the results is kept as a true significant result [158].

Sensor level

The statistical analysis for the P300 amplitude and latency features was performed using SPSS 21 (SPSS, Chicago, IL, USA). A mixed-model ANOVA and post-hoc t-tests as explained above are used for all features. Data of patient 7 was not used due to poor P300 presence.

Logistic regression analysis was performed using SPSS to test whether features could be identified that are good indicators to differentiate responders from non-responders. In logistic regression, a probability model is built based on a certain logistic function. Logistic regression is chosen since it can be used to separate categorical outcome variables, while other regression

techniques require continuous outcome variables [159]. Thus, in logistic regression, the probability of a certain level of the categorical variable is regressed with a certain feature. In this research, the created model indicates the probability that a certain value of a feature belongs to a (non-) responder. Therefore, the model can be used to separate responders from non-responders. In this research, logistic regression is performed by using the binary logistic regression functionality of SPSS. Logistic regression is calculated for those features that proved to vary significantly between responders and non-responders in the post-hoc two-tailed t-tests for the P300 amplitude. For features that proved to exhibit a significant effect of condition, the relative amplitude increase from VNS Off to On was used as feature for the logistic regression analysis. Odds ratios (OR) were calculated with 95% confidence intervals (CI). The odds ratio indicates the change in probability for a certain value to belong to a (non-) responder by a 1% increase of the value.

Receiving operating characteristic (ROC) curve analysis is performed in SPSS for those features that could be used to obtain a significant logistic regression model. A ROC curve indicates the sensitivity and specificity of a binary classifier for different cut-off values. The sensitivity is defined here as the proportion of values associated with responders that are actually classified as belonging to responders. The specificity is defined as the proportion of values associated with non-responders that are actually classified as belonging to non-responders. Also the positive and negative predictive value can be calculated. The positive predictive value is the proportion of values classified as belonging to responders, which actually belong to responders. The negative predictive value calculates the same for non-responders. These are important measures to indicate the accuracy with which a certain feature can be used to classify patients as being either responder or non-responder.

Cross-validation allows estimating how accurate an unknown patient can be classified as being either a responder or non-responder based on a certain feature. In cross-validation, the patients are divided in two groups: a validation set and a training set. First, a classification model is built based on the values present in the training set. Then, the patients in the validation set are classified, using the model that was built with the training set, as being either a responder or non-responder. The amount of patients of the validation set that are classified correctly indicate the estimation of the accuracy with which an unknown patient can be classified as being either a responder or non-responder using the given feature. In this research, a 10-fold cross-validation was calculated, meaning that the patients are divided in 10 subsets (9 sets of 2 patients and 1 set of 1 randomly chosen patient). Next, cross-validation was performed 9 times. In each of the 9 iterations, a different two-patient subset is used as validation set and the other 9 subsets are used as training set. Therefore, in each iteration two patients are classified, meaning that for each iteration the accuracy can be either 0%, 50% or 100%. After the 9 iterations, 18 patients are classified once; the randomly chosen one-patient subset is not classified. The results of these 18 classifications can be modeled by a binomial distribution since for each patients, the result can be either good or wrong. Combining the

results of the 10-fold cross-validation in a binomial distribution allows calculating mean and standard deviation for the cross-validation accuracy using a certain feature. The mean and standard deviation represent the estimation of the accuracy with which an unknown patient can be classified as being either a responder or non-responder. Cross-validation is performed in Matlab by using a generalized linear model with linear model specification for binomial distributions and with a logit link function. Both single-channel features and two-channel features are used. In the two-channel features, the P300 amplitude of two EEG channels is either used simultaneously or combined into a new single feature. No more than two features are used simultaneously due to the small amount of data points. Combining more than two features into a new single feature is not done here due to lack of time.

Source level

A flexible factorial design for the brain activity was performed using a 2^{nd}-level analysis in SPM. Contrast weights were defined as given in [160] for flexible factorial designs. P values were not FWE corrected. Data of patient 3 was not used due to irregularities in the head model. Visualization of the active dipoles was done using the SPM Anatomy toolbox (Forschungszentrum Jülich GmbH, Jülich, Germany).

Functional connectivity

Using the AAL template, 116 ROIs were defined on the template head model (Appendix Table A) [156]. By using the warping technique and SVD as described above, for each of these ROIs one activity time series was calculated. The correlation value was calculated using Matlab between the two time series for all combinations of two ROIs. Since correlation is an undirected measure, this resulted in 6670 correlation values between two different ROIs for each patient and condition. These values were analyzed by a mixed-model ANOVA and post-hoc two-tailed t-tests similar as for the sensor level. To account for the multiple comparisons, the results of the post-hoc two-tailed t-tests were analyzed twice for two different correction techniques: (1) Bonferroni correction (family wise error rate of 0.05) and (2) False Discovery Rate was controlled by using Benjamini-Hochberg approach (false discovery rate of 0.1 and significance level of 0.05).

Effective connectivity

To reduce the computation time, the 116 ROIs were reduced to 27 ROIs as indicated in section 3.5.6. The effective connectivity analysis was performed in 5 different frequency bands. These frequency bands are indicated by $\delta, \theta, \alpha, \beta$ and γ, indicating the following frequency bands: 0-4 Hz, 4-8 Hz, 8-16 Hz, 16-32 Hz and 32-64 Hz respectively. Four effective connectivity measures (iADTF, ffADTF, iAPDC, ffAPDC) were calculated between the activity time series for all

combinations of two ROIs for all patients, all conditions and all frequency bands. This was done in Matlab by using an implementation by Pieter van Mierlo [13]. The differences between the four measures are explained in section 2.5.4 of the literature review. APDC measures perform well in identifying direct information flows whereas ADTF measures perform better in identifying the cascade of information flow. The prefixes 'i' and 'ff' define the type of the used averaging method over given frequency bands. Since the result of these four effective connectivity measures is a time-dependent connection strength, time-averages and standard deviations were calculated to be able to analyze differences between groups and conditions. Time-average or mean indicates the overall strength of the connection while standard deviation reflects the time-dependent fluctuations in this strength. This means that in total 29160 different features (4 measures, 5 frequency bands, mean and standard deviation for each measure and 729 different combinations between two of the 27 ROIs) are performed to identify differences between responders vs. non-responders and VNS Off vs. On. Mixed model ANOVA and post-hoc two-tailed paired and independent samples t-tests were performed for both time-average and standard deviation of all features. Bonferroni (family wise error rate of 0.05) and Benjamini-Hochberg (false discovery rate of 0.1 and significance level of 0.05) multiple comparison corrections were applied to the post-hoc t-test results.

Brain network

A final analysis is done on the global brain network. Therefore, the brain was represented as a graph. The 27 ROIs defined in the previous section are used as nodes and the weights of the edges between them were defined by the mean effective connectivity values as calculated using iADTF, iAPDC, ffADTF and ffAPDC. Thus, the brain was represented as a directed graph. The calculation of the betweenness centrality is done for each node, for each effective connectivity measure as connection weights and in each frequency band. Therefore, difference between responders vs. non-responders and VNS Off vs. On are assessed in 540 analyses (27 nodes, 4 different connection weights and 5 frequency bands). Mixed-model ANOVA and post-hoc two-tailed independent and paired samples t-tests were used to identify differences between groups and conditions. To calculate the betweenness centrality, the MatlabBGL library was used [161].

Chapter 4

Sensor level

The locus coeruleus-norepinephrine (LC-NE) system is thought to be one of the key brain structures involved in the anti-epileptic effect of VNS. The amplitude of the P300 wave in an event-related potential (ERP) is modulated by the activity of this LC-NE system. By analyzing P300 features (latency and amplitude) between responders and non-responders (group) for both VNS On and Off (condition), statistical significant differences can be identified both with respect to group and condition.

Analyzing the extracted features is done at sensor level by performing statistical analyses directly on the P300 features. For each patient and each condition, latency is determined in the Pz channel and the P300 amplitude is extracted in all EEG channels as presented in Figure 3.4. Each measured feature value belongs to one of the following four categories: responders with VNS On, responders with VNS Off, non-responders with VNS On and non-responders with VNS Off. Therefore, data can be analyzed with respect to two factors: (1) the factor 'group' with two levels, namely responder and non-responder, and (2) the factor 'condition' with two levels, namely VNS Off and On.

Mixed-model ANOVA allows analyzing the data in three different ways depending on the factor of interest. The first comparison, the so-called main effect of group, compares responders with non-responders independent of VNS being switched On or Off. This means that the main effect of group compares groups irrespective of condition. The main effect of condition on the other hand compares conditions irrespective of group. Lastly, the mixed-model ANOVA also analyzes the so-called interaction effect, which determines if differences in a certain factor depend on the level of the factor. Thus, the interaction effect indicates if differences between responders and non-responders depend significantly on whether VNS was switched Off or On and vice versa. After the mixed-model ANOVA, the obtained results can be investigated in greater detail by post-hoc t-tests. These tests allow identifying differences for one level of a certain factor in terms of one level of the other factor, e.g. differences between responders and non-responders for VNS Off only.

Logistic Regression Analysis allows assessing whether the values of a given feature can be used to distinguish responders from non-responders. It is performed on those features that

showed significant differences between responders and non-responders for the post-hoc t-tests. Receiving Operator Characteristic (ROC) curve estimation delivers the sensitivity and specificity of the distinction between responders and non-responders for a given cut-off value of a certain feature. The sensitivity is defined here as the proportion of values associated with responders that are actually classified as belonging to responders. The specificity is defined as the proportion of values associated with non-responders that are actually classified as belonging to non-responders. ROC is performed for those features that could be used to build a statistical significant logistic regression model.

Lastly, cross-validation is applied since this technique allows making an estimation of the accuracy with which an unknown patient can be identified as being either a responder or non-responder. In cross-validation, a classification model is built based on the values of a certain feature for patients that were previously classified as responders or non-responders. Unknown patients can then be classified with this model as being either responder or non-responder by measuring the given feature for these patients. This is in contrast to the logistic regression and ROC curve since these build and characterize the classification models on known patients only. Cross-validation is performed for those features that could be used to build a statistical significant logistic regression model. In this research, 10-fold cross-validation is used to estimate the accuracy with which an unknown patient could be classified as being a responder or non-responder based on the value of a certain feature. Both single-channel and two-channel features are used. More information on the methods, data and analyses is given in Chapter 3.

4.1 Latency

A mixed-model ANOVA was performed for the latency values relative to stimulus onset. The measured values can be seen in Appendix Table B and the results are given in Appendix Table C. None of the three analyses incorporated in a mixed-model ANOVA showed significant results: (1) there is no significant difference in P300 latency between responders and non-responders irrespective of VNS, (2) nor is there a significant difference between VNS Off and On irrespective of the patient group, and (3) the difference between responders and non-responders does not depend significantly on whether VNS was switched Off or On and vice versa.

4.2 P300 amplitude

4.2.1 Influence of group and condition

The P300 amplitude in each of the 60 EEG channels is measured at the latency detected in the Pz channel. Significant influences on the P300 amplitude of being a responder or non-responders (group) and of VNS being switched On or Off (condition) are analyzed by a mixed-model ANOVA. The results are given in Appendix Table D.

No EEG channels display a significant main effect of condition. Therefore, there is no significant difference noticed between VNS On and Off irrespective of the patients being responders or non-responders for any of the EEG channels.

For the main effect of group, however, 23 EEG channels show a significant result meaning that for these channels, there is a significant difference between the P300 amplitude in responders and non-responders irrespective of VNS being switched On or Off. In these channels the P300 amplitude for non-responders is larger than for responders. The left panel of Figure 4.1 indicates the significant channels.

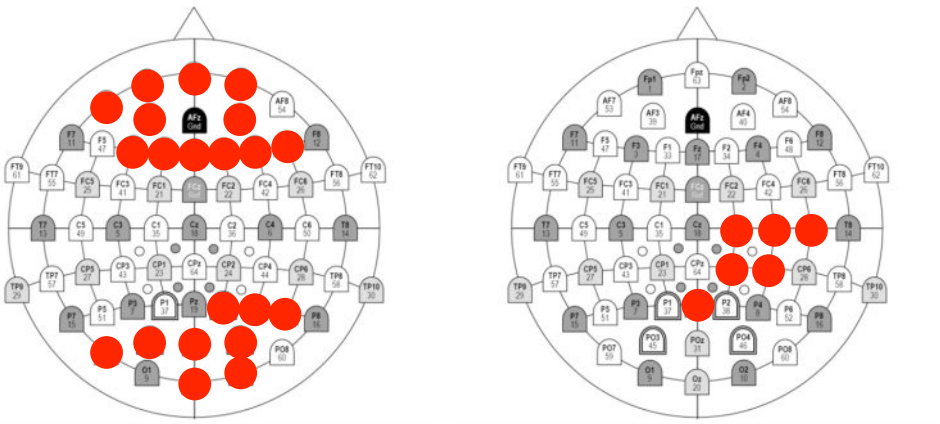

Figure 4.1: Red dots indicate the EEG channels that exhibit a significant main effect of group (left) and a significant interaction effect (right) for the P300 amplitude.

When using a mixed-model ANOVA, the result of interest is usually the interaction effect. A significant interaction effect indicates that the difference in P300 amplitude between responders and non-responders depends significantly on whether VNS was switched On or Off and vice versa. Here, 6 EEG channels show a significant interaction effect, namely CP2 (p=0.004), C2 (p=0.017), C4 (p=0.006), Pz (p=0.034), C6 (p=0.016) and CP4 (p=0.012). These channels are represented in the right panel of Figure 4.1. The interaction effects are visualized in Figure 4.2.

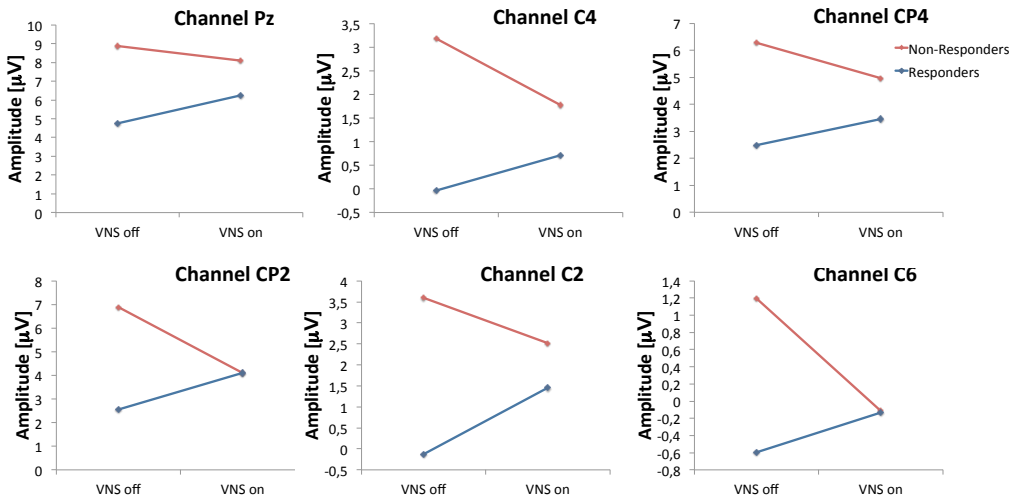

Figure 4.2: Six EEG channels show a significant interaction effect between group and condition for the P300 amplitude.

As can be seen in Figure 4.2, for each of the channels displaying a significant interaction effect the P300 amplitude is larger for non-responders than for responders both when VNS is On and Off. Also, when VNS is switched on, the P300 amplitude increases for responders while it decreases for non-responders.

To analyze the results further, post-hoc two-tailed t-tests are performed. In contrast to the analyses above, these tests analyze one level of a certain factor (e.g. responders) with respect to one level of the other factor only (e.g. VNS Off). The results can be seen in Appendix Table E. These tests reveal that for VNS Off there are 15 EEG channels that show a significant difference between responders and non-responders. For VNS On, this is the case for 20 EEG channels. For the channels that showed a significant interaction effect it can be seen that channels C4 (p=0.0079) and C6 (p=0.023) display a significant difference between VNS Off and On for non-responders. Channels CP2 (p=0.009) and Pz (p=0.014) display a significant difference between VNS Off and On for responders (Figure 4.3).

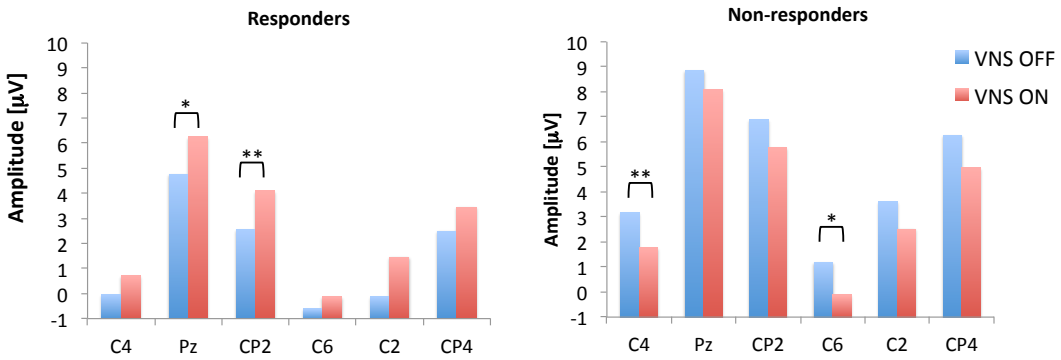

Figure 4.3: Results of the post-hoc two-tailed t-tests for the EEG channels that showed a significant interaction effect. Pz and CP2 show a significant difference between VNS Off and VNS On for responders while channels C4 and C6 show a significant difference between the two conditions for non-responders. * and ** indicate significant results at a significance level of 0.05 and 0.01 respectively.

To investigate the EEG channels further that showed a significant interaction effect, the relative change in P300 amplitude is (On-Off/On) is analyzed as well. The results are given in Appendix Table F. Only the Pz channel exhibits a significant difference (p=0.014) between responders and non-responders in terms of relative P300 amplitude change.

4.2.2 Logistic Regression Analysis

Logistic regression analysis was performed on different features (P300 amplitude in different EEG channels) to test whether these features were good indicators to differentiate responders from non-responders. Logistic regression is chosen since it can be used to regress categorical outcome variables to continuous input variables, while other regression techniques require continuous outcome variables. The analysis is performed on the EEG channels that showed a significant difference between responders and non-responders for VNS Off (15 channels) or On (20 channels) in the previous section. The relative P300 amplitude changes in the 6 channels that showed a significant interaction effect (C4, Pz, CP2, C2, C6, CP4) are also used in logistic regression. The results for VNS Off are given in Appendix Table G, for VNS On in Appendix Table H and for the relative amplitude change in Appendix Table I. More information on Logistic Regression Analysis is given in section 3.5.7 of the previous chapter.

For VNS Off, six EEG channels deliver a logistic regression analysis with statistical significance to distinguish responders from non-responders: F3 (p=0.043, OR=1.44), Pz (p=0.035, OR=0.57), P4 (p=0.042, OR=0.60), CP2 (p=0.031, OR=0.61), CP4 (p=0.03, OR=0.63) and P2 (p=0.042, OR=0.55). The OR indicates the change in probability of being a responder for a 1% increase in P300 amplitude. For example, for a 1% increase in P300 amplitude in channel F3, the probability of being a responder increases by 44%.

For VNS On, 12 EEG channels deliver a logistic regression analysis with statistical significance to distinguish responders from non-responders: F3 (p=0.049, OR=1.65), Fz (p=0.049, OR=1.72), Oz (p=0.027, OR=0.62), O2 (p=0.027, OR=0.60), PO7 (p=0.046, OR=0.66), Poz (p=0.027, OR=0.62), AF3 (p=0.019, OR=1.99), AF4 (p=0.038, OR=1.81), F1 (p=0.040, OR=1.60), PO3 (p=0.037, OR=0.64), PO4 (p=0.042, OR=0.65) and PO6 (p=0.045, OR=0.64).

For the relative P300 amplitude change, only the Pz channel (p=0.038, OR=1.05) delivers a statistical significant logistic regression model to separate responders from non-responders.

4.2.3 Receiving Operator Characteristic curve

A ROC curve indicates the sensitivity and specificity of a binary classifier for different cut-off values. The sensitivity is defined here as the proportion of values associated with responders that are actually classified as belonging to responders. The specificity is defined as the proportion of values associated with non-responders that are actually classified as belonging to non-responders. Also the positive and negative predictive value can be calculated. The positive predictive value is the proportion of values classified as belonging to responders, which actually belong to responders. The negative predictive value calculates the same but for non-responders. The ROC was calculated for statistical significant logistic regression models from the previous section. More information on the ROC analysis is given in section 3.5.7 of the previous chapter.

	Sensitivity (%)	Specificity (%)	Positive predictive value (%)	Negative predictive value (%)
F3	80	67	73	75
Pz	70	100	100	75
P4	80	67	73	75
CP2	90	78	82	88
P2	70	100	100	75
PO3	80	78	80	78
PO4	80	78	80	78
PO6	80	89	89	80

Table 4.1: ROC results for the analysis of the EEG channels for which a significant logistic regression model could be build to differentiate responders from non-responders for VNS Off.

From Table 4.1 it can be seen that several features perform good in separating responders from non-responders for VNS Off. In particular channel PO6 performs well.

	Sensitivity (%)	Specificity (%)	Positive predictive value (%)	Negative predictive value (%)
F3	90	78	82	88
Fz	80	89	89	80
Oz	80	78	80	78
O2	80	78	80	78
PO7	70	100	100	75
Poz	80	78	80	78
AF3	80	89	89	80
AF4	70	89	88	73
F1	80	78	80	78

Table 4.2: ROC results for the analysis of the EEG channels for which a significant logistic regression model could be build to differentiate responders from non-responders for VNS on.

Similarly as for VNS Off, also here for VNS On (Table 4.2) there are several features that result good in separation of responders from non-responders.

Also the relative amplitude change in the Pz channel (Table 4.3) results in good separation.

	Sensitivity (%)	Specificity (%)	Positive predictive value (%)	Negative predictive value (%)
Pz	70	89	88	73

Table 4.3: ROC results for the analysis of the Pz channel for the relative P300 amplitude increase from VNS Off to VNS on.

4.2.4 Cross-validation

Cross-validation allows estimating how accurate an unknown patient can be classified as being either a responder or non-responder based on a certain feature. In this research, a 10-fold cross-validation was calculated, meaning that the patients are divided in 10 subsets (9 sets of 2 patients and 1 set of 1 randomly chosen patient). Next, cross-validation was performed 9 times. In each of the 9 iterations, a different two-patient subset is used as validation set and the other 9 subsets are used as training set. A classification model is built based on the training set allowing to classify the patients in the validation set as being either responder or non-responder. Therefore, in each iteration two patients are classified, meaning that for each iteration the accuracy can be 0%, 50% or 100%. After the 9 iterations, 18 patients are classified once; the randomly chosen one-patient subset is not classified. The results of these 18 classifications can be modeled by a binomial distribution since for each patients, the result can be either good or wrong. Combining the results of all iterations in the 10-fold cross-validation in a single binomial distribution allows calculating mean and standard deviation for the cross-validation accuracy. The mean and standard deviation represent the estimation of the accuracy with which an unknown patient could be classified as being either a responder or non-responder. This was done for two types of features: single-channel features and two-channel features. In the two-channel features, the P300 amplitude of two EEG channels is either used simultaneously or combined into a new single feature. No more than two features are combined due to the small amount of data points. More information on the cross-validation is given in section 3.5.7 of the previous chapter.

Single channel features

	VNS Off
	μ ± σ (%)
FP2	66.67 ± 22.22
F3	66.67 ± 22.22
C4	55.56 ± 24.69
Pz	66.67 ± 22.22
CP2	72.22 ± 20.06
AF7	61.11 ± 23.77
AF3	55.56 ± 24.69
AF4	61.11 ± 23.77
F6	55.56 ± 24.69
C2	66.67 ± 22.22
CP4	72.22 ± 20.06
P2	61.11 ± 23.77
PO4	61.11 ± 23.77

Table 4.4: Resulting accuracies of the 10-fold cross-validation to separate responders from non-responders for several features for VNS Off. The results indicate the proportion of the 18 patients that were classified correctly during 10-fold cross-validation.

In Table 4.4, the most interesting results for 10-fold cross-validation to classify patients as being either a responder or non-responder for VNS Off are shown. EEG channels CP4 and CP2 perform best in classifying an unknown subject as being either a responder or non-responder. The obtained accuracy is 72.22%, meaning that 13 out of 18 patients were classified correctly during cross-validation.

	VNS On
	μ ± σ (%)
FP1	50 ± 25
Fpz	72.22 ± 20.06
F3	72.22 ± 20.06
Fz	77.78 ± 17.28
Oz	83.33 ± 13.89
O2	77.78 ± 17.28
PO7	72.22 ± 20.06
Poz	77.78 ± 17.28
AF3	77.78 ± 17.28
AF4	72.22 ± 20.06
F1	61.11 ± 23.77
F2	83.33 ± 13.89
P6	72.22 ± 20.06
PO5	66.67 ± 22.22
PO3	72.22 ± 20.06
PO4	72.22 ± 20.06
PO6	72.22 ± 20.06

Table 4.5: Resulting accuracies of the 10-fold cross-validation to separate responders from non-responders for several features for VNS On. The results indicate the proportion of the 18 patients that were classified correctly during 10-fold cross-validation.

In comparison with the results for VNS Off, several features presented in Table 4.5 for VNS On perform better in classifying an unknown patient as being a responder or non-responder. Channels Oz and F2 obtain an accuracy of 83.33%, which is relatively high and means that 15 out of 18 patients were classified correctly.

	Relative P300 amplitude change
	μ ± σ (%)
Pz	61.11 ± 23.77

Table 4.6: Resulting accuracy of the 10-fold cross-validation to separate responders from non-responders by the relative P300 amplitude change in the Pz channel. The result indicates the proportion of the 18 patients that were classified correctly during 10-fold cross-validation.

The relative P300 amplitude change in the Pz channel performs rather poor (61.11% = 11 out of 18 patients).

Two-channel features

Not only single channel features can be used in the classification of a new patient; combination of multiple features is also possible. In the following tables, only the best performing features are shown.

	Two features
	μ ± σ (%)
FPz (On) , Poz (On)	88.89 ± 9.88
FPz (On) , PO3 (On)	88.89 ± 9.88
FPz (On) , PO4 (On)	88.89 ± 9.88
PO7 (On) , AF3 (On)	88.89 ± 9.88
CP2 (Off) , PO6 (On)	88.89 ± 9.88
Poz (On) , F6 (Off)	88.89 ± 9.88
C2 (Off) , Po4 (Off)	88.89 ± 9.88

Table 4.7: Resulting accuracies of the 10-fold cross-validation to separate responders from non-responders by using the P300 amplitude in two channels simultaneously as features. The results indicate the proportion of the 18 patients that were classified correctly during 10-fold cross-validation.

It is clear from Table 4.7 that using two features results in substantially higher accuracies (up to 88.89%=16/18 correct) compared to single-channel features.

	Sum of two features
	μ ± σ (%)
FP1 (On) + F3 (On)	88.89 ± 9.88
Fpz (On) + F3 (On)	88.89 ± 9.88
Oz (On) + C2 (Off)	88.89 ± 9.88
PO7 (On) + CP2 (Off)	88.89 ± 9.88
PO7 (On) + C2 (Off)	88.89 ± 9.88
CP2 (Off) + PO4 (Off)	88.89 ± 9.88
CP2 (Off) + PO5 (On)	94.44 ± 5.25

Table 4.8: Resulting accuracies of the 10-fold cross-validation to separate responders from non-responders by using the sum of the P300 amplitudes in two channels. The results indicate the proportion of the 18 patients that were classified correctly during 10-fold cross-validation.

Using the sum of two channels as new feature results in even higher accuracies (Table 4.8). The sum of the P300 amplitude in channel CP2 for VNS Off and in channel PO5 for VNS On obtains a cross-validation accuracy of 94.44% meaning that 17 out of 18 patients were classified correctly.

	Product of two features
	μ ± σ (%)
F3 (On) x F6 (Off)	94.44 ± 5.25
CP2 (Off) x PO5 (On)	94.44 ± 5.25

Table 4.9: Resulting accuracies of the 10-fold cross-validation to separate responders from non-responders by using the product of the P300 amplitudes in two channels. The results indicate the proportion of the 18 patients that were classified correctly during 10-fold cross-validation.

Another feature that can be created is the product of the P300 amplitudes in two channels (Table 4.9). Accuracies here can be very high as well (up to 94.44%).

4.3 Conclusion

No significant differences are found for the P300 latency between groups (responders vs. non-responders) and conditions (VNS On vs. Off). A mixed-model ANOVA and post-hoc t-tests were performed for the P300 amplitude in all EEG channels. No significant differences are found for these P300 amplitudes between VNS On and Off independent of the patients being responders or non-responders. The P300 amplitude is in almost all EEG channels larger for non-responders than for responders. In 15 channels for VNS Off and 20 channels for VNS On this difference is significant. In six EEG channels, the P300 amplitude difference between groups depends significantly on the condition. In all these channels, P300 amplitude increases when VNS is switched On in responders while it decreases for non-responders. Channels Pz and CP2 show a significant increase in P300 amplitude for responders while channels C4 and C6 indicate a significant decrease for non-responders. However, the relative amplitude change (On-Off/Off) is significantly different between groups in channel Pz only.

Several EEG channels that showed significant differences in P300 amplitude between responders and non-responders can be used to build logistic regression models to separate responders from non-responders based on these amplitudes or features. For VNS Off, 6 channels result in a statistical significant logistic regression model, while this is the case for 12 channels for VNS On. When using the relative amplitude change (On-Off/Off), only the Pz channel delivers a statistical significant logistic regression model. ROC curve analyses revealed that several of these features separate groups with good sensitivity, specificity, positive predictive values and negative predictive values.

Cross-validation identifies several EEG channels that can be used to classify an unknown patient as being responder or non-responder with high accuracy. For single-channel features, 83.33% is the highest accuracy observed by using the F2 or Oz channel. By creating new features such as the sum or product of the P300 amplitudes of two EEG channels, a very good classification with accuracies of up to 94.44% can be obtained. For example, this is the case for the sum or product of CP2 (Off) with PO5 (On).

Chapter 5

Source level

A second level of analysis is the source level in which the active brain regions are assessed and compared between groups (responders vs. non-responders) and conditions (VNS On vs. Off). All brain activity was determined by ESI (see section 2.2.3 of the literature review for more details on ESI) and warped (or projected) to the template head model to be able to compare between groups and conditions. A more detailed description of the implementation of ESI, the warping process and the statistical analysis method is given in Chapter 3.

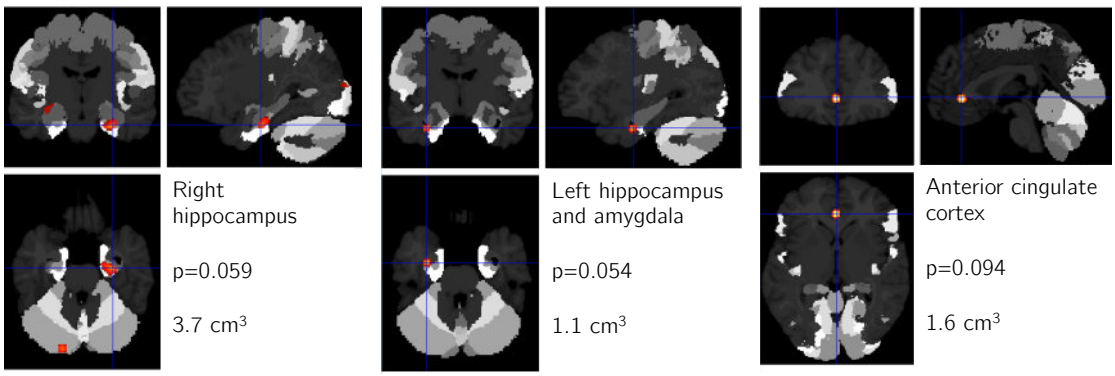

Figure 5.1: Visualization of the brain regions that are significantly more active for responders than for non-responders irrespective of VNS On or Off. The activity is determined in an 80 ms interval around the moment of P300 peak. For each figure, p indicates the significance and the size of the significant area is given.

Figure 5.1 indicates the brain regions that are significantly more active for responders than for non-responders independent of VNS being switched On or Off. The significant areas are the right hippocampus (p=0.059, 3.7 cm^3), the left hippocampus and amygdala (p=0.054, 1.1 cm^3) and the anterior cingulate cortex (p=0.094, 1.6 cm^3). It is important to notice that no regions are significantly more active for responders than for non-responders when using a 0.05 level of significance.

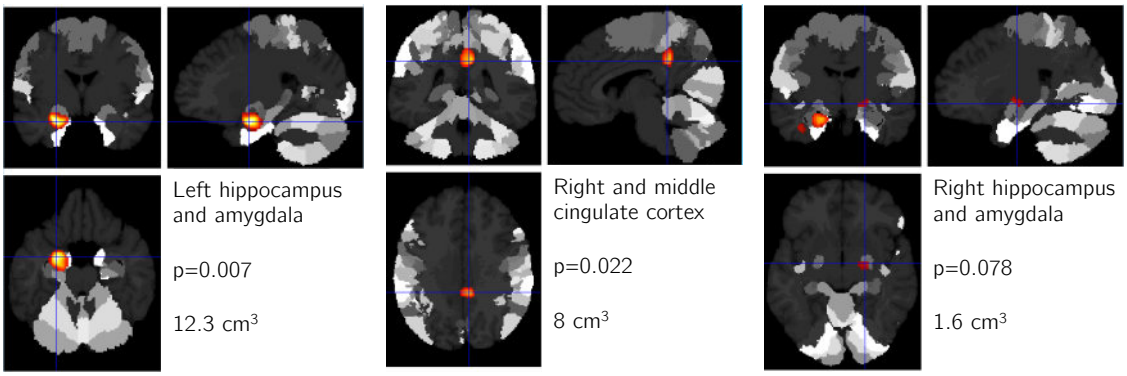

Figure 5.2: Visualization of the brain regions that are significantly more active for non-responders than for responders irrespective of VNS On or Off. The activity is determined in an 80 ms interval around the moment of P300 peak. For each figure, p indicates the significance and the size of the significant area is given.

Figure 5.2 indicates the brain regions that are significantly more active for non-responders than for responders independent of VNS being switched On or Off. The significant areas are the left hippocampus and amygdala (p=0.007, 12.3 cm^3), the right and middle cingulate cortex (p=0.022, 8 cm^3) and the right hippocampus and amygdala (p=0.078, 1.6 cm^3). In contrast to the results presented in the previous paragraph, there are regions significantly more active for non-responders than for responders at a significance level op 5%. In other words, the activity is significantly lower in the regions presented in this figure for responders.

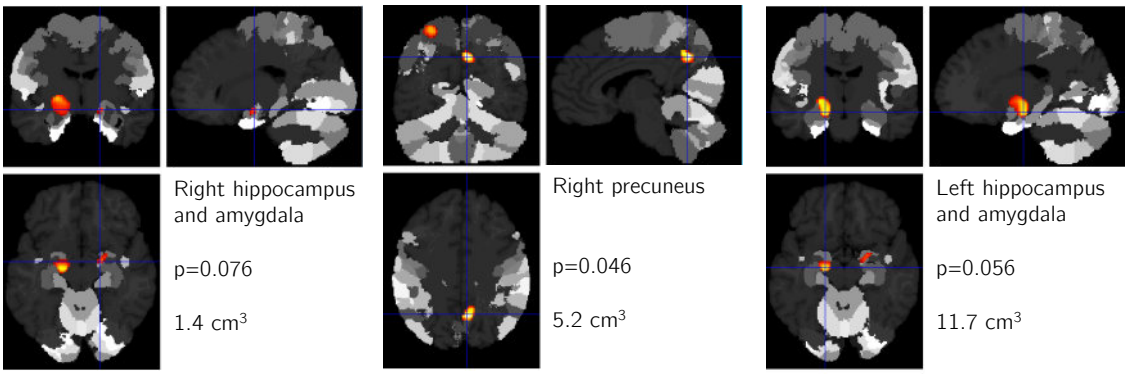

Figure 5.3: Visualization of the brain regions that are significantly more active for VNS Off than for VNS On irrespective of the patient group. The activity is determined in an 80 ms interval around the moment of P300 peak. For each figure, p indicates the significance and the size of the significant area is given.

Figure 5.3 indicates the brain regions that are significantly more active for VNS Off than for VNS On independent of the patients being responders or non-responders. The significant areas are the right hippocampus and amygdala (p=0.076, 1.4 cm^3), the right precuneus (p=0.046, 5.2 cm^3) and the left hippocampus and amygdala (p=0.056, 1.1 cm^3). These regions decrease in activity upon switching VNS On.

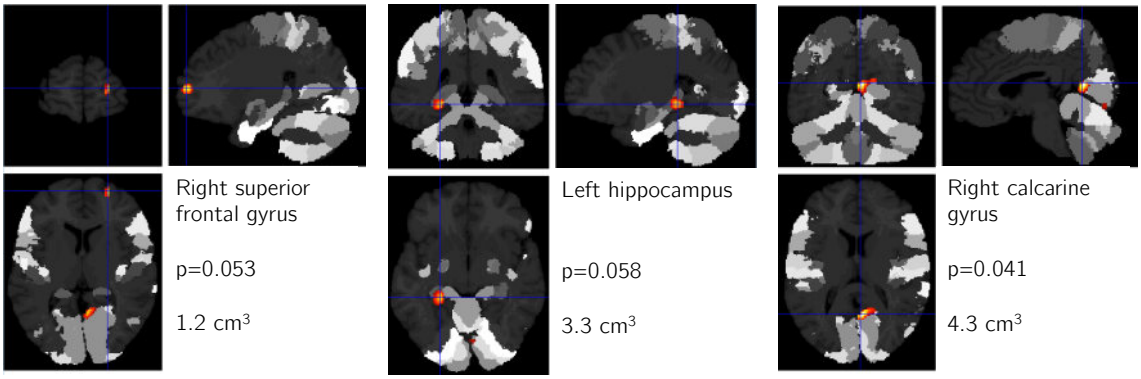

Figure 5.4: Visualization of the brain regions that are significantly more active for VNS On than for VNS Off irrespective of the patient group. The activity is determined in an 80 ms interval around the moment of P300 peak. For each figure, p indicates the significance and the size of the significant area is given.

Figure 5.4 indicates the brain regions that are significantly more active for VNS On than for VNS Off independent of the patients being responders or non-responders. The significant areas are the right superior frontal gyrus (p=0.053, 1.2 cm^3), the left hippocampus (p=0.058, 3.3 cm^3) and the right calcarine gyrus (p=0.041, 4.3 cm^3). The regions indicated here increase in activity upon switching VNS On.

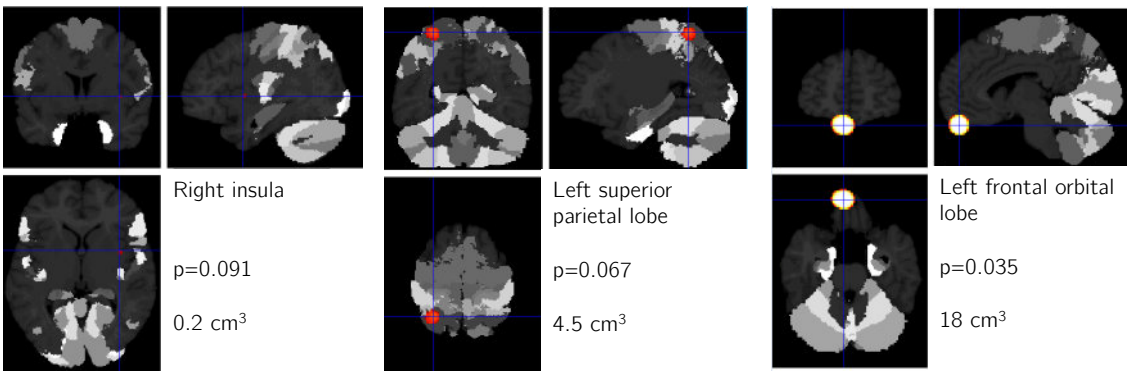

Figure 5.5: Visualization of the brain regions where the difference in activity between responders and non-responders depends significantly on whether VNS was switched On or Off and vice versa. The activity is determined in an 80 ms interval around the moment of P300 peak. For each figure, p indicates the significance and the size of the significant area is given.

Figure 5.5 indicates the brain regions where the difference in activity between responders and non-responders depends significantly on whether VNS was switched On or Off and vice versa. The significant areas are the right insula (p=0.091, 0.2 cm^3), the left superior parietal lobe (p=0.067, 4.5 cm^3) and the left frontal orbital lobe (p=0.035, 18 cm^3).

It is clear that several differences exist between responders vs. non-responders (group) and VNS On vs. Off (condition). Note that at a significance level of 0.05, main effects of group are limited to regions significantly more active for non-responders (and thus less active for responders). Interestingly, the activity of several brain regions in the temporal lobe seems to be highly dependent on whether the patient was a responder or a non-responder and whether the

VNS was switched On or Off. These brain regions include the hippocampus, the amygdala and the insula.

Chapter 6

Brain connectivity

In the previous chapter, differences in brain activity between responders vs. non-responders and between VNS On vs. Off were identified. In this chapter, the analysis of the brain activity is extended to how the active brain regions interact with each other. Also, the global brain network is modeled and specific measures are used to discover differences in the functioning of the brain network between responders vs. non-responders and VNS On vs. Off.

Using both functional and effective connectivity measures, the connections between different active brain regions is assessed. Based on the AAL brain template [156], 116 Regions of Interest (ROIs) are identified (Appendix Table A). For each of these ROIs, a time-dependent activity signal is determined. Next, correlation (a functional connectivity measure) is determined between the activity time series of two different ROIs. This is done for all combinations of two different ROIs. These analyses are done by mixed-model ANOVAs, post-hoc t-tests and Bonferroni (family wise error rate of 0.05) and Benjamini-Hochberg (false discovery rate of 0.1 and significance level of 0.05) multiple comparison corrections. More information on the ROIs, correlation and multiple comparison corrections is given in Chapter 3.

Next, effective connectivity between active brain regions is assessed. This is done by using 4 different effective connectivity measures: iADTF, iAPDC, ffADTF and ffAPDC. These four measures are explained in detail in section 2.5.4 of the literature review. APDC measures perform well in identifying direct information flows whereas ADTF performs better in identifying the cascade of information flow. The prefixes 'i' and 'ff' define the type of the used averaging over given frequency bands. The effective connectivity measures are able to analyze the influence one brain region exerts over another by the use of directed connections. These measures are applied to assess the effective connections between 27 ROIs. These 27 ROIs are identified as the second-to-last spatial division of the AAL brain template (Appendix Table A) [156]. The effective connectivity analyses are performed in different frequency bands since brain signals often have characteristic frequency ranges. These frequency bands are indicated by δ, θ, α, β and γ defining different frequency bands: 0-4 Hz, 4-8 Hz, 8-16 Hz, 16-32 Hz and 32-64

Hz respectively. Each effective connectivity measure results in a time-dependent strength of the given connection. To be able to analyze differences between responders vs. non-responders and VNS Off vs. On in statistical analyses, time-average and standard deviation of the time-dependent strengths of the connections are calculated. Time-average or mean indicates the overall strength of the connection while standard deviation reflects the time-dependent fluctuations in this strength. This means that in total 29160 different analyses (4 measures, 5 frequency bands, mean and standard deviation for each measure and 729 different combinations between two ROIs) are performed to identify differences between responders vs. non-responders and VNS Off vs. On. These analyses are done by mixed-model ANOVAs, post-hoc t-tests and Bonferroni (family wise error rate of 0.05) and Benjamini-Hochberg (false discovery rate of 0.1 and significance level of 0.05) multiple comparison corrections. More information on the implementation of the effective connectivity measures is given in Chapter 3.

The global brain network is analyzed by representing the brain network as a graph. The 27 ROIs are used as 27 nodes. The weights of the connections between these nodes are defined as the mean strengths of the connections between the appropriate regions as calculated with the effective connectivity measures (see previous paragraph). Then, betweenness centrality is calculated for each node in the overall brain network. This measure indicates the relative importance of a node in the overall network. The calculation of the betweenness centrality is done for each node, for each effective connectivity measure and in each frequency band. Therefore, differences between responders vs. non-responders and VNS Off vs. On are assessed in 540 analyses (27 nodes, 4 different connection weights and 5 frequency bands). These analyses are done by mixed-model ANOVAs and post-hoc t-tests.

More details on the applied methods are given in Chapter 3.

6.1 Functional connectivity

Correlation is calculated between all possible combinations of the 116 ROIs as defined by the AAL template (Appendix Table A). The mixed-model ANOVA revealed that 86 of the combinations show a significant interaction effect between group and condition. This means that the difference in strength of 86 functional connections between two different brain regions for responders vs. non-responders depends significantly on VNS being switched On or Off and vice versa. Post-hoc two-tailed t-tests showed that for the 86 significant combinations, there are 26 connections that show a significant difference between VNS switched Off vs. On for responders and 29 for non-responders. For VNS Off there are 20 combinations with a significant difference between responders and non-responders. Also for VNS On there are 20

combinations showing a significant difference between responders and non-responders. However, due to the relatively high number of comparisons, multiple comparison corrections had to be applied. By using Bonferroni correction (see section 3.5.7 of Chapter 3), only two combinations of two regions showed a significant result between VNS Off and On for non-responders only. These results are shown in Table 6.1 and Figure 6.1.

p	ROI 1	ROI 2
0.0003	Left inferior parietal gyrus	Cerebellum Crus 1
0.0005	Right middle occipital gyrus	Left superior temporal gyrus

Table 6.1: Significant results between conditions after Bonferroni multiple comparison correction for the post-hoc two-tailed t-tests for correlation between ROIs of non-responders. ROIs are determined by the 116 ROI system of the AAL brain template (Appendix Table A). p values indicate the uncorrected significances.

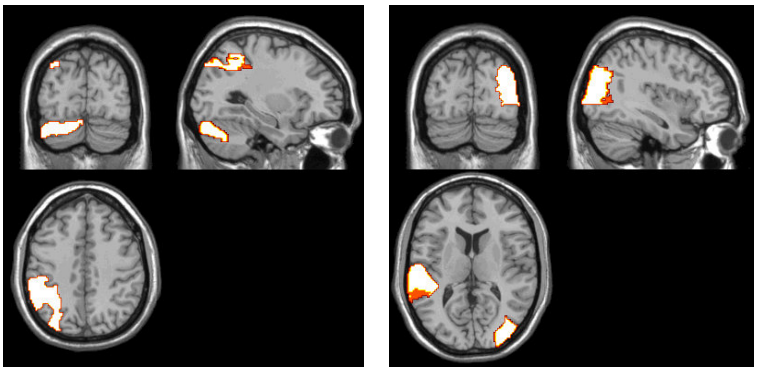

Figure 6.1: Visualization of the significant results from Table 6.1: left inferior parietal gyrus and cerebellum crus 1 (left) and right middle occipital gyrus and left superior temporal gyrus (right).

An alternative multiple comparison correction is done by controlling the false discovery rate by Benjamini-Hochberg correction (see section 3.5.7 of Chapter 3). Significant results are found for differences between VNS Off vs. On for non-responders and between responders vs. non-responders for VNS Off. The results are shown in Table 6.2, Table 6.3, Figure 6.2 and Figure 6.3.

p	ROI 1	ROI 2
0.0003	Left inferior parietal gyrus	Cerebellum Crus 1
0.0005	Right middle occipital gyrus	Left superior temporal gyrus
0.0013	Left insula	Right hippocampus
0.0018	Right calcarine fissure	Left fusiform gyrus
0.0066	Right precentral gyrus	Left postcentral gyrus
0.0067	Right insula	Let inferior parietal gyrus
0.0085	Right cuneus	Left superior parietal gyrus
0.0089	Left hippocampus	Right postcentral gyrus

Table 6.2: Significant differences between conditions after Benjamini-Hochberg correction for the post-hoc two-tailed t-tests for correlation between ROIs for non-responders. ROIs are determined by the 116 ROI system of the AAL brain template (Appendix Table A). p values indicate the uncorrected significances.

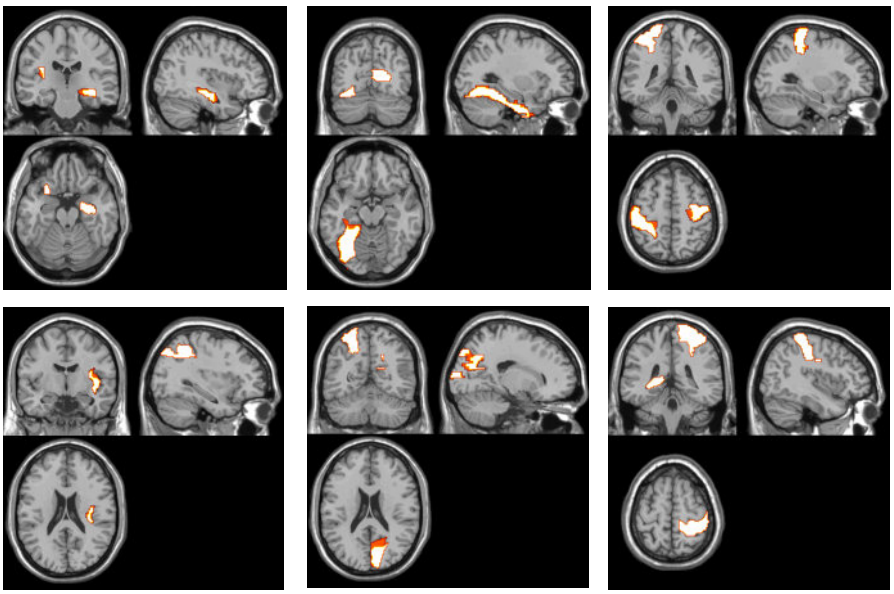

Figure 6.2: Visualization of the significant results of Table 6.2 (the first two results in Figure 6.1): left insula and right hippocampus (top left), right calcarine fissure and left fusiform gyrus (top middle), right precentral gyrus and left postcentral gyrus (top right), right insula and left inferior parietal gyrus (bottom left), right cuneus and left superior parietal gyrus (bottom middle) and left hippocampus and right postcentral gyrus (bottom right).

p	ROI 1	ROI 2
0.0017	Right olfactory cortex	Left insula
0.0029	Right supplementary motor area	Right median cingulate gyrus
0.0029	Right insula	Left inferior parietal gyrus

Table 6.3: Significant differences between groups after Benjamini-Hochberg correction for the post-hoc two-tailed t-tests for correlation between ROIs for VNS Off. ROIs are determined by the 116 ROI system of the AAL brain template (Appendix Table A). p values indicate the uncorrected significances.

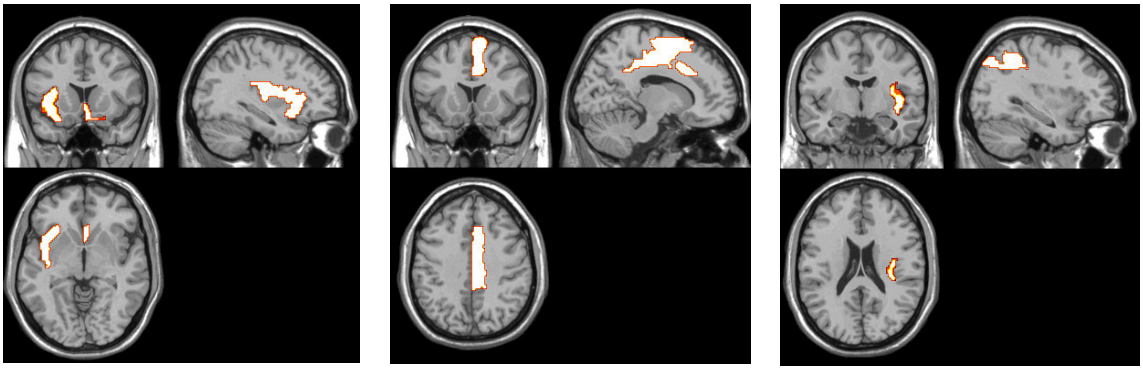

Figure 6.3: Visualization of the significant results of Table 6.3: right olfactory cortex and left insula (left), right supplementary motor area and right media cingulate gyrus (middle) and right insula and left inferior parietal gyrus (right).

Several combinations of two brain regions show significant differences between either responders vs. non-responders (group) or VNS Off vs. On (condition). These brain regions are localized in several parts of the brain. However, especially the hippocampus and the insula are bilaterally present in several significant results. In 55 of the 86 combinations that show a significant interaction effect, the correlation increases for non-responders while it decreases for responders.

6.2 Effective connectivity

Integration of different brain regions is often better represented by effective connectivity, defined as the influence one neural system exerts over another. Therefore, effective connectivity is sometimes termed 'directed functional connectivity'. Effective connectivity depends explicitly on a model of the influence. In this research, four different effective connectivity measures are used: iAPDC, iADTF, ffAPDC and ffADTF. These measures are explained in greater detail in section 2.5.4 of the literature review. The analysis of the connectivity is performed in different frequency bands using 27 ROIs. These ROIs are determined as the second-to-last split in the AAL brain template (Appendix Table A).

The result of using these connectivity measures is a time-varying connection strength between two given brain areas. In order to be able to perform statistical analyses on these results, the time-varying signals of the different measures are reduced to single values by averaging the time signal and by calculating the standard deviation. The mean indicates the overall strength of the connections while standard deviation can indicate the fluctuations in the connection strength over time. In total, 29160 different features (4 effective connectivity measures, 5 frequency bands, mean and standard deviation for each measure and 729 different combinations between two ROIs) are analyzed to identify differences between responders vs. non-responders and VNS On vs. Off.

Mixed-model ANOVAs revealed that 793 features for the mean and 795 features for standard deviation exhibit a significant interaction effect, meaning that the difference in these features between responders and non-responders depends significantly on whether VNS is switched On or Off. For these features, post-hoc two-tailed t-tests were performed to analyze them in greater detail. Bonferroni and Benjamini-Hochberg corrections were applied to the results to correct for the multiple comparisons.

For both mean and standard deviation, no significant features are found after Bonferroni correction. However, after using Benjamini-Hochberg corrections, many significant results are found, which are described below. First the results are given for the mean connection strength and further on the results for standard deviation are shown.

Mean connection strength

No significant results are found for differences in mean connection strength between (1) VNS Off and On for non-responders and (2) responders and non-responders for VNS Off. For responders, however, two features show significant differences between VNS On and Off; this is shown in Table 6.4. When VNS is switched On, for both significant results displayed in Table 6.4 the connection increases in strength. The significant connection is visualized in Figure 6.4.

p	Feature	Frequency band	ROI 1 (from)	ROI 2 (to)
0.000149	ffAPDC	β	Lateral surface of left occipital lobe	Orbital surface of right frontal lobe
0.000154	iAPDC	β	Lateral surface of left occipital lobe	Orbital surface of right frontal lobe

Table 6.4: Significant differences in time-average of iAPDC, ffAPDC, iADTF and ffADTF between VNS On and Off for responders. The p values are uncorrected. β indicates the frequency band 16-32 Hz.

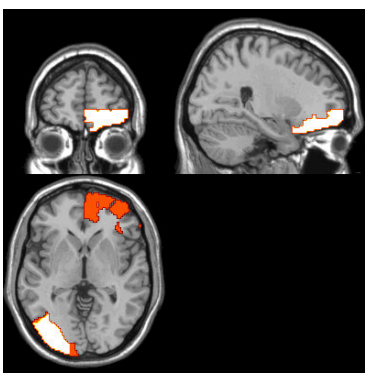

Figure 6.4: Visualization of the significant results from Table 6.4: the lateral surface of the left occipital lobe and the orbital surface of the right frontal lobe.

For VNS switched on, 50 different connections show significant differences between responders and non-responders. All together, these 50 different connections result in 312 features that

exhibit a significant difference between groups. Therefore, all of these 50 different connections show significant differences between responders and non-responders for several measures and/or frequency bands. Significant connections are spread out over the entire brain with the highest amount of significant connections in the lateral surface of the right temporal lobe, lateral surface of the left occipital lobe and the lateral surface of the right frontal lobe. Of the 312 significant features, 67 results are situated in the δ-band, 58 in the θ-band, 65 in the α-band, 56 in the β-band and 66 in the γ-band. Most of the significant results are found by iADTF and ffADTF.

Standard deviation of the connection strength

No significant results are found after Benjamini-Hochberg correction for differences between (1) VNS On and Off for responders and (2) responders vs. non-responders for VNS Off. For non-responders, nine features show significant differences between VNS On and Off; this is shown in Table 6.5. When VNS is switched On, for all significant connections displayed in Table 6.5 the connection increases in strength for non-responders. For responders, however, this is only the case for the connections involving the limbic lobe, although not significantly. The connections are visualized in Figure 6.5.

p	Feature	Frequency band	ROI 1 (from)	ROI 2 (to)
0.00008	iADTF	β	Right limbic lobe	Right limbic lobe
0.00009	iAPDC	γ	Right cerebellum	Lateral surface of left parietal lobe
0.00027	ffAPDC	γ	Right cerebellum	Lateral surface of left parietal lobe
0.00037	iAPDC	β	Right cerebellum	Lateral surface of left parietal lobe
0.00040	ffADTF	β	Right limbic lobe	Right limbic lobe
0.00053	ffAPDC	β	Right cerebellum	Lateral surface of left parietal lobe
0.00053	iADTF	β	Lateral surface of right temporal lobe	Lateral surface of right temporal lobe
0.00064	ffAPDC	α	Right cerebellum	Lateral surface of left parietal lobe
0.00069	iADTF	γ	Right limbic lobe	Right limbic lobe

Table 6.5: Significant differences in standard deviation over time of iAPDC, ffAPDC, iADTF and ffADTF between VNS On and Off for non-responders. The p values are uncorrected. α, β and γ indicate different frequency bands: 8-16 Hz, 16-32 Hz and 32-64 Hz respectively.

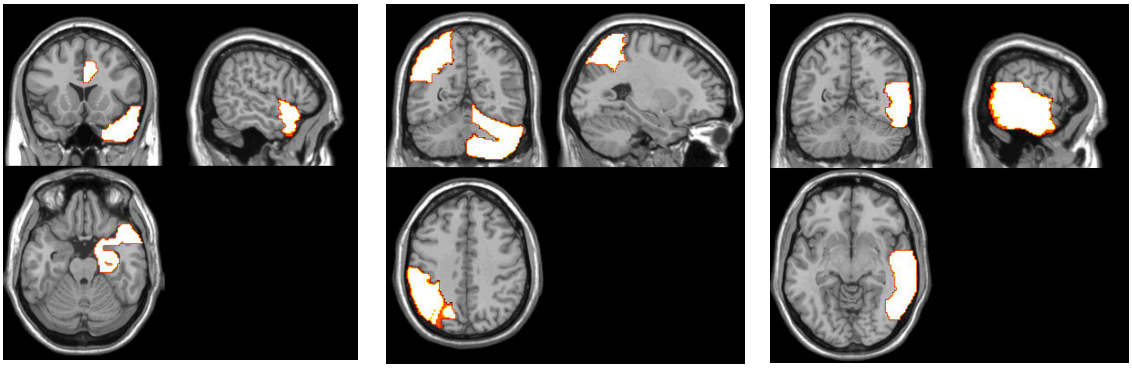

Figure 6.5: Visualization of the significant results of Table 6.5: right limbic lobe (left), right cerebellum and lateral surface of left parietal lobe (middle) and lateral surface of right temporal lobe (right).

Remarkably, 4 of the significant features consist of a connection from a certain region to itself, meaning that for these connections (right limbic lobe and the lateral surface of the right temporal lobe) the standard deviation of the autospectra are significantly different for non-responders between VNS Off and On.

For VNS On, 295 features show a significant difference between groups. These 295 significant features incorporate 47 different connections. The significant connections are spread over the entire brain with the highest amount of significant results in the central region, in the lateral surface of the right temporal lobe and the left insula. Of all 295 features, 59 are situated in the δ-band, 46 in the θ-band, 64 in the α-band, 55 in the β-band and 71 in the γ-band. Most of the significant results are found by iADTF and ffADTF.

6.3 Brain network

In the previous section, 27 ROIs were defined and by using 4 effective connectivity measures, the strengths of the directed connections between these ROIs were calculated. By using the ROIs as nodes or vertices and by labeling the edges between them with the mean connection strengths as calculated in the previous section, the brain network can be modeled. Betweenness centrality is a measure that allows indicating the importance of each node within the overall network. Differences in the relative node importance with respect to group and condition are investigated. The analysis is performed for the 27 ROIs in terms of the four effective connectivity measures of the previous section and the different frequency bands. The calculated mean betweenness centrality values are given in Appendix Table J.

Performing a mixed-model ANOVA resulted in 19 significant interaction results consisting of 8 different nodes. The results are given in Appendix Table K. Post-hoc two-tailed t-tests were

performed on these significant interaction results to identify differences in greater detail. The significant outcomes of these analyses are given in Table 6.6.

Node	p value	Measure	Frequency band	Effect
Right insula	0.0465	iADTF	θ	$R_{on}>R_{off}$
Right insula	0.0476	ffADTF	θ	$R_{on}>R_{off}$
Right limbic lobe	0.020	iAPDC	γ	$NR_{on}<R_{on}$
Right limbic lobe	0.0208	ffAPDC	γ	$NR_{on}<R_{on}$

Table 6.6: Significant results of the post-hoc two-tailed t-tests for the betweenness centrality of 27 ROIs using different effective connectivity measures in different frequency bands. The last column specifies for which category the relative node importance is highest, thus the last column indicates which significant result is identified. θ and γ indicate different frequency bands: 4-8 Hz and 32-64 Hz respectively.

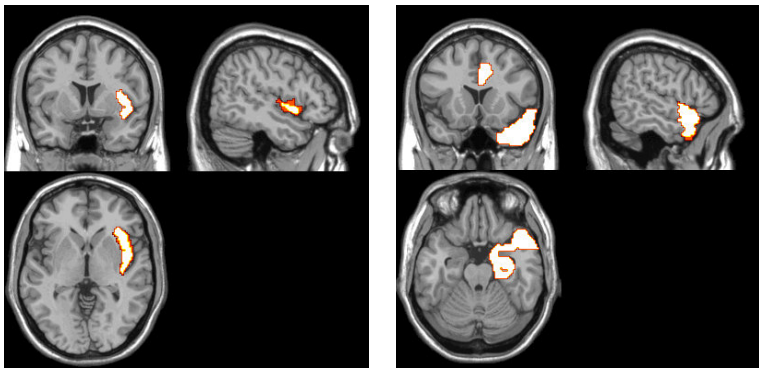

Figure 6.6: Visualization of the significant results of Table 6.6: right insula (left) and right limbic lobe (right).

For responders, the importance of the right insula in the global brain network is significantly dependent on VNS being switched On or Off. For VNS On, the importance of the right limbic lobe in the brain network is significantly dependent on whether the patient is a responder or a non-responder. The significant brain regions are visualized in Figure 6.6.

6.4 Conclusion

Performing brain connectivity and network analyses identified some key influences of group (responder vs. non-responder) and condition (VNS On vs. Off) on the brain connectivity and brain network.

By using the correlation, a functional connectivity measure, between different brain regions, several significantly altered functional connections are found. For non-responders, there is a significant influence of VNS on the correlation for 9 connections. In 3 of these connections, the (bilateral) hippocampus and/or insula play a key role. Parietal and central gyri are the main components of the other connections. For VNS Off, 3 functional connections showed significant

differences between responders and non-responders. In these significant connections, the insula plays an important role bilaterally.

Effective connectivity measures allow analyzing the influence that one neural system exerts over another. Directed connections together with a TVAR model were used to define four effective connectivity measures: iADTF, ffADTF, iAPDC, ffAPDC. Similarly as for the correlation, these measures were used to identify differences in terms of groups and condition in the connections between brain regions. For each measure, two features were made: the average and the standard deviation of the time-varying calculated connectivity strengths. The average allows comparing the overall strength of the connections, while the standard deviation reflects the time-dependent changes in the strength of the connections. These features were analyzed in 5 different frequency bands.

For the mean connection strength, significant differences are found for responders in the connection from the occipital lobe to the frontal lobe dependent on VNS On or Off. For VNS On, no less than 312 significant features are found between responders and non-responders. These consist of 50 different connections in several frequency bands and for several measures. These connections are situated over the entire brain but mainly in the lateral surface of the right temporal lobe, lateral surface of the left occipital lobe and the lateral surface of the right frontal lobe.

For the standard deviation, significant differences are found for non-responders in the connections between several regions. Remarkably, 4 of the significant features consist of a connection from a certain region to itself. This is the case for both the right limbic lobe and the lateral surface of the right temporal lobe and this means that the standard deviation of the autospectra for these regions is significantly different in non-responders between VNS switched On or Off. For VNS On, 295 features show significant differences between responders and non-responders in the standard deviation of the time-varying connection strengths. These results incorporate 47 different connections in several frequency bands and for several measures and are mainly situated in the central gyri, the lateral surface of the right temporal lobe and the left insula.

Using betweenness centrality, a measure from graph theory, the importance of each brain region in the overall brain network can be compared between groups and conditions. This allows identifying changes in the overall brain network with respect to responders vs. non-responders or VNS On vs. Off. The right insula increases in importance in the brain network for responders when VNS is switched On. This effect is observed in the τ–frequency band. In the γ–frequency band, the importance of the right limbic lobe is significantly larger for responders than for non-responders when VNS is On.

Chapter 7

Discussion

In the previous chapters, interesting results are found that indicate differences in brain functioning and activity due to vagus nerve stimulation. In this chapter, interpretation of these results is given. The results are examined and possible underlying causes or explanations are given. Results are assessed in terms of their ability to be used in clinical practice to identify unknown patients pre-operatively as being either responder or non-responder. Methods used to come to the presented results, are revised. The findings in this research are compared with other research and approaches for future work are suggested.

7.1 Sensor level

The sensor level analysis investigated the activity of the locus coeruleus-norepinephrine (LC-NE) system indirectly by means of the P300 wave in ERPs. The P300 amplitude is found to be modulated by the LC-NE activity and the LC-NE system is thought to be one of the key structures involved in the anti-epileptic effect of VNS, as supported by different studies [7]–[9], [89], [92]–[94], [96], [145]. Differences in P300 features (latency and amplitude) between responders vs. non-responders (group) and VNS Off vs. On (condition) were analyzed. The P300 features were extracted from EEG measurements of 20 patients during auditory oddball experiments. Two average P300 waves were calculated for each patient and condition, associated with the task-related target stimulus and non-task-related standard stimulus respectively. A standard sequence of data transformations was used to calculate these waveforms, which is also used in other research [8], [149]. It is important to stress the influence of several artifacts on the P300 wave. Especially ocular artifacts can have a large effect on the P300 wave [147], [162]. It is reasonable to assume that ocular artifacts are largely removed due to: (1) the fact that patients were asked to fix their eyes on a certain point during recordings, (2) vertical eye movements were recorded and removed from the EEG data, and (3) epoch

averaging was applied. A similar approach was used for cardiac and VNS related artifacts. Since the P300 wave is larger after task-related target stimuli, it was isolated by subtracting the average waveform for standard stimuli from the waveform for target stimuli, as is done in other research [8]. The target-standard difference waveform is used to extract the P300 features.

No differences in P300 latency were found between responders vs. non-responders and VNS Off vs. On. This is in agreement with other research [8], [163]. However, Neuhaus et al. reported a significant prolonged latency in non-responders [164], but the latency was detected in the Fz channel in contrast to the Pz channel in this research. Therefore, it is probable that Neuhaus et al. detected the latency of the P3a wave, since this component is mainly detected frontally, which corresponds to the location of electrode Fz. In this research, the P3b will have a larger influence on the P300 latency, since this P3b wave is detected more parietally, which corresponds to the location of the Pz channel. More information on the P3a and P3b waves was given in section 3.2. In the research by Brazdil et al., a difference between the latency at electrode Fz and Pz is shown, but no significance was reported [165].

The P300 amplitude was found not to be significantly altered between VNS Off and On, independent of the patients being responders or non-responders, which is in agreement with previous research [8], [163]–[165]. However, these studies only focused on the P300 amplitude in central electrodes, whereas in this research the same result was found for all 60 EEG channels.

In many EEG channels, the P300 amplitude was found to be larger for non-responders than for responders, which is consistent with the reported values in De Taeye et al. [8] and Neuhaus et al. for VNS Off [164]. This result was significant in 23 EEG channels and these are situated both frontally (possibly due to the P3a wave) and parietally (possible due to P3b) as shown in the left panel of Figure 4.1. The non-significant result for the Pz channel is consistent with the research of De Taeye et al. [8]. The Fz channel does indicate a significantly larger P300 amplitude for non-responders than for responders in this research, which is inconsistent with Neuhaus et al. [164]. However, in the research of Neuhaus et al., the P300 amplitude in the Fz channel was detected at the moment of peak in the Fz, while in this research it was detected at the moment of peak in the Pz channel, making the comparison difficult. To the knowledge of the author, no similar results were found in previous research where the P300 amplitude was analyzed between responders and non-responders in other channels than Pz, Cz and Fz. The result that significant differences between responders vs. non-responders are found in other EEG channels than Pz, Cz and Fz is therefore novel and is discussed further on to explore the potential of these channels to be used to separate responders from non-responders.

Analyzing the significant results in greater detail showed that 15 EEG channels exhibit a significant difference between responders and non-responders for VNS Off. For VNS On, 20 EEG channels show significant differences between responders vs. non-responders. For the midline electrodes (Fz, Cz, Pz) only the Pz channel shows a significant difference between

responders and non-responders for VNS Off while only the Fz channel shows this significant difference for VNS On. By Neuhaus et al. only a statistical trend in the difference between responders and non-responders for VNS On was given [164]. Possibly, this could point to differences mainly present in the P3a wave for VNS On and P3b for VNS Off. However, this result is to the knowledge of the author not discussed in previous research and is not investigated in other research. It therefore remains a hypothetical explanation and further research is necessary to clarify these results.

Next to the described main effects of group and condition, in six EEG channels (CP2, C2, C4, Pz, C6 and CP4) the difference in P300 amplitude between responders vs. non-responders is dependent on whether VNS was switched On or Off. For responders, the P300 amplitude increases when VNS is switched On, while it decreases for non-responders. The result for the Pz channel is consistent with the research of De Taeye et al. [8]. It is also consistent with the values reported by Neuhaus et al., however, the differences were not tested or reported [164]. Here again, the fact that the significant interaction between group and condition is present in other than the central electrodes is, to the knowledge of the author, not present in previous research and will be assessed in terms of ability to classify patients as responders and non-responders. It is important to point out that at the moment of the P300 wave, many brain regions are thought to be processing information from the stimulus. Also, the P300 is maximally recorded from the midline centroparietal regions [147]. Therefore, one should be watchful that the significant results recorded in other than centroparietal regions could also be due to activity of other brain areas. Especially the six EEG channels showing significant interactions between group and condition are situated more towards right parietal and temporal regions (right panel of Figure 4.1). A possible explanation for these results could be the VNS-dependent limbic system activity [166]–[169]. On the other hand, the origin of the P3b wave is thought to be situated somewhat more temporoparietally as well, meaning that the results could still be due to the P300 wave [139]. Further research should clarify these results.

The P300 amplitude was found to increase significantly in channels Pz and CP2 for responders only. This result for responders is consistent with the research by De Taeye et al. [8] and Neuhaus et al. [164], however in these studies only midline electrodes were used. The result for the CP2 electrode is novel. Interestingly, channels C4 and C6 show a significant decrease in P300 amplitude for non-responders only. P300 amplitudes reported in De Taeye et al. [8] and Neuhaus et al. [164] indicate a decrease for non-responders only as well, however no statistical significance was tested or reported. The result that VNS induces not only P300 amplitude changes for responders but also specific changes for non-responders is interesting and could lead to more efficient separation of responders from non-responders.

The relative amplitude increase (On-Off/On) was analyzed as well between responders and non-responders. This relative increase was significant for channel Pz only, a result consistent with research of De Taeye et al. [8].

The results of P300 increase for responders and P300 decrease for non-responders support the hypothesis that electrical stimulation of the vagus nerve activates the LC-NE system and that this activation is critically linked to the anti-epileptic effect of VNS. This hypothesis points to the use of the amount of NE release in the brain as biomarker for the therapeutic efficacy of VNS and is supported by evidence in literature [7], [89], [92]–[94], [96], [170]–[172].

Activation of the LC-NE system in response to an important stimulus resets ongoing functional networks to be able to respond rapidly to the given stimulus. Therefore, activating the LC-NE system induces an inhibitory brain signal [142]. The results that the P300 amplitudes for non-responders are larger than for responders in many EEG channels could be linked to this LC-NE inhibition [8], [139]. Responders show an increase in P300 wave when VNS is switched On, meaning that in these patients there is an increased inhibitory signal from the active LC-NE system. This is not the case in non-responders since they do not show increased P300 wave amplitude upon VNS being switched On. Therefore, it is possible that responders show lower voltages due to the effective LC-NE inhibition during the VNS treatment period. This inhibition would then be less effective for non-responders, resulting in the higher voltages measured in the EEG for non-responders. However, a power analysis was performed on the original EEG spectrum, but no differences were found between responders and non-responders in that respect. Therefore, the amplitude difference between responders and non-responders is specifically found in the P300 wave, showing a specific key role for the LC-NE inhibitory system in the difference between these two groups. The inhibitory function of the LC-NE system is proposed to be a key anti-epileptic actor as a consequence of VNS since the inhibition is thought to arrest and cancel the spatial spread of seizures, which is nicely linked to the better VNS outcome for responders, since only in these patients an increase in P300 amplitude is observed upon VNS being switched On [7].

Clinically, the results presented above would be interesting if they could be used to accurately predict whether a patient would benefit from VNS therapy or not. Therefore, logistic regression analysis, ROC curve estimation and 10-fold cross-validation are used to indicate the capability of several features to be used as biomarkers for VNS efficacy (thus to separate responders from non-responders). Logistic regression analysis and ROC curve indicate that several features (i.e. P300 amplitudes in several EEG channels) can be used to distinguish responders from non-responders. For the relative change in P300 amplitude in the Pz channel, results are the same as found by De Taeye et al. [8]. In this research, however, several other features are found that can separate responders from non-responders with higher sensitivity and specificity. This result is interesting since it indicates that although the P300 wave is maximally presented at midline positions, P300 amplitudes in other EEG channels can perform better in separating responders from non-responders. This could indicate that measuring the P300 wave as a biomarker for VNS efficacy should be done in non-midline electrodes. However, as indicated above, it is possible that the results in non-midline electrodes are due to other VNS dependent brain

activities, such as the limbic system activity [166]–[169]. Therefore, it is also possible that these results point to biomarker presence in the VNS dependent auditory ERP that provides more accurate separation between responders and non-responders than the P300 wave.

In contrast to other research, cross-validation was used in this research next to logistic regression and ROC curve analyses to indicate the capability of P300 features to separate responders from non-responders. Interestingly, in cross-validation the accuracy of classifying unknown patients as being either responder or non-responders is estimated, which is not the case for logistic regression and ROC curves. In cross-validation, a classification model is built based on the values of a certain feature for patients that were previously classified as responders or non-responders. Unknown patients can then be classified with this model as being either responder or non-responder by the measured value of the given feature for these patients. This is in contrast to logistic regression analysis and ROC since these methods build and characterize the classification models on known patients only. Therefore, cross-validation is very useful with respect to the accurate pre-operative prediction of whether a patient would benefit from VNS therapy or not in clinical practice.

In this research, both single-channel and two-channel features were tested. In the two-channel features, the P300 amplitudes of two EEG channels are either used simultaneously or combined into a new single feature. No more than two features are combined due to the small amount of data points. As a rule of thumb, 15 data points are required per simultaneously used feature. Combining more than two features into a new single feature is not done here due to lack of time. For VNS Off, channels CP4 and CP2 perform best when used to classify an unknown subject as being either a responder or non-responder. The estimated accuracy is 72%, which is not superb. For VNS On, however, channels Oz an F2 obtain accuracies of 83%, which is relatively high. In previous research by De Taeye et al., the relative amplitude increase of the P300 amplitude in the Pz channel was proposed as a biomarker to assess the VNS efficacy [8]. However, using cross-validation, in this research it was found that this feature only obtains 61% classification accuracy. This is an important result and could possibly result in shifting the focus of future research to identify clinically applicable biomarkers for VNS efficacy. Again, it is important to be cautious about the results presented here, because it is not clear whether they originate from the P300 wave or from other VNS dependent brain signals. Future research should provide a clearer insight.

Two-channel features are split up in using two features simultaneously or combining two features into a new single feature. Using two features simultaneously results in accuracies of 89% for several features. Remarkably, using the sum of the P300 amplitudes in two EEG channels can obtain accuracies as high as for the simultaneous use of two features (89%) and summing the P300 amplitudes of channels CP2 for VNS Off and PO5 for VNS On even leads to an estimated accuracy of 94%. Multiplying the P300 amplitudes in (1) channels F3 for VNS On and F6 for VNS Off, and (2) channels CP2 for VNS Off and PO5 for VNS On can also be

used to obtain an accuracy of 94%. To the knowledge of the author, the results presented here for cross-validation are not yet reported or investigated in previous research.

The novel results for logistic regression, ROC curve and cross-validation analyses indicate intriguing possibilities to find biomarkers to assess the clinical efficacy of VNS treatment. However, these results also point to the main drawback of this research. As is indicated before, one of the main objectives of this research was to identify predictive biomarkers, which could be used to accurately predict whether a patient would benefit from VNS therapy or not before surgery. Therefore, these predictive biomarkers should be identified in ERPs of patients that have not yet received VNS surgery. All data in this research was recorded in patients that underwent VNS surgery and received at least 18 months of VNS therapy. It is attempted to overcome this problem by recording ERPs of patients when VNS was switched Off. However, in research it was shown that the anti-epileptic effect of VNS is present during Off-time as well [88]. Results shown in this research are thus possibly poor indicators of differences between responders and non-responders pre-operatively. Therefore, the biomarkers presented in this research are interesting but have little predictive value in clinical practice.

The results at sensor level remain valuable since they point out that P300 features that were previously thought to be good biomarkers for VNS efficacy are out-performed by novel features presented in this research. These results can point to one or both of the following hypotheses: (1) P300 features recorded from other than midline electrodes can be used to obtain the best results in assessing VNS efficacy and (2) other VNS dependent brain signals than the P300 wave can be used to assess VNS efficacy with a much larger accuracy.

7.2 Source level

In the source level analysis, the activity of specific brain regions was compared between responders vs. non-responders and between VNS On vs. Off. These results were obtained by using Electrical Source Imaging (ESI) and are analyzed by statistical parametric software (SPM) using a flexible factorial design. For patients with good quality MRI images, individual head models were used, which were warped to the template head model. For the others, the template head model was used.

When VNS is switched On, activity decreases in hippocampus and amygdala bilaterally as well as in the right precuneus, irrespective of the patients being responders or non-responders. Activity increases when VNS is switched On in the right superior frontal gyrus, the left hippocampus and right calcarine gyrus. The part of the hippocampus that is decreased in activity is however larger than the part that is increased in activity upon VNS switched On.

Differences between responders and non-responders irrespective of VNS being switched On vs. Off are situated in the hippocampus and amygdala bilaterally as well as in the anterior, middle and right cingulate cortex. Importantly, when using the commonly chosen 0.05 significance level, the only significant differences between responders and non-responders are brain regions that show larger activity for non-responders than for responders. These brain regions include the left hippocampus and amygdala and the right and middle cingulate cortex. This result can be linked to the discussion presented above on the larger P300 amplitudes for non-responders and the connection to the inhibitory function of the LC-NE system. It is conceivable that this more effective inhibition due to the VNS induced activation of the LC-NE system is the reason for the significantly lower activity in responders.

Interestingly, in this research also an interaction effect was investigated between group (responders vs. non-responders) and condition (VNS On vs. Off). The brain regions displaying significant results here are the right insula, left superior parietal lobe and left frontal orbital lobe. In these regions, the change in activity between VNS On and Off depends significantly on whether the patient is responder or non-responder and therefore these results can indicate crucial regions that can point to key structures for VNS efficacy.

In research on the same topic, many inconsistencies are present and little research exists where differences between responders and non-responders are incorporated. On top of that, most research is done for depression and not for epilepsy. Therefore, it is conceivable that results presented in literature are poorly applicable to epilepsy patients due to the possible differences between an epileptic and a depressed brain. Conway et al. [173] found that the activity in the orbitofrontal cortex, cingulate cortex and frontal cortex is increased due to VNS, while it is decreased for the temporal cortex and several parietal areas. Bohning et al. [174] found influences of VNS on the orbitofrontal, parieto-occipital and temporal cortices as well as on the hypothalamus and amygdala. Zobel et al. [175] found increased activity in the middle frontal gyrus and decreased activity in amygdala, hippocampus, cingulate cortex, thalamus and brain stem. Kraus et al. [176] indicated decreased activity in the limbic lobe and increased activity in the insula, precentral gyrus and thalamus. The diminished activity of the limbic lobe was also found by Henry et al. [168], [177], Devous et al. [178], Barnes et al. [179], Vonck et al. [167] and Van Laere et al. [180]. Also, recent research by Willeke Staljanssens in the MEDISIP group at Ghent University, Belgium obtained similar results for the active brain regions.

In this research, several brain regions are found to be significantly influenced by VNS, which are also reported in previous research. The main result consistent with previous research is the diminished activity of the limbic system (hippocampus and amygdala). Also the differences between responders vs. non-responders and VNS Off vs. On in activity of the insular region and frontal orbital lobe are interesting and can be linked to the reported VNS dependent changes in activity in these regions in other research.

7.3 Brain connectivity

In recent literature on epilepsy, brain connectivity and whole-brain network measures are presented as important tools to analyze the altered epileptic brain [152]–[155]. Therefore, in this research, ESI was combined with functional connectivity, effective connectivity and graph theory analyses to indicate differences in the brain connectivity and network between responders vs. non-responders and VNS On vs. Off. In this research, ROIs were defined using the AAL template [156].

Functional connectivity between 116 ROIs was determined using the correlation measure. The only differences between VNS On and Off were found in non-responders and are in the connections between the hippocampus and insula bilaterally. Also the parietal and central gyri are present in these significantly different connections. For VNS Off, correlations of several brain regions with the insula are statistically different between responders and non-responders. These results again indicate an important role for the limbic lobe, as is also presented in other research [167], [168], [177].

Effective connectivity was analyzed using iADTF, iAPDC, ffADTF and ffAPDC based on a TVAR model. To reduce the computation time, the 116 ROIs were reduced to 27 ROIs based on the second-to-last regional split in the AAL template. The connections between the 27 ROIs were analyzed for all four measures and in five frequency bands. These frequency bands are indicated by δ, θ, α, β and γ, indicating different frequency bands: 0-4 Hz, 4-8 Hz, 8-16 Hz, 16-32 Hz and 32-64 Hz respectively. Analyzing connectivity in the brain of epilepsy patients by ADTF is also done by Wilke et al. [135] where connectivity between EEG electrodes was used in the presurgical assessment. The analysis in different frequency bands is done in many researches [135], [181]–[183]. Both mean and standard deviation of the time-dependent connectivity calculations are analyzed. This technique was also used by Pittau et al. [184], where the average BOLD time course was compared between different ROIs. For responders, differences are found in the mean connection from occipital to frontal lobe when VNS is On vs. Off. For VNS On, many mean connection strengths show significant differences between responders and non-responders. These connections mainly involve the lateral surface of the right temporal lobe, the lateral surface of the left occipital lobe and the lateral surface of the right frontal lobe.

When analyzing the standard deviation of the time series for the different measures, for non-responders, the autospectra for the right limbic lobe and right temporal lobe are significantly different for VNS On vs. Off. This again indicates a substantial effect of VNS on the activity and connectivity with and within the right temporal lobe and limbic lobe, as was also discussed in the discussion of the source level analysis. For VNS On, similarly as for the mean connection strength, the standard deviation is significantly different between responders and non-responders in many connections. These connections are situated in the central gyri, the lateral surface of

the right temporal lobe and the left insula. As discussed above, many studies assess the connectivity between the time series of the electrode potentials. The strength of this research is to analyze connectivity between activity time series of brain regions and not between EEG electrode potentials. This approach is interesting because it can provide insight in the involved brain areas and allows easier clinical and physiological interpretation. This was also done by Pittau et al. [184] and they mainly found decreased connectivity between the hippocampus and the amygdala and the default mode network. These researchers specifically chose small ROIs in the hippocampus and amygdala, which allowed having precise results in this area of the brain. Due to the larger 27 ROIs used in this work, it is difficult to interpret the results of this report in terms of the default mode network. The altered connectivity with the default mode network was also presented by Fang et al. [185], who analyzed differences in connectivity due to VNS. Next to that, in the results presented in this report, the presence of the limbic lobe, temporal lobe and insula is convincing and these brain areas are also presented in the research by Fang et al. [185] and Pittau et al. [184].

The results for effective connectivity indicate a clear difference in connectivity between responders and non-responders especially for VNS On. This is consistent with research indicating an important role for connectivity analysis in understanding the epileptic brain and the anti-epileptic effect of VNS. Similar brain regions seem to be involved in the altered connections as discussed in the previous section on source level analysis. Although few research exists in which the connectivity is analyzed between activity time series of brain regions and not between electrodes potentials, the presence of the temporal area with inclusion of the limbic system and insula, is undeniable and is presented by other research as well [184], [185]. However, in literature, the connections of temporal lobe structures with the default mode network is often indicated as being significantly altered, but this is difficult to compare with the research in this report due to the choice of ROIs.

Using a graph theory approach, a final analysis was performed to identify differences in the brain between responders vs. non-responders and VNS On vs. Off. The 27 ROIs as defined in the effective connectivity analysis, are now used as 27 nodes or vertices and the mean effective connectivity values are used as weights or labels of the edges connecting the 27 ROIs. Betweenness centrality was calculated for each node to be compared between groups and conditions. This measure indicates the relative importance of a node in the network and was used in previous researches as well [135], [186]–[189]. The right insula was found to be of higher importance in the brain network of responders when VNS was switched On than when VNS was Off. This result was present only in the θ-band. The θ-band is found to be crucially involved in epileptic brain alterations [135], [181], [182]. When VNS is switched On, the right limbic lobe was found to be of higher importance in the γ-band in responders than in non-responders. For both the right insula and limbic lobe, the relative importance increases when VNS is switched On for responders while it decreases for non-responders.

In research on the brain network for epilepsy patients, many inconsistencies are present, but a main conclusion is that a shift towards a less efficient organization increases the epilepsy burden [189]–[194]. Therefore, research indicates that inducing a more efficient organization could reduce that epilepsy burden. Fraschini et al. [181] indeed found this result when comparing responders and non-responders for VNS Off and On. In this research, a minimum spanning tree was computed to characterize VNS-induced alterations in the network topology. They found that there is a more integrated network based on several minimum spanning tree measures. For the results of this report, the right insula and limbic lobe increase in importance in responders when VNS is switched On while it decreases for non-responders. Also, these nodes are relatively more important in responders than non-responders. It is possible that these nodes perform a hub-like function and therefore can relay information more efficient to more nodes. This would be consistent with the increased integrated network presented by Fraschini et al. [181]. However, they also showed an increased minimum spanning tree hierarchy in responders only, which indicates a decreased overloading of central nodes. It is important to stress that Fraschini et al. used EEG electrodes as nodes whereas in this research brain areas were used as nodes. Therefore, comparison between this research and Fraschini et al. is not trivial.

Importantly, again the insular and limbic area in the brain again seem to be critically involved in analyzing differences between responders vs. non-responders and VNS On vs. Off. This result is consistent with the conclusions in the source level analysis and the effective connectivity results. However, to the knowledge of the author, the approach to use brain areas as nodes in contrast to EEG electrodes for graph theory analyses of epileptic brains has little or no precedents.

7.4 Limitations

The limited amount of patients and the absence of pre-operative recordings reduce the clinical applicability of the results. Therefore, the biomarkers presented in this research are interesting but have little predictive value in clinical practice. P300 amplitudes were extracted in all EEG channels at the moment of peak in the Pz channel. A more detailed extraction of the P300 amplitudes would be achieved by detecting the P300 peak in each channel separately. The P300 can be split up into P3a and P3b. As was shown in this research, both components seem to generate specific results. Therefore, treating and investigating them separately seems appropriate. Also, using more patients will allow using more features simultaneously in the cross-validation for classification of patients as responders or non-responders.

In the source level analysis, due to the lack of time, no post-hoc t-tests were performed, which could identify differences between responders vs. non-responders and VNS On vs. Off in greater detail. Also, although warping the head models to the template head models was

performed accurately, the anatomically defined ROIs on the template head model do not perfectly delineate the same brain regions in the individual head models. There is a clear advantage when using individual head models, but the ROIs should therefore also be defined individually.

For the brain connectivity analysis, the 116-regional ROI system was reduced to 27 ROIs. Therefore, differences between some small ROIs are removed, limiting the anatomical accuracy of the results. Due to computational issues in the ESI, EEG signals of 9 s were used. This is short compared to the recordings of over 10 min and could possibly generalize the results inaccurately. Multiple comparison corrections are performed for all significance values of the post-hoc t-tests simultaneously. However, results in different frequency bands could be seen separate from each other and in that case they should be corrected separately.

Due to the lack of time, only betweenness centrality for each node was used as measure in the brain network analysis. This technique fails to indicate overall network characteristics.

In this research, no influences of the AEDs or administration regime were included. It is possible that AEDs altered brain functioning in patients and this effect should be investigated in other research.

7.5 Future research

Results in this research indicate possible methods to indicate features in the auditory oddball ERPs of patients to identify them as being either responder or non-responder. Future work should compare pre- and post-operative recordings with each other to come to predictive biomarkers. This research is currently being performed at the Reference Center for Refractory Epilepsy, Ghent University, Ghent, Belgium. The P300 wave should be investigated separately for P3a and P3b and all P300 features should be extracted from each EEG channel separately. Cross-validation should be used to estimate the clinical classification efficacy pre-operatively.

The use of individual head models is a good approach, but this should also be reflected in the definition of individual ROIs. The activity of the limbic and temporal brain areas was omnipresent in this research in the differences between responders and non-responders. Future work should focus on further elucidating the effect VNS has on these brain regions and what the contribution of them is to the anti-epileptic effect of VNS.

To the author's opinion, graph theory analyses could be of great help to unravel the mechanism of action of VNS. Importantly, the ROIs should be well chosen. A possible approach could be to start with large ROIs and to increase ROI resolution in those areas that show significant results. To overcome some computational issues, a simpler ESI technique could be used. Future

research should focus on using several graph theory measures to identify influences of VNS treatment on the brain. Brain areas should be used as nodes instead of using EEG electrodes as nodes, since this will generate results with high clinical interpretability, as is done in this research. Graph theory measures should be used that allow easy interpretation and that give interesting information on the mechanism of action of VNS.

Chapter 8

Conclusion

In this research, the effect of vagus nerve stimulation on the brain of epilepsy patients was assessed. The effects were explored at three levels: sensor level, source level and brain connectivity level. Possible biomarkers for pre-operative assessment of the VNS efficacy are analyzed and discussed.

An increase in P300 amplitude for responders only is reported in literature on several occasions and is confirmed in this research with the extension of finding a significant decrease in P300 amplitude for non-responders as well. Results in this research indicate that treating the P3a and P3b P300 components separately could be valuable. Importantly, cross-validation revealed that several features in the ERP can be used to obtain better accuracies in estimating the VNS efficacy of an unknown patient than the P300 amplitude recorded from the midline electrodes, which is proposed in literature. The results in this research point to one or both of the following hypotheses: (1) P300 features recorded from other than midline electrodes can be used to obtain better accuracies in assessing VNS efficacy and (2) other VNS dependent brain signals than the P300 wave can be used to assess VNS efficacy with a much larger accuracy. However, the reported biomarkers are no predictive biomarkers due to the absence of ERP recordings pre-operatively.

Several brain regions are found that are influenced by VNS treatment, including the limbic system, insula, frontal orbital lobe and several temporal structures. Therefore, these results are consistent with the VNS mediated activity in limbic and temporal lobe structures, as reported in literature. Analyzing the brain connectivity and whole-brain network identified shifts in the brain functioning between responders and non-responders due to VNS. The importance of the insular and limbic area in brain functioning seems to be altered between responders and non-responders. Future research should elaborate on unraveling the role of these structures in the anti-epileptic effect of VNS. Consistent with literature, connectivity and graph theory measures prove to be helpful tools to study the epileptic brain and provide useful insights in the mechanism of action of VNS.

Appendix

116 ROIs	27 ROIs
Precentral gyrus Postcentral gyrus Rolandic operculum	Central region
Superior frontal gyrus, dorsolateral Middle frontal gyrus Inferior frontal gyrus, opercular part Inferior frontal gyrus, triangular part	Lateral surface of frontal lobe
Superior frontal gyrus, medial Supplementary motor area Paracentral lobule	Medial surface of frontal lobe
Superior frontal gyrus, orbital part Superior frontal gyrus, medial orbital part Middle frontal gyrus, orbital part Inferior frontal gyrus, orbital part Gyrus rectus Olfactory cortex	Orbital surface of frontal lobe
Superior temporal gyrus Heschl gyrus Middle temporal gyrus Inferior temporal gyrus	Lateral surface of temporal lobe
Superior parietal gyrus Inferior parietal, but supramarginal and angular gyri Angular gyrus Supramarginal gyrus	Lateral surface of parietal lobe
Precuneus	Medial surface of parietal lobe
Superior occipital gyrus Middle occipital gyrus Inferior occipital gyrus	Lateral surface of occipital lobe
Cuneus Calcarine fissure and surrounding cortex Lingual gyrus Fusiform gyrus	Medial and inferior surfaces of occipital lobe
Temporal pole: superior temporal gyrus Temporal pole: middle temporal gyrus Anterior cingulate and paracingulate gyri Median cingulate and paracingulate gyri Posterior cingulate gyrus Hippocampus Parahippocampal gyrus	Limbic lobe

Insula	Insula
Amygdala Caudate nucleus Lenticular nucleus, putamen Lenticular nucleus, pallidum Thalamus	Sub cortical gray nuclei
Cerebellum Crus1 Cerebellum Crus2 Cerebellum 3 Cerebellum 4-5 Cerebellum 6 Cerebellum 7 Cerebellum 8 Cerebellum 9 Cerebellum 10	Cerebellum
Vermis 1-2 Vermis 3 Vermis 4-5 Vermis 6 Vermis 7 Vermis 8 Vermis 9 Vermis 10	Vermis

Appendix Table A: Detailed description of the two ROIs systems used in this research. All regions are present bilaterally except the vermis. These systems were defined in [156].

Patient	Group	Latency Off (s)	Latency On (s)
P1	R	0.586	0.656
P2	R	0.527	0.840
P3	NR	0.453	0.598
P4	NR	0.516	0.453
P5	NR	0.426	0.480
P8	NR	0.656	0.668
P9	R	0.469	0.441
P10	R	0.313	0.313
P11	NR	0.477	0.457
P12	R	0.477	0.469
P13	R	0.477	0.879
P14	R	0.691	0.754
P15	NR	0.406	0.422
P16	R	0.434	0.453
P17	NR	0.620	0.625
P18	NR	0.668	0.770
P19	R	0.711	0.594
P20	NR	0.590	0.570
P21	R	0.543	0.531

Appendix Table B: Observed values for the latency of the P300 peak in the target-standard difference waveform. The latency is automatically detected in the Pz channel for each patient and each condition. For each patient it is indicated whether it is a responder (R) or non-responders (NR). Latency is measured relative to stimulus onset.

R		**NR**		**Statistical analysis**		
Off	On	Off	On	Group df = 1,17	Condition df = 1,17	Group x condition df = 1,17
$\mu \pm \sigma$ (s)		$\mu \pm \sigma$ (s)		F=0.038	F=2.089	F=0.451
0.523±0.119	0.593±0.186	0.535±0.101	0.560±0.117	p=0.847	p=0.167	p=0.511

Appendix Table C: Results of the mixed-model ANOVA statistical analysis for the P300 latency.

	R		NR		Statistical analysis					
	Off	On	Off	On	Group		Condition		Group x condition	
					df=1,17		df=1,17		df=1,17	
	μ ± σ (μV)				F	p	F	p	F	p
Fp1	-3.82 ± 4.00	-2.99 ± 4.21	-9.04 ± 8.72	-7.41 ± 5.09	4.65	0.05	0.78	0.39	0.08	0.78
Fpz	-0.72 ± 11.36	-1.39 ± 5.27	-9.45 ± 7.23	-8.48 ± 4.89	7.21	0.02	0.01	0.94	0.17	0.68
Fp2	-3.46 ± 3.05	-2.51 ± 5.08	-9.21 ± 6.70	-7.83 ± 6.56	9.98	0.01	0.42	0.53	0.01	0.91
F7	-2.62 ± 3.50	-4.18 ± 4.20	-7.23 ± 4.17	-6.01 ± 4.06	3.92	0.06	0.04	0.84	2.74	0.12
F3	-3.08 ± 2.37	-2.73 ± 2.36	-7.84 ± 4.79	-6.86 ± 4.00	11.13	0.00	0.56	0.46	0.13	0.73
Fz	-4.25 ± 2.72	-2.77 ± 2.57	-6.77 ± 5.33	-6.59 ± 3.44	5.94	0.03	0.63	0.44	0.39	0.54
F4	-3.07 ± 1.90	-2.49 ± 2.50	-5.25 ± 4.21	-4.77 ± 1.42	5.26	0.04	0.48	0.50	0.01	0.94
F8	-2.79 ± 2.36	-4.09 ± 3.40	-5.35 ± 2.40	-4.86 ± 3.29	1.95	0.18	0.47	0.50	2.22	0.16
T7	-0.84 ± 3.64	-2.24 ± 3.59	-4.42 ± 4.84	-3.78 ± 5.52	2.06	0.17	0.15	0.70	1.10	0.31
C3	-1.00 ± 3.84	-0.49 ± 3.69	-1.39 ± 2.79	-1.81 ± 3.54	0.31	0.58	0.01	0.93	0.86	0.37
Cz	-1.34 ± 4.28	0.23 ± 2.87	1.93 ± 4.79	1.15 ± 4.74	1.37	0.26	0.29	0.60	2.63	0.12
C4	-0.03 ± 3.26	0.71 ± 2.92	3.18 ± 3.19	1.77 ± 2.91	2.44	0.14	0.93	0.35	9.76	0.01
T8	-1.21 ± 4.23	-3.03 ± 3.83	-0.80 ± 4.68	-2.02 ± 4.90	0.15	0.70	3.18	0.09	0.12	0.73
P7	2.01 ± 3.80	1.11 ± 4.27	2.25 ± 4.37	2.37 ± 4.41	0.19	0.67	0.18	0.68	0.31	0.59
P3	4.01 ± 2.30	4.47 ± 4.25	5.74 ± 3.31	4.78 ± 1.39	0.66	0.43	0.17	0.69	1.38	0.26
Pz	4.75 ± 2.49	6.25 ± 3.83	8.86 ± 3.43	8.09 ± 3.60	4.12	0.06	0.55	0.47	5.33	0.03
P4	4.28 ± 1.98	5.04 ± 2.90	7.74 ± 3.35	7.38 ± 2.44	7.76	0.01	0.09	0.77	0.69	0.42
P8	1.35 ± 4.23	0.52 ± 3.98	4.41 ± 5.15	4.46 ± 3.85	4.04	0.06	0.17	0.69	0.22	0.65
O1	3.10 ± 3.99	1.52 ± 3.72	5.36 ± 5.35	5.93 ± 3.21	3.67	0.07	0.44	0.52	2.02	0.17
Oz	3.08 ± 3.87	1.99 ± 3.12	5.52 ± 5.23	6.20 ± 2.88	4.49	0.05	0.06	0.81	1.11	0.31
O2	2.91 ± 3.96	2.11 ± 2.91	5.48 ± 5.08	6.22 ± 3.01	4.69	0.05	0.00	0.97	0.83	0.37
FC5	-2.31 ± 1.41	-3.36 ± 3.13	-5.88 ± 3.53	-5.54 ± 4.68	4.13	0.06	0.35	0.56	1.35	0.26
FC1	-3.66 ± 3.41	-2.32 ± 2.20	-4.12 ± 5.49	-4.27 ± 3.39	0.66	0.43	0.45	0.51	0.71	0.41
FC2	-2.89 ± 3.47	-1.23 ± 2.85	-1.91 ± 4.74	-2.31 ± 3.74	0.00	0.98	0.76	0.40	2.04	0.17
FC6	-2.39 ± 2.58	-2.45 ± 2.86	-2.74 ± 2.48	-3.08 ± 2.43	0.20	0.66	0.18	0.67	0.09	0.77
PO7	2.86 ± 3.16	1.39 ± 4.51	4.88 ± 4.23	5.63 ± 2.42	4.46	0.05	0.19	0.67	1.79	0.20
PO8	2.50 ± 4.90	0.60 ± 7.92	5.57 ± 4.86	5.71 ± 3.24	3.06	0.10	0.72	0.41	0.97	0.34
CP1	2.09 ± 3.36	2.83 ± 3.53	4.75 ± 2.43	4.75 ± 4.66	2.22	0.15	0.38	0.55	0.40	0.54
CP2	2.54 ± 2.88	4.09 ± 3.02	6.89 ± 3.73	5.78 ± 4.30	3.77	0.07	0.30	0.59	10.96	0.00
CP6	1.55 ± 2.56	1.60 ± 2.69	4.24 ± 3.18	3.08 ± 2.47	3.37	0.08	1.06	0.32	1.29	0.27
Poz	5.19 ± 3.66	4.93 ± 2.80	8.74 ± 4.69	8.71 ± 2.75	6.73	0.02	0.03	0.86	0.02	0.89
AF7	-2.53 ± 4.23	-3.37 ± 3.80	-7.91 ± 6.14	-6.95 ± 3.45	7.97	0.01	0.00	0.97	0.46	0.51
AF3	-3.98 ± 2.74	-2.92 ± 2.20	-7.96 ± 4.31	-6.90 ± 2.55	13.77	0.00	1.44	0.25	0.00	1.00
AF4	-3.51 ± 2.37	-2.68 ± 2.85	-7.37 ± 4.72	-6.55 ± 2.68	10.87	0.00	0.79	0.39	0.00	0.99
AF8	-2.66 ± 3.85	-4.32 ± 5.07	-6.82 ± 3.67	-5.45 ± 5.40	3.39	0.08	0.01	0.93	0.99	0.33
F5	-4.00 ± 4.21	-4.03 ± 4.53	-8.45 ± 4.56	-6.45 ± 3.33	3.66	0.07	1.95	0.18	2.03	0.17
F1	-3.90 ± 2.66	-2.85 ± 2.30	-6.92 ± 4.48	-6.60 ± 3.44	8.95	0.01	0.47	0.50	0.13	0.72
F2	-3.80 ± 2.31	-1.99 ± 3.29	-5.92 ± 4.84	-5.44 ± 2.70	4.97	0.04	1.51	0.24	0.52	0.48
F6	-2.18 ± 3.49	-2.41 ± 2.87	-6.82 ± 5.17	-5.22 ± 10.41	5.99	0.03	0.09	0.77	0.15	0.70
FC3	-2.66 ± 2.79	-2.05 ± 2.72	-5.03 ± 3.99	-4.54 ± 4.12	2.89	0.11	0.69	0.42	0.01	0.93
FCz	-4.06 ± 3.95	-2.50 ± 2.92	-3.85 ± 6.47	-4.47 ± 4.40	0.23	0.64	0.21	0.65	1.17	0.30
FC4	-2.15 ± 2.74	-1.18 ± 2.81	-1.39 ± 2.92	-2.15 ± 2.80	0.01	0.94	0.06	0.81	4.20	0.06
C5	0.28 ± 4.48	-0.60 ± 4.13	-2.55 ± 3.33	-3.11 ± 4.36	2.15	0.16	2.11	0.17	0.10	0.76
C1	-1.27 ± 4.01	-0.17 ± 3.03	0.51 ± 3.40	-0.12 ± 3.49	0.38	0.55	0.15	0.70	2.03	0.17
C2	-0.13 ± 3.43	1.45 ± 2.72	3.60 ± 4.09	2.52 ± 4.41	2.20	0.16	0.24	0.63	6.93	0.02
C6	-0.60 ± 3.69	-0.14 ± 3.84	1.20 ± 2.78	-0.11 ± 2.56	0.38	0.55	1.64	0.22	7.15	0.02
CP3	2.06 ± 3.37	2.35 ± 3.93	3.07 ± 2.73	1.91 ± 2.49	0.04	0.85	1.03	0.33	2.86	0.11

CP5	1.50 ± 2.69	0.82 ± 2.72	0.72 ± 3.49	-0.12 ± 3.91	0.39	0.54	2.04	0.17	0.02	0.89
CP4	2.48 ± 2.50	3.45 ± 3.31	6.27 ± 3.22	4.97 ± 2.99	4.01	0.06	0.17	0.68	7.88	0.01
P5	3.15 ± 2.35	2.58 ± 2.57	4.21 ± 3.78	3.65 ± 2.57	0.84	0.37	0.92	0.35	0.00	0.99
P1	4.47 ± 2.40	5.19 ± 4.32	7.16 ± 2.81	6.35 ± 2.03	2.27	0.15	0.01	0.94	1.85	0.19
P2	4.33 ± 2.00	5.80 ± 3.38	8.41 ± 3.73	7.77 ± 3.48	4.82	0.04	0.68	0.42	4.29	0.05
P6	2.79 ± 2.70	2.86 ± 2.59	6.33 ± 3.60	5.92 ± 2.37	9.84	0.01	0.05	0.83	0.09	0.77
PO5	2.61 ± 4.46	1.06 ± 5.54	5.69 ± 4.56	6.06 ± 2.39	4.63	0.05	0.56	0.47	1.48	0.24
PO3	4.77 ± 3.21	3.75 ± 3.08	6.97 ± 4.28	7.01 ± 2.18	4.32	0.05	0.47	0.50	0.54	0.47
PO4	3.41 ± 4.62	2.60 ± 7.47	8.10 ± 3.97	8.20 ± 2.61	5.87	0.03	0.14	0.71	0.22	0.64
PO6	2.78 ± 4.90	1.33 ± 7.67	7.08 ± 3.98	7.38 ± 2.55	5.63	0.03	0.34	0.57	0.78	0.39
FT7	-1.62 ± 2.82	-3.40 ± 3.28	-5.60 ± 4.71	-4.82 ± 4.58	2.73	0.12	0.46	0.51	3.08	0.10
FT8	-1.44 ± 3.20	-3.04 ± 4.17	-2.85 ± 3.67	-3.64 ± 3.67	0.40	0.54	4.47	0.05	0.51	0.49
TP7	0.38 ± 3.64	-0.67 ± 3.55	-1.15 ± 4.10	-0.60 ± 5.03	0.20	0.66	0.07	0.79	0.78	0.39

Appendix Table D: Results and descriptive statistics of mixed-model ANOVA for the P300 amplitude in all 60 EEG channels. Group indicates responders vs. non-responders while condition indicates VNS On vs. VNS Off. Group x condition represents the interaction effect between the factors group and condition. Significant results are marked in gray.

	Group				**Condition**			
	Off (df=17)		**On (df=17)**		**R (df=9)**		**NR (df=8)**	
	t	**p**	**t**	**p**	**t**	**p**	**t**	**p**
Fp1	1.728	0.102	1.95	0.068				
Fpz	2.011	0.06	2.738	0.014				
Fp2	2.452	0.025	1.988	0.063				
F3	2.794	0.0125	2.777	0.013				
Fz	1.316	0.206	2.763	0.013				
F4	1.478	0.158	2.41	0.028				
C4	-2.166	0.045	-0.796	0.437	-1.366	0.205	3.519	0.0079
Pz	-3.015	0.008	-1.08	0.295	-3.042	0.014	0.875	0.407
P4	-2.744	0.014	-1.889	0.076				
Oz	-1.164	0.261	-3.035	0.007				
O2	-1.236	0.233	-3.019	0.008				
PO7	-1.19	0.25	-2.504	0.023				
CP2	-2.864	0.011	-1.002	0.33	-3.329	0.009	1.681	0.131
Poz	-1.853	0.081	-2.966	0.009				
AF7	2.245	0.038	2.141	0.047				
AF3	2.433	0.026	3.654	0.002				
AF4	2.284	0.036	3.049	0.007				
F1	1.809	0.088	2.821	0.012				
F2	1.239	0.232	2.486	0.024				
F6	2.315	0.033	0.821	0.423				
C2	-2.16	0.045	-0.645	0.528	-1.837	0.099	2.303	0.05
C6	-1.186	0.252	-0.015	0.988	-0.986	0.35	2.808	0.023
CP4	-2.883	0.01	-1.044	0.311	-1.957	0.082	1.996	0.081
P2	-3.012	0.008	-1.255	0.226				
P6	-2.436	0.026	-2.678	0.016				

PO5	-1.484	0.156	-2.499	0.023				
PO3	-1.282	0.217	-2.633	0.017				
PO4	-2.361	0.03	-2.128	0.048				
PO6	-2.086	0.052	-2.25	0.038				

Appendix Table E: Results of post-hoc two-tailed two tailed t-tests for EEG channels that exhibit significant main effect of group and/or significant interaction effect for the P300 amplitude. To investigate the influence of the group, independent samples t-tests are used for both VNS Off and On. To investigate the influence of the condition paired samples t-tests are used.

	Relative amplitude change	
	t (df=17)	**p**
C4	-0.05	0.961
Pz	2.742	0.014
CP2	0.743	0.486
C6	1.056	0.306
C2	1.141	0.27
CP4	1.033	0.316

Appendix Table F: Results for post-hoc two-tailed independent samples t-tests for the relative (on-off/off) amplitude change of the P300 amplitude.

	VNS Off			
	OR	**CI (lower-upper)**		**p**
Fp2	1.289	0.989	1.68	0.06
F3	1.444	1.012	2.06	0.043
C4	0.72	0.507	1.021	0.065
Pz	0.574	0.343	0.963	0.035
P4	0.595	0.361	0.981	0.042
CP2	0.614	0.394	0.957	0.031
AF7	1.251	0.98	1.598	0.072
AF3	1.388	0.999	1.928	0.051
AF4	1.407	0.978	2.024	0.066
F6	1.392	0.978	1.981	0.066
C2	0.742	0.538	1.024	0.069
CP4	0.629	0.414	0.957	0.03
P2	0.55	0.309	0.979	0.042
P6	0.681	0.459	1.01	0.056
PO4	0.728	0.522	1.015	0.061

Appendix Table G: Results of the logistic regression analysis for VNS Off. The analysis is performed on the EEG channels that showed a significant difference between responders and non-responders for VNS Off by post-hoc two-tailed independent samples t-test. OR indicates the odds ratio and CI the confidence interval.

	VNS On			
	OR	CI (lower-upper)		p
Fp1	1.274	0.963	1.684	0.09
Fpz	1.582	0.986	2.536	0.057
F3	1.654	1.003	2.729	0.049
Fz	1.715	1.002	2.934	0.049
F4	2.357	0.955	5.82	0.063
P4	0.706	0.469	1.062	0.095
Oz	0.622	0.409	0.947	0.027
O2	0.598	0.379	0.944	0.027
PO7	0.655	0.432	0.992	0.046
Poz	0.617	0.403	0.946	0.027
AF7	1.36	0.967	1.912	0.077
AF3	1.988	1.122	3.52	0.019
AF4	1.814	1.034	3.18	0.038
F1	1.599	1.022	2.5	0.04
F2	2.24	0.926	5.418	0.074
P6	0.546	0.296	1.007	0.053
PO5	0.625	0.381	1.025	0.063
PO3	0.639	0.419	0.973	0.037
PO4	0.654	0.435	0.984	0.042
PO6	0.644	0.419	0.99	0.045

Appendix Table H: Results of the logistic regression analysis for VNS on. The analysis is performed on the EEG channels that showed a significant difference between responders and non-responders for VNS On by post-hoc two-tailed independent samples t-test. OR indicates the odds ratio and CI the confidence interval.

	Relative amplitude change			
	OR	CI (lower-upper)		p
C4	1	0.996	1.004	0.958
Pz	1.052	1.003	1.103	0.038
CP2	1.003	0.996	1.009	0.453
C2	1.001	0.998	1.005	0.402
C6	1	1	1	0.59
CP4	1.006	0.994	1.019	0.308

Appendix Table I: Results of the logistic regression analysis for the relative P300 amplitude change. The analysis is performed on the EEG channels that showed a significant difference between VNS On and Off for either responders or non-responders for by post-hoc two-tailed related samples t-test. OR indicates the odds ratio and CI the confidence interval.

ROI	NR (Off)	NR (On)	R (Off)	R (On)
1	4.53	22.28	5.19	8.86
2	14.80	17.89	18.89	16.31
3	1.60	7.92	31.50	14.92
4	5.63	9.01	7.43	18.69
5	16.41	8.70	11.67	5.82
6	30.57	9.88	28.45	18.11
7	13.16	4.39	9.62	9.73
8	8.61	7.09	7.37	16.76
9	3.60	0.51	5.30	2.59
10	5.25	12.64	16.99	12.83
11	0.82	1.39	3.94	1.81
12	3.89	5.08	14.06	13.73
13	11.30	2.11	13.25	7.52
14	13.16	9.10	22.58	25.02
15	1.76	7.99	4.19	1.80
16	2.99	6.37	17.72	8.23
17	6.40	13.14	16.01	14.19
18	16.20	22.07	22.09	26.56
19	26.01	20.39	8.03	10.96
20	28.63	9.51	16.37	35.83
21	18.23	27.58	8.89	5.68
22	18.02	4.32	20.11	38.70
23	4.20	9.43	7.54	9.46
24	16.54	19.62	14.15	27.36
25	3.83	3.24	15.68	12.51
26	9.93	20.09	17.52	11.80
27	13.76	8.86	11.25	13.63

Appendix Table J: Mean betweenness centrality measures for groups, conditions and ROIs.

Node	p value	Measure	Frequency band	R_{on}-R_{off}	NR_{on}-NR_{off}
Frontal surface of left frontal lobe	0.0265	iADTF	γ	<0	>0
Medial surface of right frontal lobe	0.0328	iADTF	α	>0	<0
	0.0137	ffADTF	γ	<0	>0
Lateral surface of right temporal lobe	0.0426	ffADTF	β	<0	>0
Lateral surface of left parietal lobe	0.0233	ffADTF	γ	<0	>0
Lateral surface of left occipital lobe	0.0392	ffADTF	γ	<0	>0
Left limbic lobe	0.0212	iADTF	γ	>0	<0
Right limbic lobe	0.0393	iAPDC	δ	>0	<0
	0.0271	iAPDC	θ	>0	<0
	0.0170	iAPDC	α	>0	<0
	0.0140	iAPDC	γ	>0	<0
	0.0390	ffAPDC	δ	>0	<0
	0.0275	ffAPDC	θ	>0	<0
	0.0167	ffAPDC	α	>0	<0
	0.0163	ffAPDC	γ	>0	<0
Right insula	0.0253	iADTF	θ	>0	<0
	0.0417	iADTF	α	>0	<0
	0.0266	ffADTF	θ	>0	<0
	0.0492	ffADTF	α	>0	<0

Appendix Table K: Significant results for interaction effect of betweenness centrality for different nodes, measures and frequency bands. δ, θ, α, β and γ indicate different frequency bands: 0-4 Hz, 4-8 Hz, 8-16 Hz, 16-32 Hz and 32-64 Hz respectively.

References

[1] K. Vonck, V. De Herdt, and P. Boon, "Vagal nerve stimulation--a 15-year survey of an established treatment modality in epilepsy surgery," *Adv. Tech. Stand. Neurosurg.*, vol. 34, pp. 111–146, 2009.

[2] L. Forsgren, E. Beghi, A. Oun, and M. Sillanpää, "The epidemiology of epilepsy in Europe - a systematic review," *Eur. J. Neurol. Off. J. Eur. Fed. Neurol. Soc.*, vol. 12, no. 4, pp. 245–253, Apr. 2005.

[3] F. A. Al-Otaibi, C. Hamani, and A. M. Lozano, "Neuromodulation in epilepsy," *Neurosurgery*, vol. 69, no. 4, pp. 957–979; discussion 979, Oct. 2011.

[4] E. Ben-Menachem, "Vagus-nerve stimulation for the treatment of epilepsy," *Lancet Neurol.*, vol. 1, no. 8, pp. 477–482, Dec. 2002.

[5] K. Vonck, V. D. Herdt, M. Sprengers, and E. Ben-Menachem, "Neurostimulation for epilepsy," *Handb. Clin. Neurol.*, vol. 108, pp. 956–970, 2012.

[6] P. Boon, K. Vonck, J. D. Reuck, and J. Caemaert, "Vagus nerve stimulation for refractory epilepsy," *Seizure Eur. J. Epilepsy*, vol. 10, no. 6, pp. 456–460, 2001.

[7] F. Fornai, R. Ruffoli, F. S. Giorgi, and A. Paparelli, "The role of locus coeruleus in the antiepileptic activity induced by vagus nerve stimulation," *Eur. J. Neurosci.*, vol. 33, no. 12, pp. 2169–2178, Jun. 2011.

[8] L. De Taeye, K. Vonck, M. van Bochove, P. Boon, D. Van Roost, L. Mollet, A. Meurs, V. De Herdt, E. Carrette, I. Dauwe, S. Gadeyne, P. van Mierlo, T. Verguts, and R. Raedt, "The P3 event-related potential is a biomarker for the efficacy of vagus nerve stimulation in patients with epilepsy," *Neurother. J. Am. Soc. Exp. Neurother.*, vol. 11, no. 3, pp. 612–622, Jul. 2014.

[9] S. Nieuwenhuis, G. Aston - Jones, and J. D. Cohen, "Decision Making, the P3, and the Locus Coeruleus--Norepinephrine System," *Psychol. Bull.*, vol. 131, no.

4, 2006.

[10] D. R. White and S. P. Borgatti, "Betweenness centrality measures for directed graphs," *Soc. Netw.*, vol. 16, no. 4, pp. 335–346, Oct. 1994.

[11] D. Purves, *Neuroscience*, 5th ed. Sunderland, Mass: Sinauer, 2012.

[12] F. A. C. Azevedo, L. R. B. Carvalho, L. T. Grinberg, J. M. Farfel, R. E. L. Ferretti, R. E. P. Leite, W. Jacob Filho, R. Lent, and S. Herculano-Houzel, "Equal numbers of neuronal and nonneuronal cells make the human brain an isometrically scaled-up primate brain," *J. Comp. Neurol.*, vol. 513, no. 5, pp. 532–541, Apr. 2009.

[13] Pieter van Mierlo, "Epileptic focus localization using functional brain connectivity," 2013.

[14] C. Petersen, "The action potential," presented at the Lectures "Neurosciences - Cellular mechanisms of brain function.," Ecole Polytechnique Fédérale de Lausanne, 24-Sep-2014.

[15] C. Petersen, "Membrane potential," presented at the Lectures "Neurosciences - Cellular mechanisms of brain function.," Ecole Polytechnique Fédérale de Lausanne, 17-Sep-2014.

[16] C. Petersen, "Neurotransmitter release," presented at the Lectures "Neurosciences - Cellular mechanisms of brain function.," Ecole Polytechnique Fédérale de Lausanne, 10-Jan-2014.

[17] C. Petersen, "GABAergic inhibition," presented at the Lectures "Neurosciences - Cellular mechanisms of brain function.," Ecole Polytechnique Fédérale de Lausanne, 15-Oct-2014.

[18] C. Petersen, "Glutamate receptors," presented at the Lectures "Neurosciences - Cellular mechanisms of brain function.," Ecole Polytechnique Fédérale de Lausanne, 10-Aug-2014.

[19] C. Petersen, "Postsynaptic potentials," presented at the Lectures "Neurosciences - Cellular mechanisms of brain function.," Ecole Polytechnique Fédérale de Lausanne, 10-Aug-2014.

[20] R. Carter, *The Brain Book*. Dorling Kindersley Ltd, 2014.

[21] S. A. Bunge and I. Kahn, "Cognition: An Overview of Neuroimaging Techniques." Elsevier Ltd, 2009.

[22] M. Demitri and M. D. ~ 2 min read, "Types of Brain Imaging Techniques," *Psych Central.com*. [Online]. Available: http://psychcentral.com/lib/types-of-brain-imaging-techniques/0001057. [Accessed: 14-Apr-2015].

[23] B. He and Z. Liu, "Multimodal Functional Neuroimaging: Integrating Functional MRI and EEG/MEG," *IEEE Rev. Biomed. Eng.*, vol. 1, no. 2008, pp. 23–40, Nov. 2008.

[24] S. Baillet, J. C. Mosher, and R. M. Leahy, "Electromagnetic brain mapping," *Signal Process. Mag. IEEE*, vol. 18, no. 6, pp. 14–30, 2001.

[25] M. Haemaelaeinen, R. Hari, R. J. Ilmoniemi, J. Knuutila, and O. V. Lounasmaa, "Magnetoencephalography---theory, instrumentation, and applications to noninvasive studies of the working human brain," *Rev. Mod. Phys.*, vol. 65, no. 2, 1993.

[26] Hallez Hans, Vanrumste Bart, Grech Roberta, Muscat Joseph, De Clercq Wim, Vergult Anneleen, D'Asseler Yves, Camilleri Kenneth, Fabri Simon, Van Huffel Sabine, and Lemahieu Ignace, "Review on solving the forward problem in EEG source analysis," *J. NeuroEngineering Rehabil. JNER*, vol. 4, no. 1, p. 46, 2007.

[27] N. Schaul, "The fundamental neural mechanisms of electroencephalography," *Electroencephalogr. Clin. Neurophysiol.*, vol. 106, no. 2, pp. 101–107, 1998.

[28] C. Petersen, "Glutamatergic circuits," presented at the Lectures "Neurosciences - Cellular mechanisms of brain function.," Ecole Polytechnique Fédérale de Lausanne, 10-Aug-2014.

[29] S. Lefort, C. Tomm, J.-C. Floyd Sarria, and C. C. H. Petersen, "The excitatory neuronal network of the C2 barrel column in mouse primary somatosensory cortex," *Neuron*, vol. 61, no. 2, pp. 301–316, Jan. 2009.

[30] UC Regents Davis campus, "Brainmaps.org."

[31] "tDCS - Album on," *Imgur*. [Online]. Available: http://imgur.com/a/CrzTG/embed. [Accessed: 14-Apr-2015].

[32] M. Teplan, "Fundamentals of EEG measurement," in *Measurement Science Review*, vol. 2, Bratislave, Slovakia: Institute of Measurement Science.

[33] H. Hallez, "Incorporation of Anisotropic Conductivities in EEG source Analysis," Ghent University, Faculty of Engineering, Ghent, Belgium, 2008.

[34] S. Vandenberghe, "Neuro imaging: electrical signals from the brain," Ghent, Belgium, 2014-2013.

[35] G. Strobbe, "Advanced Forward Models for EEG Source Imaging."

[36] J. C. de Munck, B. W. van Dijk, and H. Spekreijse, "Mathematical dipoles are adequate to describe realistic generators of human brain activity," *IEEE Trans. Biomed. Eng.*, vol. 35, no. 11, pp. 960–966, Nov. 1988.

[37] K. Kaiboriboon, H. O. Lüders, M. Hamaneh, J. Turnbull, and S. D. Lhatoo, "EEG source imaging in epilepsy--practicalities and pitfalls," *Nat. Rev. Neurol.*, vol. 8, no. 9, pp. 498–507, Sep. 2012.

[38] P. K. Banerjee, *The Boundary Element Methods in Engineering*, Rev Sub edition. London ; New York: Mcgraw-Hill College, 1994.

[39] Y. K. Cheung, S. H. Lo, and A. Y. T. Leung, *Finite Element Implementation*, 1 edition. Oxford, England ; Cambridge, Mass., USA: Wiley-Blackwell, 1996.

[40] A. R. Mitchell and D. F. Griffiths, *The Finite Difference Method in Partial Differential Equations*, 1 edition. Chichester Eng. ; New York: Wiley, 1980.

[41] P. Van Hese, "Detection and analysis of epileptiform activity in the electroencephalogram," dissertation, Ghent University, 2008.

[42] J. C. Mosher, P. S. Lewis, and R. M. Leahy, "Multiple dipole modeling and localization from spatio-temporal MEG data," *IEEE Trans. Biomed. Eng.*, vol. 39, no. 6, pp. 541–557, Jun. 1992.

[43] R. Willoughby, "Solutions of Ill-Posed Problems (A. N. Tikhonov and V. Y. Arsenin)," *SIAM Rev.*, vol. 21, no. 2, pp. 266–267, Apr. 1979.

[44] P. Hansen, "Analysis of Discrete Ill-Posed Problems by Means of the L-Curve," *SIAM Rev.*, vol. 34, no. 4, pp. 561–580, Dec. 1992.

[45] A. T. Berg, S. F. Berkovic, M. J. Brodie, J. Buchhalter, J. H. Cross, W. Van Emde Boas, J. Engel, J. French, T. A. Glauser, G. W. Mathern, S. L. Moshé, D. Nordli, P. Plouin, and I. E. Scheffer, "Revised terminology and concepts for organization of seizures and epilepsies: Report of the ILAE Commission on Classification and Terminology, 2005–2009," *Epilepsia*, vol. 51, no. 4, pp. 676–685, 2010.

[46] J. S. Duncan, J. W. Sander, S. M. Sisodiya, and M. C. Walker, "Adult epilepsy," *Lancet*, vol. 367, no. 9516, pp. 1087–1100, Apr. 2006.

[47] R. S. Fisher, C. Acevedo, A. Arzimanoglou, A. Bogacz, J. H. Cross, C. E. Elger, J. Engel, L. Forsgren, J. A. French, M. Glynn, D. C. Hesdorffer, B. I. Lee, G. W. Mathern, S. L. Moshé, E. Perucca, I. E. Scheffer, T. Tomson, M. Watanabe, and S. Wiebe, "ILAE official report: a practical clinical definition of epilepsy," *Epilepsia*, vol. 55, no. 4, pp. 475–482, Apr. 2014.

[48] R. S. Fisher, W. van Emde Boas, W. Blume, C. Elger, P. Genton, P. Lee, and J. Engel, "Epileptic seizures and epilepsy: definitions proposed by the International League Against Epilepsy (ILAE) and the International Bureau for Epilepsy (IBE)," *Epilepsia*, vol. 46, no. 4, pp. 470–472, Apr. 2005.

[49] D. J. Thurman, E. Beghi, C. E. Begley, A. T. Berg, J. R. Buchhalter, D. Ding, D. C. Hesdorffer, W. A. Hauser, L. Kazis, R. Kobau, B. Kroner, D. Labiner, K. Liow, G. Logroscino, M. T. Medina, C. R. Newton, K. Parko, A. Paschal, P.-M. Preux, J. W. Sander, A. Selassie, W. Theodore, T. Tomson, S. Wiebe, and ILAE Commission on Epidemiology, "Standards for epidemiologic studies and surveillance of epilepsy," *Epilepsia*, vol. 52 Suppl 7, pp. 2–26, Sep. 2011.

[50] T. R. Browne and G. L. Holmes, "Epilepsy.(Review Article)," *N. Engl. J. Med.*, vol. 344, no. 15, p. 1145, 2001.

[51] C. P. Panayiotopoulos, "The new ILAE report on terminology and concepts for organization of epileptic seizures: a clinician's critical view and contribution," *Epilepsia*, vol. 52, no. 12, pp. 2155–2160, Dec. 2011.

[52] S. D. Shorvon, "The etiologic classification of epilepsy," *Epilepsia*, vol. 52, no. 6, pp. 1052–1057, Jun. 2011.

[53] "WHO | Epilepsy," *WHO*. [Online]. Available: http://www.who.int/topics/epilepsy/en/. [Accessed: 15-Apr-2015].

[54] N. Savage, "Epidemiology: The complexities of epilepsy," *Nature*, vol. 511, no. 7508, pp. S2–S3, Jul. 2014.

[55] L. Sörnmo and P. Laguna, *Bioelectrical signal processing in cardiac and neurological applications*. Academic Press, 2005.

[56] C. P. Panayiotopoulos, *A Clinical Guide to Epileptic Syndromes and their Treatment*. London: Springer London, 2010.

[57] S. Noachtar and J. Rémi, "The role of EEG in epilepsy: A critical review," *Epilepsy Behav.*, vol. 15, no. 1, pp. 22–33, May 2009.

[58] M. Javidan, "Electroencephalography in Mesial Temporal Lobe Epilepsy: A Review," *Epilepsy Res. Treat.*, vol. 2012, p. e637430, Jun. 2012.

[59] V. Keereman, "Introduction to neuroanatomy, neurphysiology and neurological diseases," Ghent, Belgium, 2014-2013.

[60] M. J. Brodie, S. J. E. Barry, G. A. Bamagous, J. D. Norrie, and P. Kwan, "Patterns of treatment response in newly diagnosed epilepsy," *Neurology*, vol. 78, no. 20, pp. 1548–1554, May 2012.

[61] P. Kwan, A. Arzimanoglou, A. T. Berg, M. J. Brodie, W. Allen Hauser, G. Mathern, S. L. Moshé, E. Perucca, S. Wiebe, and J. French, "Definition of drug resistant epilepsy: Consensus proposal by the ad hoc Task Force of the ILAE Commission on Therapeutic Strategies," *Epilepsia*, vol. 51, no. 6, pp. 1069–1077, Jun. 2010.

[62] V. Keereman, "Neuromodulation," Ghent, Belgium, 2014-2013.

[63] F. Rosenow and H. Lüders, "Presurgical evaluation of epilepsy," *Brain J. Neurol.*, vol. 124, no. Pt 9, pp. 1683–1700, Sep. 2001.

[64] Medtronic, "Medtronic Receives European CE Mark Approval for Deep Brain Stimulation Therapy for Refractory Epilepsy." 16-Sep-2010.

[65] C. M. DeGiorgio, D. Murray, D. Markovic, and T. Whitehurst, "Trigeminal nerve stimulation for epilepsy: long-term feasibility and efficacy," *Neurology*, vol. 72, no. 10, pp. 936–938, Mar. 2009.

[66] F. Fregni, P. T. M. Otachi, A. Do Valle, P. S. Boggio, G. Thut, S. P. Rigonatti, A. Pascual-Leone, and K. D. Valente, "A randomized clinical trial of repetitive transcranial magnetic stimulation in patients with refractory epilepsy," *Ann. Neurol.*, vol. 60, no. 4, pp. 447–455, Oct. 2006.

[67] "Press Announcements - FDA approves medical device to treat epilepsy." [Online]. Available: http://www.fda.gov/newsevents/newsroom/pressannouncements/ucm375041.htm. [Accessed: 16-Apr-2015].

[68] "Photos of the Day: Top 10 Medical Innovations for 2014," *Medical Design Technology*. [Online]. Available: http://www.mdtmag.com/news/2013/10/photos-day-top-10-medical-innovations-2014. [Accessed: 16-Apr-2015].

[69] Odier, "Manuel de Médecine Pratique." 1811.

[70] "Epilepsy and other chronic convulsive diseases : their causes, symptoms, & treatment : Gowers, W. R. (William Richard), 1845-1915 : Free Download & Streaming," *Internet Archive*. [Online]. Available: https://archive.org/details/epilepsyotherchr00goweuoft. [Accessed: 18-Apr-2015].

[71] P. Andrews and I. Lawes, "A protective role for vagal afferents, a hypothesis.," *Neuroanat. Physiol. Abdom. Vagal Afferents*, p. 221.

[72] P. Rajna and C. Lona, "Sensory stimulation for inhibition of epileptic seizures," *Epilepsia*, vol. 30, no. 2, pp. 168–174, Apr. 1989.

[73] K. Vonck, V. Thadani, K. Gilbert, S. Dedeurwaerdere, L. De Groote, V. De Herdt, L. Goossens, F. Gossiaux, E. Achten, E. Thiery, G. Vingerhoets, D. Van Roost, J. Caemaert, J. De Reuck, D. Roberts, P. Williamson, and P. Boon, "Vagus Nerve Stimulation for Refractory Epilepsy: A Transatlantic Experience:," *J. Clin. Neurophysiol.*, vol. 21, no. 4, pp. 283–289, Jul. 2004.

[74] K. Vonck, S. Dedeurwaerdere, L. D. Groote, V. Thadani, P. Claeys, F. Gossiaux, D. V. Roost, and P. Boon, "Generator replacement in epilepsy patients treated with vagus nerve stimulation," *Seizure*, vol. 14, no. 2, pp. 89–99, Mar. 2005.

[75] Cyberonics, "http://us.cyberonics.com/en/vns-therapy-for-epilepsy/healthcare-professionals/vns-therapy/about-products/." .

[76] C. for D. and R. Health, "Recently-Approved Devices - VNS Therapy System - P970003s050." [Online]. Available: http://www.fda.gov/MedicalDevices/ProductsandMedicalProcedures/DeviceApprovalsandClearances/Recently-ApprovedDevices/ucm078532.htm. [Accessed: 17-Apr-2015].

[77] Cyberonics, "Overview to Cyberonics." .

[78] S. Benbadis, S. Helmers, L. Hirsch, J. Sirven, F. L. Vale, and J. Wheless, "Yes, neurostimulation has a role in the management of epilepsy," *Neurology*, vol. 83, no. 9, pp. 845–847, Aug. 2014.

[79] P. Boon, V. De Herdt, K. Vonck, and D. Van Roost, "Clinical experience with vagus nerve stimulation and deep brain stimulation in epilepsy," *Acta Neurochir. Suppl.*, vol. 97, no. 2, pp. 273–80, 2007.

[80] E. Ben-Menachem, "Vagus nerve stimulation, side effects, and long-term safety," *J. Clin. Neurophysiol. Off. Publ. Am. Electroencephalogr. Soc.*, vol. 18, no. 5, pp. 415–418, Sep. 2001.

[81] C. Hoppe, "Vagus nerve stimulation: Urgent need for the critical reappraisal of clinical effectiveness," *Seizure J. Br. Epilepsy Assoc.*, vol. 22, no. 1, 2012.

[82] E. García-Navarrete, C. V. Torres, I. Gallego, M. Navas, J. Pastor, and R. G. Sola, "Response to 'Vagus nerve stimulation: Urgent need for the critical reappraisal of clinical effectiveness,'" *Seizure-Eur. J. Epilepsy*, vol. 22, no. 6, pp. 490–491, 2013.

[83] D. J. Englot, "Vagus nerve stimulation versus 'best drug therapy' in epilepsy patients who have failed best drug therapy," *Seizure*, vol. 22, no. 5, pp. 409–410, Jun. 2013.

[84] S. Ogbonnaya and C. Kaliaperumal, "Vagal nerve stimulator: Evolving trends," *J. Nat. Sci. Biol. Med.*, vol. 4, no. 1, pp. 8–13, Jan. 2013.

[85] G. K. Bergey, "Neurostimulation in the treatment of epilepsy," *Exp. Neurol.*, vol. 244, p. 87, 2013.

[86] B. M. Uthman, A. M. Reichl, J. C. Dean, S. Eisenschenk, R. Gilmore, S. Reid,

S. N. Roper, and B. J. Wilder, "Effectiveness of vagus nerve stimulation in epilepsy patients A 12-year observation," *Neurology*, vol. 63, no. 6, pp. 1124–1126, 2004.

[87] F. Marrosu, A. Serra, A. Maleci, M. Puligheddu, G. Biggio, and M. Piga, "Correlation between GABA(A) receptor density and vagus nerve stimulation in individuals with drug-resistant partial epilepsy," *Epilepsy Res.*, vol. 55, no. 1–2, pp. 59–70, Jul. 2003.

[88] E. Ben-Menachem, A. Hamberger, T. Hedner, E. J. Hammond, B. M. Uthman, J. Slater, T. Treig, H. Stefan, R. E. Ramsay, and J. F. Wernicke, "Effects of vagus nerve stimulation on amino acids and other metabolites in the CSF of patients with partial seizures," *Epilepsy Res.*, vol. 20, no. 3, pp. 221–227, Mar. 1995.

[89] S. E. Krahl, K. B. Clark, D. C. Smith, and R. A. Browning, "Locus Coeruleus Lesions Suppress the Seizure-Attenuating Effects of Vagus Nerve Stimulation," *Epilepsia*, vol. 39, no. 7, 1998.

[90] C. Jimenez-Rivera, A. Voltura, and G. K. Weiss, "Effect of locus ceruleus stimulation on the development of kindled seizures," *Exp. Neurol.*, vol. 95, no. 1, pp. 13–20, Jan. 1987.

[91] D. A. Groves and V. J. Brown, "Vagal nerve stimulation: a review of its applications and potential mechanisms that mediate its clinical effects," *Neurosci. Biobehav. Rev.*, vol. 29, no. 3, pp. 493–500, May 2005.

[92] P. Follesa, F. Biggio, G. Gorini, S. Caria, G. Talani, L. Dazzi, M. Puligheddu, F. Marrosu, and G. Biggio, "Vagus nerve stimulation increases norepinephrine concentration and the gene expression of BDNF and bFGF in the rat brain," *Brain Res.*, vol. 1179, pp. 28–34, 2007.

[93] R. W. Roosevelt, D. C. Smith, R. W. Clough, R. A. Jensen, and R. A. Browning, "Increased extracellular concentrations of norepinephrine in cortex and hippocampus following vagus nerve stimulation in the rat," *Brain Res.*, vol. 1119, no. 1, pp. 124–132, 2006.

[94] D. L. Hassert, T. Miyashita, and C. L. Williams, "The effects of peripheral vagal nerve stimulation at a memory-modulating intensity on norepinephrine output in the basolateral amygdala," *Behav. Neurosci.*, vol. 118, no. 1, 2004.

[95] L. V. Borovikova, S. Ivanova, M. Zhang, H. Yang, G. I. Botchkina, L. R. Watkins, H. Wang, N. Abumrad, J. W. Eaton, and K. J. Tracey, "Vagus nerve stimulation attenuates the systemic inflammatory response to endotoxin,"

Nature, vol. 405, no. 6785, pp. 458–462, May 2000.

[96] R. Raedt, R. Clinckers, L. Mollet, K. Vonck, el Tahry, T. Wyckhuys, de Herdt, E. Carrette, W. J. Wadman, Y. Michotte, I. Smolders, P. Boon, and A. Meurs, "Increased hippocampal noradrenaline is a biomarker for efficacy of vagus nerve stimulation in a limbic seizure model.," *J. Neurochem.*, vol. 117, 2011.

[97] J. L. Vincent, G. H. Patel, M. D. Fox, A. Z. Snyder, J. T. Baker, D. C. Van Essen, J. M. Zempel, L. H. Snyder, M. Corbetta, and M. E. Raichle, "Intrinsic functional architecture in the anaesthetized monkey brain," *Nature*, vol. 447, no. 7140, pp. 83–86, May 2007.

[98] C. D. F. K. J. Friston, "Time-dependent changes in effective connectivity measured with PET," *Hum. Brain Mapp.*, vol. 1, no. 1, 1993.

[99] K. J. Friston, C. D. Frith, P. F. Liddle, and R. S. Frackowiak, "Functional connectivity: the principal-component analysis of large (PET) data sets," *J. Cereb. Blood Flow Metab. Off. J. Int. Soc. Cereb. Blood Flow Metab.*, vol. 13, no. 1, pp. 5–14, Jan. 1993.

[100] K. J. Friston, "Functional and Effective Connectivity: A Review," *Brain Connect.*, vol. 1, no. 1, pp. 13–36, Jan. 2011.

[101] D. Goldenberg and A. Galván, "The use of functional and effective connectivity techniques to understand the developing brain," *Dev. Cogn. Neurosci.*, vol. 12, pp. 155–164, Apr. 2015.

[102] L. Lee, L. M. Harrison, and A. Mechelli, "A report of the functional connectivity workshop, Dusseldorf 2002," *NeuroImage*, vol. 19, no. 2 Pt 1, pp. 457–465, Jun. 2003.

[103] P. J. Basser, J. Mattiello, and D. LeBihan, "MR diffusion tensor spectroscopy and imaging," *Biophys. J.*, vol. 66, no. 1, pp. 259–267, Jan. 1994.

[104] P. Hagmann, L. Jonasson, P. Maeder, J.-P. Thiran, V. J. Wedeen, and R. Meuli, "Understanding Diffusion MR Imaging Techniques: From Scalar Diffusion-weighted Imaging to Diffusion Tensor Imaging and Beyond1," *RadioGraphics*, vol. 26, no. suppl_1, pp. S205–S223, Oct. 2006.

[105] Siemens Healthcare, "RESOLVE," *Experience a higher level of diagnostic confidence with sharp, high-resolution diffusion-weighted images largely free of geometric distortions.* [Online]. Available: https://www.healthcare.siemens.com/magnetic-resonance-imaging/options-and-upgrades/clinical-applications/syngo-resolve. [Accessed: 19-Apr-2015].

[106] K. M. Li, L. Guo, J. X. Nie, G. Li, and T. M. Liu, "Review of methods for functional brain connectivity detection using fMRI," *Comput. Med. IMAGING Graph.*, vol. 33, no. 2, pp. 131–139, 2009.

[107] E. Pereda, R. Q. Quiroga, and J. Bhattacharya, "Nonlinear multivariate analysis of neurophysiological signals," *Prog. Neurobiol.*, vol. 77, no. 1–2, pp. 1–37, Oct. 2005.

[108] G. M. Jenkins and D. G. Watts, *Spectral analysis and its applications*. Holden-Day, 1969.

[109] J. P. Lachaux, E. Rodriguez, J. Martinerie, and F. J. Varela, "Measuring phase synchrony in brain signals," *Hum. Brain Mapp.*, vol. 8, no. 4, pp. 194–208, 1999.

[110] C. E. Shannon and W. Weaver, *The Mathematical Theory of Communication*, First Edition. Urbana: University of Illinois Press, 1975.

[111] R. Chavarriaga Lozano, "Feature selection," Ecole Polytechnique Fédérale de Lausanne, 11-Mar-2014.

[112] R. Chavarriaga Lozano, "Decision Trees," Ecole Polytechnique Fédérale de Lausanne, 11-Oct-2014.

[113] R. Quian Quiroga, A. Kraskov, T. Kreuz, and P. Grassberger, "Performance of different synchronization measures in real data: A case study on electroencephalographic signals," *Phys. Rev. E*, vol. 65, no. 4, p. 041903, Mar. 2002.

[114] A. J. Tomarken and N. G. Waller, "Structural equation modeling: strengths, limitations, and misconceptions," *Annu. Rev. Clin. Psychol.*, vol. 1, pp. 31–65, 2005.

[115] W. Gersch and G. V. Goddard, "Epileptic focus location: spectral analysis method," *Science*, vol. 169, no. 3946, pp. 701–702, Aug. 1970.

[116] B. Gourévitch, R. L. Bouquin-Jeannès, and G. Faucon, "Linear and nonlinear causality between signals: methods, examples and neurophysiological applications," *Biol. Cybern.*, vol. 95, no. 4, pp. 349–369, Oct. 2006.

[117] A. B. Barrett, L. Barnett, and A. K. Seth, "Multivariate Granger Causality and Generalized Variance," *Phys. Rev. E*, vol. 81, no. 4, Apr. 2010.

[118] S. L. Bressler and A. K. Seth, "Wiener–Granger Causality: A well established methodology," *NeuroImage*, vol. 58, no. 2, pp. 323–329, Sep. 2011.

[119] C. W. J. Granger, "Investigating Causal Relations by Econometric Models and Cross-Spectral Methods," *Econometrica*, vol. 37, no. 3, pp. 424–38, 1969.

[120] V. Sakkalis, "Review of advanced techniques for the estimation of brain connectivity measured with EEG/MEG," *Comput. Biol. Med.*, vol. 41, no. 12, pp. 1110–1117, Dec. 2011.

[121] M. J. Kaminski and K. J. Blinowska, "A new method of the description of the information flow in the brain structures," *Biol. Cybern.*, vol. 65, no. 3, pp. 203–210, Jul. 1991.

[122] L. A. Baccalá and K. Sameshima, "Partial directed coherence: a new concept in neural structure determination," *Biol. Cybern.*, vol. 84, no. 6, pp. 463–474, Jun. 2001.

[123] L. Astolfi, F. Cincotti, D. Mattia, F. De Vico Fallani, A. Tocci, A. Colosimo, S. Salinari, M. G. Marciani, W. Hesse, H. Witte, M. Ursino, M. Zavaglia, and F. Babiloni, "Tracking the time-varying cortical connectivity patterns by adaptive multivariate estimators," *IEEE Trans. Biomed. Eng.*, vol. 55, no. 3, pp. 902–913, Mar. 2008.

[124] H. Akaike, "A new look at the statistical model identification," *IEEE Trans. Autom. Control*, vol. 19, no. 6, pp. 716–723, Dec. 1974.

[125] G. Schwarz, "Estimating the Dimension of a Model," *Ann. Stat.*, vol. 6, no. 2, pp. 461–464, Mar. 1978.

[126] J. Pardey, S. Roberts, and L. Tarassenko, "A review of parametric modelling techniques for EEG analysis," *Med. Eng. Phys.*, vol. 18, no. 1, pp. 2–11, Jan. 1996.

[127] Y. Saito and H. Harashima, "Tracking of Information within Multichannel {EEG} record Causal analysis in {EEG}," in *Recent Advances in EEG and EMG Data Processing*, N. Yamaguchi and K. Fujisawa, Eds. Elsevier, 1981, pp. 133–146.

[128] G. Wang and M. Takigawa, "Directed coherence as a measure of interhemispheric correlation of EEG," *Int. J. Psychophysiol. Off. J. Int. Organ. Psychophysiol.*, vol. 13, no. 2, pp. 119–128, Sep. 1992.

[129] M. A. L. Nicolelis, *Methods for NEURAL ENSEMBLE RECORDINGS*. CRC Press, 2010.

[130] C. Wilke, L. Ding, and B. He, "Estimation of time-varying connectivity patterns through the use of an adaptive directed transfer function," *IEEE Trans. Biomed. Eng.*, vol. 55, no. 11, pp. 2557–2564, Nov. 2008.

[131] M. Arnold, W. H. Miltner, H. Witte, R. Bauer, and C. Braun, "Adaptive AR modeling of nonstationary time series by means of Kalman filtering," *IEEE*

Trans. Biomed. Eng., vol. 45, no. 5, pp. 553–562, May 1998.

[132] A. Schlogl, S. J. Roberts, and G. Pfurtscheller, "A criterion for adaptive autoregressive models," in *Proceedings of the 22nd Annual International Conference of the IEEE Engineering in Medicine and Biology Society, 2000*, 2000, vol. 2, pp. 1581–1582 vol.2.

[133] P. J. Franaszczuk, G. K. Bergey, and M. J. Kamiński, "Analysis of mesial temporal seizure onset and propagation using the directed transfer function method," *Electroencephalogr. Clin. Neurophysiol.*, vol. 91, no. 6, pp. 413–427, Dec. 1994.

[134] P. J. Franaszczuk and G. K. Bergey, "Application of the directed transfer function method to mesial and lateral onset temporal lobe seizures," *Brain Topogr.*, vol. 11, no. 1, pp. 13–21, 1998.

[135] C. Wilke, W. van Drongelen, M. Kohrman, and B. He, "Identification of epileptogenic foci from causal analysis of ECoG interictal spike activity," *Clin. Neurophysiol. Off. J. Int. Fed. Clin. Neurophysiol.*, vol. 120, no. 8, pp. 1449–1456, Aug. 2009.

[136] A. Korzeniewska, M. Mańczak, M. Kamiński, K. J. Blinowska, and S. Kasicki, "Determination of information flow direction among brain structures by a modified directed transfer function (dDTF) method," *J. Neurosci. Methods*, vol. 125, no. 1–2, pp. 195–207, May 2003.

[137] R. Diestel, *Graph Theory*, 4th ed. 2010. Corr. 3rd printing 2012 edition. Heidelberg ; New York: Springer, 2010.

[138] K. Ruohonen, "Graph Theory."

[139] J. Polich, "Updating P300: An integrative theory of P3a and P3b," *Clin. Neurophysiol.*, vol. 118, no. 10, pp. 2128–2148, 2007.

[140] C. C. Duncan, R. J. Barry, J. F. Connolly, C. Fischer, P. T. Michie, R. Näätänen, J. Polich, I. Reinvang, and C. Van Petten, "Event-related potentials in clinical research: Guidelines for eliciting, recording, and quantifying mismatch negativity, P300, and N400," *Clin. Neurophysiol.*, vol. 120, no. 11, pp. 1883–1908, 2009.

[141] P. R. Murphy, I. H. Robertson, J. H. Balsters, and R. G. O' Connell, "Pupillometry and P3 index the locus coeruleus–noradrenergic arousal function in humans," *Psychophysiology*, vol. 48, no. 11, 2011.

[142] S. J. Sara, "The locus coeruleus and noradrenergic modulation of cognition," *Nat. Rev. Neurosci.*, vol. 10, no. 3, 2009.

[143] S. Nieuwenhuis, de Geus, and G. Aston-Jones, "The anatomical and functional relationship between the P3 and autonomic components of the orienting response," *Psychophysiology*, vol. 48, no. 2.

[144] G. Aston-jones and J. D. Cohen, "An integrative theory of locus coeruleus-norepinephrine function: adaptive gain and optimal performance," *Annu. Rev. Neurosci.*, vol. 28, pp. 403–50, 2005.

[145] J. A. Pineda, S. L. Foote, and H. J. Neville, "Effects of locus coeruleus lesions on auditory, long-latency, event-related potentials in monkey," *J. Neurosci. Off. J. Soc. Neurosci.*, vol. 9, no. 1, pp. 81–93, 1989.

[146] C. W. Berridge and B. D. Waterhouse, "The locus coeruleus–noradrenergic system: modulation of behavioral state and state-dependent cognitive processes," *Brain Res. Rev.*, vol. 42, no. 1, pp. 33–84, 2003.

[147] T. W. Picton, "The P300 wave of the human event-related potential.," *J. Clin. Neurophysiol.*, vol. 9, no. 4, pp. 456–479, 1992.

[148] Steven J. Luck, *An introduction to the event-related potential technique*, 2nd ed. Cambridge, Mass: The MIT Press, 2014.

[149] T. w Picton, S. Bentin, P. Berg, E. Donchin, S. a Hillyard, R. Johnson, G. a Miller, W. Ritter, D. s Ruchkin, M. d Rugg, and M. j Taylor, "Guidelines for using human event-related potentials to study cognition: Recording standards and publication criteria," *Psychophysiology*, vol. 37, no. 2, 2000.

[150] G. Strobbe, P. van Mierlo, M. De Vos, B. Mijović, H. Hallez, S. Van Huffel, J. D. López, and S. Vandenberghe, "Multiple sparse volumetric priors for distributed EEG source reconstruction," *NeuroImage*, vol. 100, pp. 715–724, Oct. 2014.

[151] W. Staljanssens, "Source localization of the P300 event-related potential as a biomarker for the efficacy of vagus nerve stimulation in patients with epilepsy."

[152] P. M. Francesca Pittau, "Mapping Epileptic Activity: Sources or Networks for the Clinicians?," *Front. Neurol.*, vol. 5, p. 218, 2014.

[153] E. van Diessen, W. M. Otte, K. P. J. Braun, C. J. Stam, and F. E. Jansen, "Improved Diagnosis in Children with Partial Epilepsy Using a Multivariable Prediction Model Based on EEG Network Characteristics," *PLoS ONE*, vol. 8, no. 4, p. e59764, Apr. 2013.

[154] J. Engel, P. M. Thompson, J. M. Stern, R. J. Staba, A. Bragin, and I. Mody, "Connectomics and epilepsy," *Curr. Opin. Neurol.*, vol. 26, no. 2, pp. 186–194, Apr. 2013.

[155] J. R. Terry, O. Benjamin, and M. P. Richardson, "Seizure generation: the role of nodes and networks," *Epilepsia*, vol. 53, no. 9, pp. e166–169, Sep. 2012.

[156] N. Tzourio-Mazoyer, B. Landeau, D. Papathanassiou, F. Crivello, O. Etard, N. Delcroix, B. Mazoyer, and M. Joliot, "Automated anatomical labeling of activations in SPM using a macroscopic anatomical parcellation of the MNI MRI single-subject brain," *Neuroimage*, vol. 15, no. 1, pp. 273–289, 2002.

[157] O. J. Dunn, "Estimation of the Medians for Dependent Variables," *Ann. Math. Stat.*, vol. 30, no. 1, pp. 192–197, Mar. 1959.

[158] Y. Benjamini and Y. Hochberg, "Controlling the false discovery rate: a practical and powerful approach to multiple testing," *J. R. Stat. Soc. Ser. B Methodol.*, vol. 57, no. 1, pp. 289–300, 1995.

[159] "Statistical Models," *Cambridge University Press*. [Online]. Available: http://www.cambridge.org/us/academic/subjects/statistics-probability/statistical-theory-and-methods/statistical-models-theory-and-practice-2nd-edition. [Accessed: 13-May-2015].

[160] J. Gläscher and D. Gitelman, "Contrast weights in flexible factorial design with multiple groups of subject." Caltech, 19-Mar-2008.

[161] D. Gleich, "MatlabBGL - File Exchange - MATLAB Central." [Online]. Available: http://www.mathworks.com/matlabcentral/fileexchange/10922-matlabbgl. [Accessed: 17-May-2015].

[162] H. V. Semlitsch, P. Anderer, P. Schuster, and O. Presslich, "A Solution for Reliable and Valid Reduction of Ocular Artifacts, Applied to the P300 ERP," *Psychophysiology*, vol. 23, no. 6, pp. 695–703, Nov. 1986.

[163] E. J. Hammond, B. M. Uthman, S. A. Reid, and B. J. Wilder, "Electrophysiologic Studies of Cervical Vagus Nerve Stimulation in Humans: II. Evoked Potentials," *Epilepsia*, vol. 33, no. 6, 1992.

[164] A. H. Neuhaus, A. Luborzewski, J. Rentzsch, E. L. Brakemeier, C. Opgen-Rhein, J. Gallinat, and M. Bajbouj, "P300 is enhanced in responders to vagus nerve stimulation for treatment of major depressive disorder," *J. Affect. Disord.*, vol. 100, no. 1, pp. 123–128, 2007.

[165] M. Brázdil, P. Chadim, P. Daniel, R. Kuba, I. Rektor, Z. Novák, and J. Chrastina, "Effect of vagal nerve stimulation on auditory and visual event-related potentials," *Eur. J. Neurol. Off. J. Eur. Fed. Neurol. Soc.*, vol. 8, no. 5, pp. 457–461, Sep. 2001.

[166] J.-H. Chae, Z. Nahas, M. Lomarev, S. Denslow, J. P. Lorberbaum, D. E.

Bohning, and M. S. George, "A review of functional neuroimaging studies of vagus nerve stimulation (VNS)," *J. Psychiatr. Res.*, vol. 37, no. 6, pp. 443–455, Nov. 2003.

[167] K. Vonck, V. De Herdt, T. Bosman, S. Dedeurwaerdere, K. Van Laere, and P. Boon, "Thalamic and limbic involvement in the mechanism of action of vagus nerve stimulation, a SPECT study," *Seizure*, vol. 17, no. 8, pp. 699–706, Dec. 2008.

[168] T. R. Henry, R. A. Bakay, J. R. Votaw, P. B. Pennell, C. M. Epstein, T. L. Faber, S. T. Grafton, and J. M. Hoffman, "Brain blood flow alterations induced by therapeutic vagus nerve stimulation in partial epilepsy: I. Acute effects at high and low levels of stimulation," *Epilepsia*, vol. 39, no. 9, pp. 983–990, Sep. 1998.

[169] T. R. Henry, "Therapeutic mechanisms of vagus nerve stimulation," *Neurology*, vol. 59, no. 6 Suppl 4, pp. 3–14, 2002.

[170] E. J. Van Bockstaele, J. Peoples, and P. Telegan, "Efferent projections of the nucleus of the solitary tract to peri-locus coeruleus dendrites in rat brain: evidence for a monosynaptic pathway," *J. Comp. Neurol.*, vol. 412, no. 3, pp. 410–28, 1999.

[171] D. A. Groves, E. M. Bowman, and V. J. Brown, "Recordings from the rat locus coeruleus during acute vagal nerve stimulation in the anaesthetised rat," *Neurosci. Lett.*, vol. 379, no. 3, pp. 174–179, 2005.

[172] A. E. Dorr and G. Debonnel, "Effect of vagus nerve stimulation on serotonergic and noradrenergic transmission," *J. Pharmacol. Exp. Ther.*, vol. 318, no. 2, pp. 890–8, 2006.

[173] C. R. Conway, Y. I. Sheline, J. T. Chibnall, M. S. George, J. W. Fletcher, and M. A. Mintun, "Cerebral blood flow changes during vagus nerve stimulation for depression," *Psychiatry Res. Neuroimaging*, vol. 146, no. 2, pp. 179–184, Mar. 2006.

[174] D. E. Bohning, M. P. Lomarev, S. Denslow, Z. Nahas, A. Shastri, and M. S. George, "Feasibility of vagus nerve stimulation-synchronized blood oxygenation level-dependent functional MRI," *Invest. Radiol.*, vol. 36, no. 8, pp. 470–479, Aug. 2001.

[175] A. Zobel, A. Joe, N. Freymann, H. Clusmann, J. Schramm, M. Reinhardt, H.-J. Biersack, W. Maier, and K. Broich, "Changes in regional cerebral blood flow by therapeutic vagus nerve stimulation in depression: An exploratory approach,"

Psychiatry Res. Neuroimaging, vol. 139, no. 3, pp. 165–179, Aug. 2005.

[176] T. Kraus, K. Hösl, O. Kiess, A. Schanze, J. Kornhuber, and C. Forster, "BOLD fMRI deactivation of limbic and temporal brain structures and mood enhancing effect by transcutaneous vagus nerve stimulation," *J. Neural Transm.*, vol. 114, no. 11, pp. 1485–1493, Jun. 2007.

[177] T. R. Henry, R. A. E. Bakay, P. B. Pennell, C. M. Epstein, and J. R. Votaw, "Brain blood-flow alterations induced by therapeutic vagus nerve stimulation in partial epilepsy: II. prolonged effects at high and low levels of stimulation," *Epilepsia*, vol. 45, no. 9, pp. 1064–1070, Sep. 2004.

[178] M. H. M. D. Devous, "Effects of VNS on regional cerebral blood flow in depressed subjects," *Eur. Psychiatry - EUR PSYCHIAT*, vol. 17, pp. 113–114, 2002.

[179] A. Barnes, R. Duncan, J. A. Chisholm, K. Lindsay, J. Patterson, and D. Wyper, "Investigation into the mechanisms of vagus nerve stimulation for the treatment of intractable epilepsy, using 99mTc-HMPAO SPET brain images," *Eur. J. Nucl. Med. Mol. Imaging*, vol. 30, no. 2, pp. 301–305, Feb. 2003.

[180] K. Van Laere, K. Vonck, P. Boon, J. Versijpt, and R. Dierckx, "Perfusion SPECT changes after acute and chronic vagus nerve stimulation in relation to prestimulus condition and long-term clinical efficacy," *J. Nucl. Med. Off. Publ. Soc. Nucl. Med.*, vol. 43, no. 6, pp. 733–744, Jun. 2002.

[181] M. Fraschini, M. Demuru, M. Puligheddu, S. Floridia, L. Polizzi, A. Maleci, M. Bortolato, A. Hillebrand, and F. Marrosu, "The re-organization of functional brain networks in pharmaco-resistant epileptic patients who respond to VNS," *Neurosci. Lett.*, vol. 580, pp. 153–157, 19.

[182] L. Douw, E. van Dellen, M. de Groot, J. J. Heimans, M. Klein, C. J. Stam, and J. C. Reijneveld, "Epilepsy is related to theta band brain connectivity and network topology in brain tumor patients," *BMC Neurosci.*, vol. 11, p. 103, 2010.

[183] L. Douw, M. de Groot, E. van Dellen, J. J. Heimans, H. E. Ronner, C. J. Stam, and J. C. Reijneveld, "'Functional Connectivity' Is a Sensitive Predictor of Epilepsy Diagnosis after the First Seizure," *PLoS ONE*, vol. 5, no. 5, p. e10839, May 2010.

[184] F. Pittau, C. Grova, F. Moeller, F. Dubeau, and J. Gotman, "Patterns of altered functional connectivity in mesial temporal lobe epilepsy," *Epilepsia*, vol. 53, no. 6, pp. 1013–1023, Jun. 2012.

[185] J. Fang, P. Rong, Y. Hong, Y. Fan, J. Liu, H. Wang, G. Zhang, X. Chen, S. Shi, L. Wang, R. Liu, J. Hwang, Z. Li, J. Tao, Y. Wang, B. Zhu, and J. Kong, "Transcutaneous Vagus Nerve Stimulation Modulates Default Mode Network in Major Depressive Disorder," *Biol. Psychiatry*.

[186] M. A. Kramer, E. D. Kolaczyk, and H. E. Kirsch, "Emergent network topology at seizure onset in humans," *Epilepsy Res.*, vol. 79, no. 2–3, pp. 173–186, May 2008.

[187] Z. Zhang, W. Liao, H. Chen, D. Mantini, J.-R. Ding, Q. Xu, Z. Wang, C. Yuan, G. Chen, Q. Jiao, and G. Lu, "Altered functional–structural coupling of large-scale brain networks in idiopathic generalized epilepsy," *Brain*, vol. 134, no. 10, pp. 2912–2928, Oct. 2011.

[188] E. van Dellen, L. Douw, A. Hillebrand, P. C. de Witt Hamer, J. C. Baayen, J. J. Heimans, J. C. Reijneveld, and C. J. Stam, "Epilepsy surgery outcome and functional network alterations in longitudinal MEG: a minimum spanning tree analysis," *NeuroImage*, vol. 86, pp. 354–363, Feb. 2014.

[189] B. C. Bernhardt, Z. Chen, Y. He, A. C. Evans, and N. Bernasconi, "Graph-theoretical analysis reveals disrupted small-world organization of cortical thickness correlation networks in temporal lobe epilepsy," *Cereb. Cortex N. Y. N 1991*, vol. 21, no. 9, pp. 2147–2157, Sep. 2011.

[190] W. M. Otte, R. M. Dijkhuizen, M. P. A. van Meer, W. S. van der Hel, S. A. M. W. Verlinde, O. van Nieuwenhuizen, M. A. Viergever, C. J. Stam, and K. P. J. Braun, "Characterization of functional and structural integrity in experimental focal epilepsy: reduced network efficiency coincides with white matter changes," *PloS One*, vol. 7, no. 7, p. e39078, 2012.

[191] M. Chavez, M. Valencia, V. Navarro, V. Latora, and J. Martinerie, "Functional modularity of background activities in normal and epileptic brain networks," *Phys. Rev. Lett.*, vol. 104, no. 11, p. 118701, Mar. 2010.

[192] F. Bartolomei, G. Bettus, C. J. Stam, and M. Guye, "Interictal network properties in mesial temporal lobe epilepsy: a graph theoretical study from intracerebral recordings," *Clin. Neurophysiol. Off. J. Int. Fed. Clin. Neurophysiol.*, vol. 124, no. 12, pp. 2345–2353, Dec. 2013.

[193] M.-T. Horstmann, S. Bialonski, N. Noennig, H. Mai, J. Prusseit, J. Wellmer, H. Hinrichs, and K. Lehnertz, "State dependent properties of epileptic brain networks: comparative graph-theoretical analyses of simultaneously recorded EEG and MEG," *Clin. Neurophysiol. Off. J. Int. Fed. Clin. Neurophysiol.*, vol.

121, no. 2, pp. 172–185, Feb. 2010.

[194] E. van Dellen, L. Douw, J. C. Baayen, J. J. Heimans, S. C. Ponten, W. P. Vandertop, D. N. Velis, C. J. Stam, and J. C. Reijneveld, "Long-Term Effects of Temporal Lobe Epilepsy on Local Neural Networks: A Graph Theoretical Analysis of Corticography Recordings," *PLoS ONE*, vol. 4, no. 11, p. e8081, Nov. 2009.